SNOWPACK ESTIMATION AND MODELLING ACROSS SCALES USING FIELD-BASED AND REMOTELY SENSED DATA IN A FORESTED REGION OF CENTRAL ONTARIO

A Thesis Submitted to the Committee on Graduate Studies in Partial Fulfillment of the Requirements for the Degree of Doctor of Philosophy in the Faculty of Arts and Science

Trent University

Peterborough, Ontario, Canada

May 2023

Abstract

Snowpack Estimation and Modelling Across Scales Using Field-Based and Remotely Sensed Data in a Forested Region of Central Ontario

Andrew Donald John Beaton

Understanding snowpack variability is important as it plays an imperative role in environmental, hydrologic, and atmospheric systems. Research questions related to three linked areas were investigated in this thesis: 1) scaling issues in snow hydrology, 2) forest-snowpack relationships, and 3) methods of integrating snow water equivalent (SWE) into a hydrologic model for a large, forested drainage basin in central Ontario. The first study evaluated differences in SWE across process, measurement, and model scales. Point scale snowpack measurements could be bias corrected using scaling factors derived from a limited number of transect measurements and appropriately stratified point scale measurements may be suitable for replacing transect scale mean SWE when transect data are not possible to collect. Comparison of modelled products to measurements highlighted the importance of understanding the spatial representativeness of *in-situ* measurements and the processes those measurements represent when validating snow products or assimilating data into models.

The second study investigated the efficacy of field-based, and remotely sensed datasets to describe forest structure and resolve forest-snowpack relationships. Canopy cover was highly correlated with melt rate and timing at the site scale however, significant correlations were present in 2016 but not 2017, which was attributed to interannual differences in climate. Peak SWE metrics did not correlate well with forest metrics. This was likely due to mid-winter melt events throughout both study years,

where a mix of accumulation and melt processes confounded forest-snowpack relationships.

The third study evaluated the accuracy of the Copernicus SWE product and assessed the impact of calibrating and assimilating SWE data on model performance. The bias corrected Copernicus product agreed with measured data and provided a good estimate of mean basin SWE. Calibration of a hydrologic model to subbasin SWE substantially improved modelled SWE performance. Modelled SWE skill was not improved by assimilating SWE into the calibrated model. All models evaluated had similar streamflow performance, indicating streamflow in the study basin can be accurately estimated using a model with a poor representation of SWE. The findings from this work improved knowledge and understanding of snow processes in the hydrologically significant Great Lakes-St Lawrence Forest region of central Ontario.

Keywords

scale, snow depth, snow water equivalent (SWE), remote sensing, forest structure, multi-objective calibration, data assimilation, hydrologic model, Great Lakes-St. Lawrence Forest.

Acknowledgements

I am very grateful for the opportunity I had to learn from my supervisors and committee members; Dr. Robert Metcalfe, Dr. James Buttle, Dr. Steven Franklin, and Dr. Bryan Tolson. I am very fortunate to work with highly regarded experts in the field of hydrology and remote sensing with a broad range of specialties. They provided encouragement, advice, and thoughtful comments on this work. I am very thankful for and would like to acknowledge the assistance and support from Dr. Chris Derksen, James English, Max Debues, Wes Greenwood, Halya Petzold, Dr. Carly Armstrong and especially Dr. Jamie Luce. Their assistance in the field and numerous conversations about snow processes during long car rides to the field sites helped shape the contents of this thesis. Support from the Ministry of Natural Resources and Forestry organization and staff including Dave Burritt and Kathy Woeller are much appreciated, and especially Frank Kenny who helped initiate my studies and provided support and encouragement throughout. The authors also thank Dr. Jamie Luce, Dr. Lawrence Mudryk, Dr. Kari Luojus, Ian Sinclair, and Dr. Ming Han for providing access to models and data. Finally, I would like to thank my family and in particular my wife Carly Armstrong for all the love and support over the course of my graduate studies. This research was partially funded through the Canada-Ontario Agreement Fund.

Co-authorship Statement

This thesis consists of three manuscripts. Andy Beaton is the primary author of all manuscripts. He designed the study, analyzed the data, and wrote the manuscripts with guidance, input, and suggestions from coauthors identified on the title page of each

manuscript. Dr. Ming Han provided a hydrologic model that was used in the third manuscript (described in Chapter 4).

Table of Contents

List of Figures

List of Tables

List of abbreviations and symbols

2D	Two-Dimensional
3D	Three-Dimensional
BL	Baseline Model Calibrated to Discharge and Lake Levels
BLS	Baseline Model Calibrated to Discharge, Lake Levels and Subbasin SWE
CC	Canopy Cover
CMC	Canadian Meteorological Centre
CON	Coniferous
DBH	Diameter at Breast Height
DBH_{max}	Maximum Diameter at Breast Height
DDS	Dynamically Dimensioned Search Algorithm
DEC	Deciduous
DTB_{field}	Distance to Closest Tree Bole Derived from Field Measurements
DTB_{LiDAR}	Distance to Closest Tree Bole Derived from LiDAR
GEM	Global Environmental Multiscale
GF_{55}	Hemispheric Photo Derived Gap Fraction at a 55° Zenith Angle
GHz	Gigahertz
GLSF	Great Lakes-St. Lawrence Forest
GPS	Global Positioning System
HP	Hemispheric Photo
HRU	Hydrologic Response Unit
IMS	Ice Mapping System
KGE	Kling Gupta Efficiency
KGED	Kling Gupta Efficiency Deviation
LAI	Leaf Area Index
LiDAR	Light Detection and Ranging
MAD	Mean Absolute Difference
masl	Metres Above Sea Level
MB	Mean Bias
MERRA-2	Modern-Era Retrospective Analysis
MIX	Mixed Woods
MODIS	Moderate Resolution Imaging Spectroradiometer
MSC	Meteorological Service of Canada
NASA	National Aeronautics and Space Administration
NDVI	Normalized Difference Vegetation Index
NIR	Near Infrared
NOAA	National Oceanic and Atmospheric Administration

NSIDC	National Snow and Ice Data Centre
P	Days Between Snow Surveys
PA-DDS	Pareto Archived Dynamically Dimensioned Search
PDEM	Provincial Digital Elevation Model
$PEAK_{doy}$	Maximum SWE Day of Year for Each Year
PET	Potential Evapotranspiration
PF	Particle Filter Model
$PGRND_{PPC}$	Percentage of Points that Reach the Ground
POR	Period of Record
PPC	Photogrammetric Point Cloud
PRMS	Precipitation-Runoff Modelling System
RSE	Relative Standard Error
RTK	Real-time Kinematic
SACSMA	Sacramento Soil Moisture Accounting Model
SCA	Snow Covered Area
SCOOP	South-Central Ontario Orthophoto Project
SF_{doy}	Snow Free Day of Year
SMR	Snowmelt Rate
SSMIS	Special Sensor Microwave Imager/Sounder
SWE	Snow Water Equivalent
SWE_{peak}	Maximum SWE Within Each Year
TL	Time-lapse
WET	Wetland
$zmax_{LiDAR}$	Maximum Point Cloud Heights
$zmax_{LiDAR}$	Mean of Point Cloud Heights
zsd_{LiDAR}	Standard Deviation of Point Cloud Heights

Chapter 1 General introduction

1.1 Background

Accurate representation of snow water equivalent (SWE) distribution through time in snow-dominated basins is critical for assessing hydrologic processes, numerical weather prediction and for evaluating the Earth's water balance, ecosystem function and the potential impacts of a changing climate on water resources (Luce *et al.*, 1998; Pomeroy *et al.*, 2004; Barnett *et al.*, 2005; Kinar and Pomeroy, 2015). Understanding SWE distribution remains a significant scientific challenge and requires consideration of scaling issues and complex physical processes (Steppuhn and Dyck, 1974; Blöschl, 1999; Watson *et al.*, 2006; Jost *et al.*, 2007). Extensive research has been conducted in this area, but important research gaps remain, particularly related to understanding variables and processes that control snow distribution across scales (Blöschl, 1999; Sturm, 2015; Dong, 2018). Blöschl (1999) defines three conceptual scales: 1) the process scale which represents the true process, 2) the measurement scale, which is the scale of the collected data, and 3) the model scale, which is defined by the model dimensions and elements (e.g., model grid). Observed SWE data are rarely available as measurement of SWE in the field is labor intensive and expensive. Field-based measurement of SWE typically captures less than 1% of a basin's snowpack and spatially distributed measurements are infrequent (Sturm, 2015). Remotely sensed and modelled gridded SWE products provide estimates across larger extents and at higher frequencies than can feasibly be measured in the field but these data are often at resolutions too coarse to resolve important variations and processes and suffer from limitations that degrade product accuracy (Dong, 2018). In addition, validating products remains a significant challenge, attributed to differences

in scale between ground truth and model data (Mudryk *et al.*, 2015). Differences in snowpack estimates and the processes they represent across scales, the error introduced using fine scale measurements to represent coarser extents, assimilation of fine scale data into gridded datasets, and validation of coarse scale modeled snowpack using fine scale data remain unresolved and require further investigation (Peters-Lidard *et al.*, 2017).

Factors affecting the spatial variability of snowpack are hierarchically scale dependent (Blöschl, 1999; Clark *et al.*, 2011). In non-mountainous forested landscapes, topography and land cover are the physical characteristics that drive basin scale variability of SWE (Jiusto and Kaplan, 1972; Anderton *et al.*, 2004; Clark *et al.*, 2011). At the forest stand scale, vegetation structure plays the largest role along with slope and aspect (Metcalfe and Buttle, 1998; Jost *et al.*, 2007; Varhola *et al.*, 2010b). At the site scale, vegetation, micro-topography, and ground surface features such as boulders, branches, and ponded water are the physical factors that affect snow depth and SWE variability (López-Moreno *et al.*, 2011). Field based forest structure data for evaluating forest-snowpack relationships are time consuming to measure and difficult to distribute over larger areas (Varhola *et al.*, 2012; Moeser *et al.*, 2014). Spatially-distributed two-dimensional (2D) forest metrics have been derived from remote sensing data and related to snowpack data (Metcalfe and Buttle, 1998; Essery *et al.*, 2008). More recently, three-dimensional (3D) forest metrics have been derived from light detection and ranging (LiDAR) data and photogrammetric point clouds (PPCs). Several studies have used LiDAR derived forest metrics to assess forest-snowpack relationships while use of PPC data for this purpose is limited (Morsdorf *et al.*, 2006; Essery *et al.*, 2008; Moeser *et al.*, 2015b; Zheng *et al.*, 2018). The Ontario government collects and disseminates LiDAR

and orthophoto-derived spectral and point cloud data across regions of the province. These data may be valuable for addressing unresolved questions related to factors and processes that control forest-snowpack relationships across scale and climate, warranting investigation (Varhola *et al.*, 2010b; Land Information Ontario, 2022a, 2022b).

Assessing flood risk, hydropower production, aquatic ecosystems, water supply and the impacts of climate change on water resources requires accurate estimates of streamflow (Barnett et al., 2005; Beaton and Bradford, 2013; Musselman et al., 2018). Hydrologic models are valuable tools for estimating SWE and streamflow and can facilitate planning, prediction and decision making (Luce *et al.*, 1998; Jenicek *et al.*, 2016; Hammond *et al.*, 2018). SWE is typically a state variable within hydrologic models that can be improved by calibrating to snowpack data or assimilating snowpack data into the model. Multi-objective calibration has been used to constrain hydrologic models with measured and remotely sensed snowpack data and discharge observations (Gao et al., 2017; Tuo et al., 2018; Nemri and Kinnard, 2020). Many studies have investigated assimilation of snowpack data into hydrologic models to improve simulations for practical applications and to explore processes (e.g. Vuyovich and Jacobs, 2011; Bergeron et al., 2016; Dziubanski and Franz, 2016; Griessinger et al., 2016; Huang et al., 2017a, 2017b; Leach et al., 2018; Zahmatkesh et al., 2019; Micheletty et al., 2021). While previous research has focused on multi-objective calibration using SWE or SWE assimilation, the comparative effect of these two approaches on model performance remains unresolved.

1.2 Thesis objectives and structure

Three inter-related objectives were addressed in Chapters 2 to 4. The objective of Chapter 2 was to improve understanding of snow distribution across scale. Chapter 3 focused on the use of remotely sensed forest structure metrics to assess forest-snowpack relationships, and the objective of Chapter 4 was to evaluate the effects of incorporating SWE into a hydrologic model by multi-objective calibration and data assimilation.

Chapter 2 objectives were met by assessing differences in the mean and variability of snowpack across measurement and model scales and exploring how these scales represent true processes and their statistical moments. Two main questions were addressed:

- *What snow processes do measurements at different scales represent?*
- *How do daily SWE and snow depth mean, and variability compare across scale?*

Variable effects of vegetation on SWE were observed and it was hypothesized that the simple comparison of canopy cover with mean SWE in Chapter 2 was not adequate for capturing the interactions between vegetation and snow cover. This hypothesis was explored in Chapter 3 by comparing several forest and snowpack metrics. Interannual differences in the effect of vegetation on snowpack metrics were found in Chapter 2 and explored in more depth in Chapter 3.

Chapter 2 provided insight and quantified the error associated with using fine scale measurements to represent SWE at coarser scales. These findings informed the upscaling of point data for the validation of a remotely sensed SWE product in Chapter 4. The comparison of measurement and model scale values in Chapter 2 highlighted important considerations that informed the use of remotely sensed SWE in Chapter 4.

The objective of Chapter 3 was accomplished using Ontario orthophotos and LiDAR data sets to address the following questions:

- *How do forest metrics compare to peak SWE and snowmelt?*
- *How and why do relationships between forest structure and snowpack vary inter-annually?*

The results of Chapter 3 helped inform model development in Chapter 4.

The objectives of Chapter 4 were accomplished using a baseline hydrologic model calibrated to lake levels and basin outlet discharge developed by Han et al. (2021), a model calibrated to subbasin SWE, lake levels, and outlet discharge, and a model that assimilated remotely sensed SWE. The following research question was addressed:

- *What are the relative effects of calibrating to subbasin SWE and assimilating remotely sensed SWE on the performance of modelled SWE and discharge?*

1.3 Contributions of research

The study was conducted in the Great Lakes-St. Lawrence Forest (GLSF) region. The GLSF covers a broad swath of central Ontario and southern Quebec and plays an important role in regulating water inputs to the Great Lakes. These lakes contain nearly 20% of the earth's freshwater, are a vital source of drinking water, food, energy, transportation, and recreation, and support a diverse ecosystem (Ontario Ministry of the Environment, 2016). The GLSF's hydrology is dominated by a response to seasonal snow cover and improved understanding of SWE and melt processes is therefore critical to enhance understanding of water inputs to the Great Lakes basin. A unique dataset was collected in this environment for the specific purpose of addressing the research questions in this thesis. Previous studies investigating scaling issues and forest-

snowpack relationships have primarily been conducted in coniferous forests and alpine regions (Penn *et al.*, 2012), creating a research gap in non-mountain mixed hardwood and coniferous forests.

Previous efforts to assess snowpack across scale typically focused on differences over a single conceptual scale (e.g. measurement; Neumann *et al.*, 2006) (model; Derksen *et al.*, 2005b; Meromy *et al.*, 2013), have used data with a limited repeat frequency, and have not discussed process scale in detail. This research extends existing literature by considering all three conceptual model scales, assessing how scaling issues change over time (within and across winter seasons) and by explicitly focusing on snow processes.

The comparison of field-based, 2D and 3D orthophoto- and LiDAR-derived metrics for the purposes of characterizing a snowpack builds on previous studies, which typically have focused on a single remotely sensed data set to derive the required forest metrics (Varhola *et al.*, 2010a; Moeser *et al.*, 2015b). To the knowledge of the author, this was the first study to use Ontario imagery and LiDAR data to assess forest-snowpack relationships. This thesis also evaluated both field and remotely sensed canopy and tree bole characteristics whereas most previous studies focused on a single category of metrics.

To the author's knowledge this is the first study to validate Copernicus SWE product at the basin scale, assimilate Copernicus SWE into a hydrologic model, and assimilate SWE using the Raven hydrologic modelling framework. This research contributes to snow hydrology science by elucidating the accuracy and value of a readily available, spatially distributed SWE dataset for hydrologic modelling at the basin scale in

a mixed forest region and the relative impact of SWE calibration and SWE data assimilation on model performance.

Chapter 2 Investigating snowpack across scale in the Great Lakes-St. Lawrence Forest region of central Ontario, Canada

A version of this chapter is published in the journal Hydrological Processes

Beaton AD, Metcalfe RA, Buttle JM, Franklin SE. 2019. Investigating snowpack across scale in the northern Great Lakes–St. Lawrence Forest region of Central Ontario, Canada. *Hydrological Processes* **33** (26): 3310–3329 DOI: 10.1002/hyp.13558

*A.D. Beaton is the primary author of this paper. He designed the study, analyzed the data, and wrote the primary manuscript with guidance, input, and suggestions from coauthors. Dr. Jamie Luce collected and processed the aerial imagery.

Abstract

This study investigates scaling issues by evaluating snow processes and quantifying bias in snowpack properties across scale in a northern Great Lakes-St. Lawrence Forest. Snow depth and density were measured along transects stratified by land cover over the 2015/16 and 2016/17 winters. Daily snow depth was measured using three rulers and a time-lapse camera (TL) at each transect. Semivariogram analysis of the transect data was conducted and no autocorrelation was found, indicating little spatial structure along the transects. Pairwise differences in snow depth and snow water equivalent (SWE) between land covers were calculated and compared across scales. Differences in snowpack between TL measurements in forested land cover types corresponded to differences in canopy cover but this relationship was not evident at the transect scale, indicating a difference in observed process across scale. TL and transect estimates had substantial bias but consistency in error was observed which indicates that scaling coefficients may be derived to improve point scale estimates. TL and transect measurements were upscaled to estimate grid scale means. Upscaled estimates were

compared and found to be consistent indicating that appropriately stratified point scale measurements can be used to approximate a grid scale mean when transect data are not available. These findings are important in remote regions such as the study area where frequent transect data may be difficult to obtain. TL, transect and upscaled means were compared to modelled depth and SWE. Model comparisons to TL and transect data indicated that bias was dependent on land cover, measurement scale and seasonality. Modelled means compared well with upscaled estimates, but model SWE was underestimated during spring melt. These findings highlight the importance of understanding the spatial representativeness of *in-situ* measurements and the processes those measurements represent when validating gridded snow products or assimilating data into models.

2.1 Introduction

Understanding snow water equivalent (SWE) distribution through time in snow-dominated basins is essential for assessing hydrologic processes, numerical weather prediction, understanding water balance and ecosystem function and assessing the potential impacts of a changing climate (Luce *et al.*, 1998; Pomeroy *et al.*, 2004; Barnett *et al.*, 2005; Kinar and Pomeroy, 2015). Accurate estimates of distributed SWE remain a significant scientific challenge and require consideration of scaling issues, measurement uncertainty and complex physical processes (Steppuhn and Dyck, 1974; Blöschl, 1999; Watson *et al.*, 2006; Jost *et al.*, 2007). Extensive research has been conducted in this area, but important research gaps remain, particularly related to understanding processes that control snow distribution across scales (Blöschl, 1999; Sturm, 2015; Dong, 2018). Peters-Lidard et al. (2017) assert that scaling issues are one of the major impediments to

advancing understanding of hydrologic processes. They suggest scaling become the fourth paradigm (in addition to empiricism, theory, and computational simulation) in hydrologic research and a focal point for current, intensive investigation.

Blöschl (1999) defines three conceptual scales. The process scale represents the true process and has statistical moments that define the natural variability. The measurement scale is the scale of the collected data and has statistical moments defined by the processes measured by the dimensions of the instrument and sample design. The model scale is defined by the model dimensions and elements (e.g., model grid) which represent aggregated variability within model elements (e.g., sub grid variability) and spatial variability between elements. The term scaling can be defined as a change across scales and can consist of aggregation (upscaling) from fine to coarser scales or disaggregation (downscaling) from coarse to finer scales (Blöschl, 1999). Fundamental questions arise related to the representativeness of the statistical moments of the measurement and model scale represented by the data versus the true patterns and processes being investigated (Blöschl and Sivapalan, 1995; Blöschl, 2006). Snow depth and SWE measured at one scale may not be representative of another scale due to the complex non-linear interactions of snowpack and factors that control snow distribution during accumulation and ablation (Blöschl and Sivapalan, 1995; Blöschl, 1999; Molotch and Bales, 2005; Meromy *et al.*, 2013).

The term scale can be defined as a characteristic dimension of space or time (Blöschl, 1999). Temporal scales investigated in snow hydrology range from sub-daily to event based, seasonal, annual, decadal and centennial time-periods depending on the research questions being addressed (Sturm, 2015). Spatial scale can be defined by the

scale triplet which includes the support (area covered by a single measurement), spacing (distance between individual measurements), and extent (distance or area between all measurements)(Blöschl and Sivapalan, 1995; Blöschl, 1999). This traditional scale triplet has been extended to define characteristics of snowpack measurements including repeat frequency, accuracy, and work effort (Sturm, 2015). Due to limitations in instrumentation and the work effort required to collect distributed snowpack data, point measurements with low support and extent at a high repeat frequency (e.g. sub-daily ultrasonic depth measurements) or distributed measurements at low repeat frequency (e.g. bi-monthly snow surveys) are often the only ground based data possible to collect (Neumann *et al.*, 2006; Kinar and Pomeroy, 2015; Sturm, 2015). Research has shown that a very small fraction of a basin's snowpack, ranging from 1% for small basins to a fraction of a percent for larger basins, can be measured feasibly using ground based methods (Sturm, 2015). As a result, point and single transect measurements are routinely used operationally for assessing regional scale hazard risks (Provincial Flood Forecasting and Warning Committee, 2014) and wildlife vulnerability (Warren *et al.*, 1998), and are assimilated into regional scale models of snowpack, often times without careful consideration of measurement representativeness of the surrounding area (Meromy *et al.*, 2013).

Remote sensing and modelling can provide snowpack estimates across larger support, extent and repeat frequencies but these data are often at resolutions too coarse to resolve important variability and processes and suffer from limitations that degrade product accuracy (Dong, 2018). In addition, validating products remains a significant challenge due to differences in scale between ground truth and model data (Mudryk *et*

al., 2015). Single point climate stations and transect data that capture a small fraction of model grid extent are inadequate for validating modelled and remotely sensing snow datasets but are routinely used due to limitations in instrumentation and data availability (Hancock *et al.*, 2013; Snauffer *et al.*, 2016; Larue *et al.*, 2017).

The purpose of this paper is to evaluate differences in snowpack estimates and the process they represent across common measurement (point and transect) and model scales to provide insight into the error introduced by using fine scale measurements to represent coarser extents, assimilation of fine scale data into gridded datasets, and validation of coarse scale modeled snowpack using fine scale data. This is accomplished by assessing differences in mean and variability of snowpack across measurement and model scales and exploring how these scales may represent true processes and their statistical moments in a Great Lakes-St. Lawrence Forest (GLSF) basin. Two main questions are addressed:

1. *What snow processes do measurements at different scales represent; and*
2. *How do estimates of snowpack mean and variability compare across scale?*

Previous effort to assess snowpack across scale have typically focused on differences over a single conceptual scale (e.g. measurement; Neumann *et al.*, 2006) (model; Derksen *et al.*, 2005b; Meromy *et al.*, 2013), have used data with a limited repeat frequency, and have not discussed process scale in detail. This study extends existing literature by considering all three conceptual scales, assessing how scaling issues change over time (within and across winter seasons) and by explicitly focusing on snow processes. In addition, previous literature focused on northern boreal or montane environments, whereas this study is in the less studied GLSF. This landscape exerts

critical control on water resources (e.g., flood risk and aquatic ecology) of numerous downstream communities.

2.2 Methods

2.2.1 Study area

The study area is in central Ontario in the southwest corner of Algonquin Provincial Park and covers an area of ~ 13 km² (Figure 2.1). It is within the GLSF region, characterized by deciduous, coniferous and mixed forests of uneven ages dominated by maple (*Acer*), oak (*Quercus*), birch, (*Betula*), pine (*Pinus*), cedar (*Cedrus*), hemlock (*Tsuga*) and spruce (*Picea*) genera (Cumming, 2009). The study area is in the Canadian Shield physiographic region, which has a generally thin soil layer over Precambrian bedrock and a large number of waterbodies within the drainage networks (Singer and Cheng, 2002). It is also situated on the Algonquin dome, one of the highest elevations in Ontario reaching 580 meters above sea level approximately 40 km northeast of the study area. This typically results in lower temperatures and greater precipitation than the surrounding region. Monthly average annual temperatures ranges from −19.2 °C in January to 18.8 °C in July and mean daily temperature for the year is 2°C (Environment and Climate Change Canada, 2019). Annual total precipitation is ~ 1100 mm and the region has an average of 90 frost-free days per year. The study area is leeward of Georgian Bay, which influences the regional climate and results in lake-effect precipitation (Scott and Huff, 1996; Cumming, 2009).

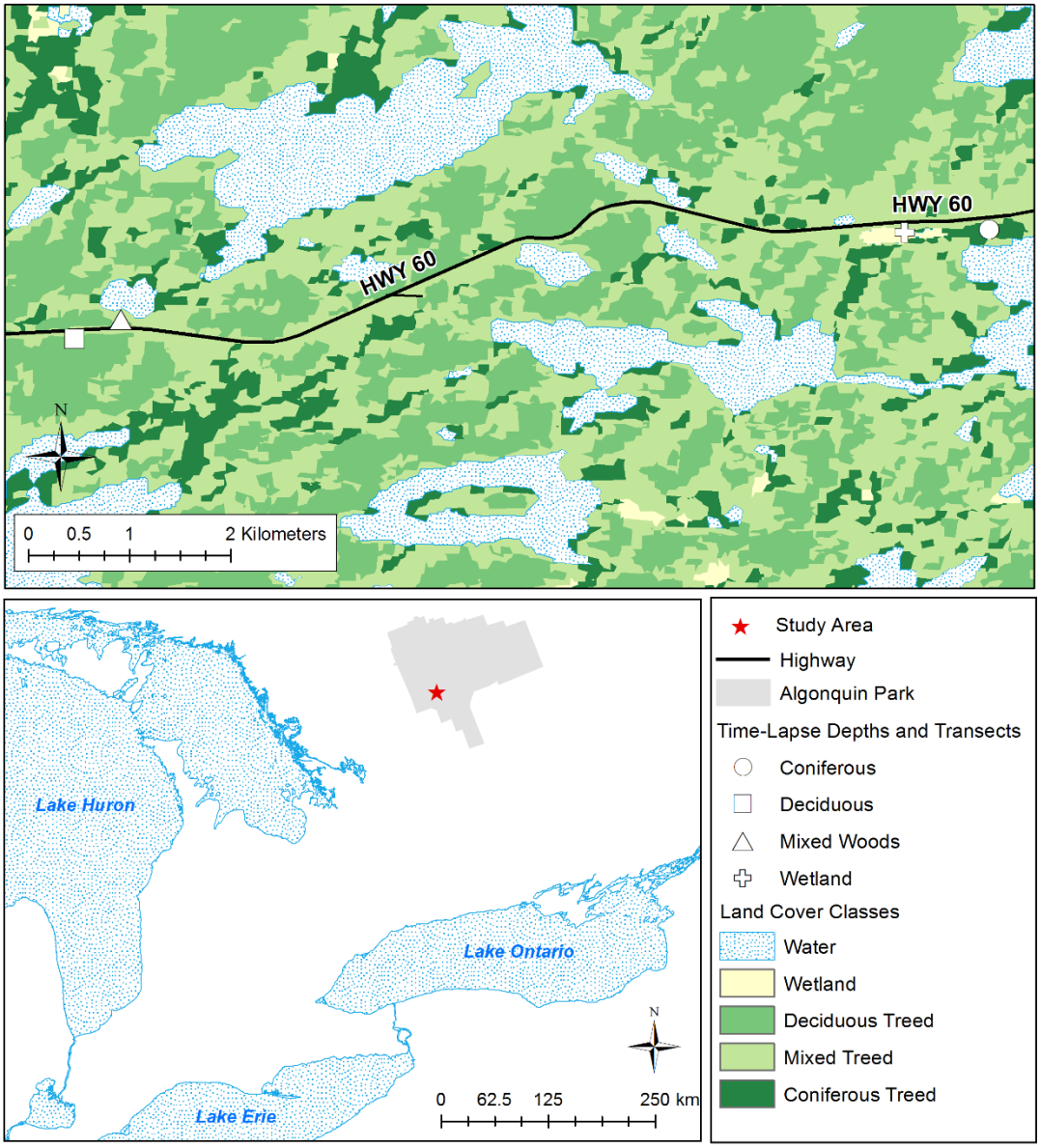

Figure 2.1: Study area with sample locations and land cover.

2.2.2 Snow data

Snow depth and density measurements were stratified across land cover type and taken in relatively flat areas to restrict the primary factors influencing snow processes to snow-vegetation interaction (Table 2.1; Figure 2.1 and Figure 2.2). Relatively homogeneous land cover classes were identified using the Ontario Land Cover Classification (OLCC), Forest Resource Inventory datasets and field scouting (Ontario

Ministry of Natural Resources and Forestry, 2007, 2014). Snow measurements were taken in four land cover types including forested (coniferous, deciduous, and mixed woods) and open (wetland) areas (Figure 2.1).

Table 2.1: Vegetative cover, elevation, and slope across land cover types.

	Vegetative Cover (%)		Elevation (m)		Slope (degrees)	
	Time-lapse	Transect†	Time-lapse	Transect†	Time-lapse	Transect†
Coniferous	70	69, (31-97)	431	431, (431 - 433)	0.6	2.0, (0.6 - 5.2)
Mixed	16	45, (8-96)	455	449, (446 - 455)	4.2	6.1, (4.1 - 9.4)
Deciduous	12	6, (2-12)	476	477, (475 - 478)	1.8	1.2, (0.4, 2.3)
Wetland	16	26, (0-55)	431	430, (429 - 430)	0.8	0.7, (0.3 - 1.2)

†mean, (min-max)

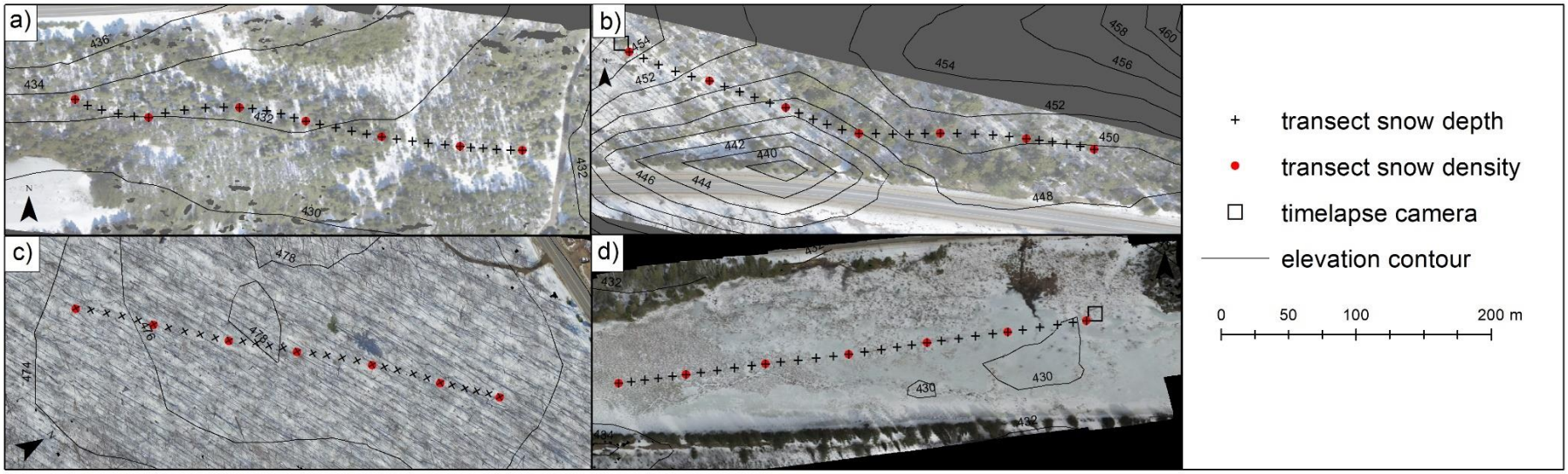

Figure 2.2: Time-lapse camera, transect measurement locations, elevation contours and orthophotos showing vegetative cover for the (a) coniferous, (b) mixed forest (c) deciduous and (d) wetland land cover type.

Measurements were taken at similar elevations and in relatively level areas to control for the effects of slope, aspect, and elevation along the transects. Low sloping areas were identified using the 30 m resolution Provincial Digital Elevation Model (PDEM) combined with field scouting (Ontario Ministry of Natural Resources and Forestry, 2018). Difference in mean elevation between land cover types was less than 45 m and the mean transect slopes were less than 6.1˚ (Table 2.1). Snow depth and density measurements were taken along one 300 m linear transect in each land cover type. A total of 31 depth measurements and seven density measurements were taken at each transect spaced approximately 10 m and 50 m apart, respectively (Figure 2.2). Snow density was measured using an ESC-30 gravimetric sampler, averaged for the transect, and used to calculate SWE at all depth points for a given date (Dickinson and Whiteley, 1972; Jost *et al.*, 2007). The relationship between measured and estimated (depth x mean density) SWE was significant at 99% for all surveys, justifying the use of this approach (Derksen *et al.*, 2005a). Surveying with a snow tube can introduce bias of up to 12% depending on snow conditions with more error observed during melt when liquid water is present (Farnes *et al.*, 1982; Goodison *et al.*, 1987). Surveying on the wetland introduced uncertainty due to the indefinite boundary between ice and snow, and saturation from underlying water. In addition, ice conditions during some surveys, were unsafe to access the wetland, preventing measurement of the entire transect. In the 2015/16 season, 10 surveys were conducted across each of the four land cover types from February 6th to April 22nd, 2016. In the 2016/17 season, a total of eight snow surveys were conducted beginning December 16th, 2016 and finishing April 13th, 2017.

Daily snow depths were measured at one point along each transect using Cuddeback model C and Moultrie 880 time-lapse (TL) game cameras and three rulers spaced approximately 2 m apart (Figure 2.2 and Figure 2.3). TL photos were used to provide automated higher temporal frequency measurements, estimate meter scale variability, and provide visual, qualitative information about snow processes (Figure 2.3). A series of hourly photos was taken each day and the earliest clear photo used to produce three daily snow depth time series at each land cover. The TL cameras performed well with less than 1% of data having gaps due to equipment malfunction or climate conditions that prevented ruler visibility. TL depth data were typically digitized within an error margin of ± 1 cm but during ablation additional uncertainty of up to ± 3 cm was introduced at some locations due to wells forming around the rulers. Average density measurements from the snow transects for each date and site were linearly interpolated and then used to calculate daily SWE within each land cover type from the TL depths (Varhola *et al.*, 2014). Snow density is a conservative variable (McCreight and Small, 2014) where simple estimates such as the climatological normal (Mizukami and Perica, 2008) or linear approximations (Bormann *et al.*, 2013) have been shown to accurately represent daily values. While attempts were made to randomly locate the TL cameras and linear transects within each land cover, bias towards more open areas that were easier to sample may have been inadvertently introduced.

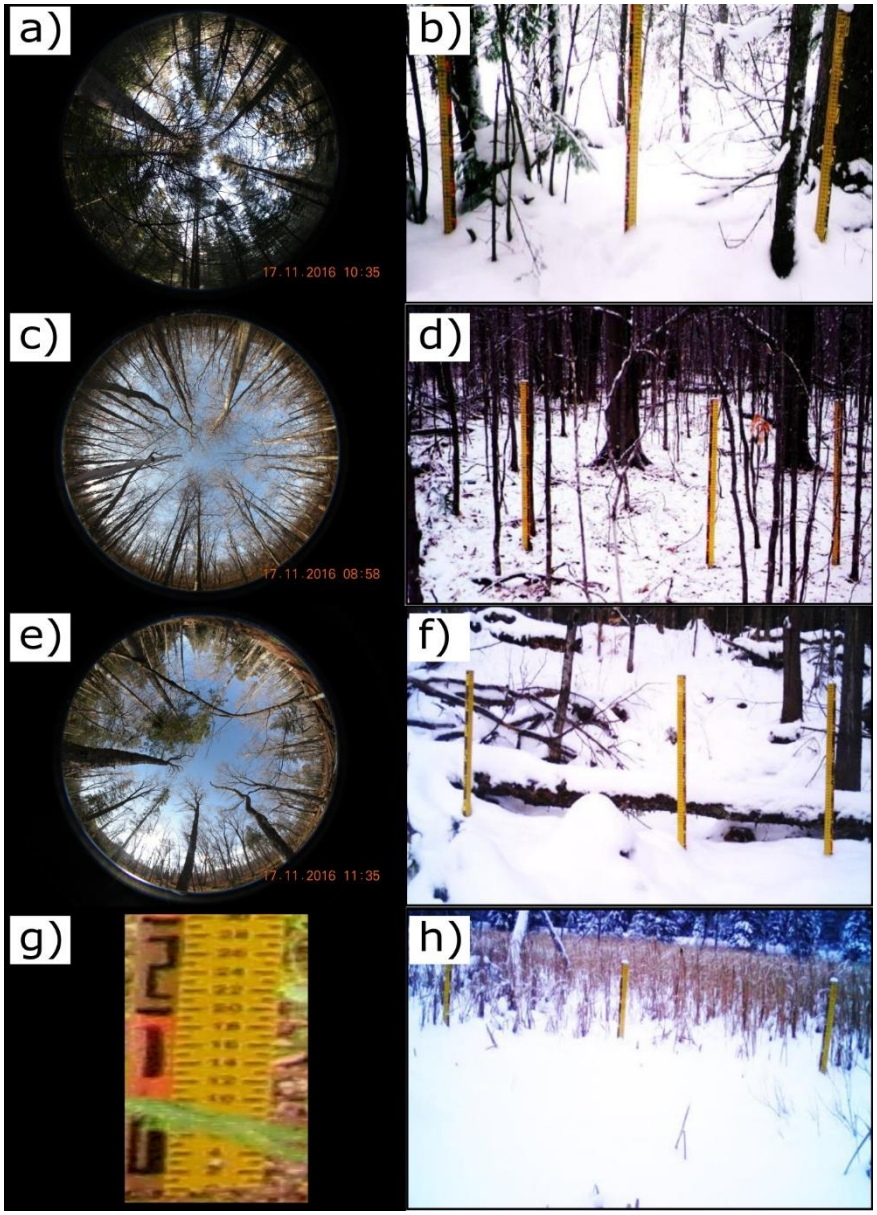

Figure 2.3: Hemispheric photo and example time-lapse photo at the coniferous site (a) and (b), the deciduous site (c) and (d) and the mixed site (e) and (f), respectively. Photo showing the base of the coniferous ruler (g) and a time-lapse photo at the wetland site (h).

2.2.3 Model data

The Globsnow SWE and the Canadian Meteorological Centre (CMC) data were selected for this study as they are generated using a combination of modelling, remote

sensing and data assimilation and have similar spatial and temporal resolution (Takala *et al.,* 2011 and Brown *et al.,* 2003, respectively). The CMC snow depth product uses optimal interpolation to assimilate Meteorological Service of Canada (MSC) synoptic snow depth observations and aviation reports with a background field of snow depth derived from the CMC Global Environmental Multiscale (GEM) forecast model (Brasnett, 1999). The CMC depth product has an error 22% smaller than the climatological normal when tested over the Northern Hemisphere (Brasnett, 1999). The product is disseminated by the National Snow and Ice Data Centre (NSIDC) in polar stereographic projection at a 24x24 km resolution (Figure 2.4; (Ross and Brasnett, 2014). Measurements were made in the southeast corner of the CMC cell (Figure 2.4). The CMC values within this cell were compared to surrounding cells and the pattern and values were similar with a mean absolute difference (MAD) of 1.2 cm across all three adjacent cells.

Globsnow combines passive microwave derived SWE with a background field of SWE generated from kriged snow depth observations and estimated densities (Pulliainen and Hallikainen, 2001; Luojus *et al.*, 2010; Takala *et al.*, 2011). SWE is derived from passive microwave signals as the spectral difference between horizontally polarized brightness temperatures of 16-18 GHz (sensitive to underlying surface) and 37 GHz (prone to volume scattering of snowpack) (Dietz *et al.*, 2012). Globsnow has a root mean square error less than 50 mm for SWE accumulations of less than 150 mm when tested at the regional scale within a similar environment to the study area (Larue *et al.*, 2017). Globsnow is disseminated by the NSIDC in EASE grid projection at 25x25 km resolution (Takala *et al.*, 2011; Figure 2.4).

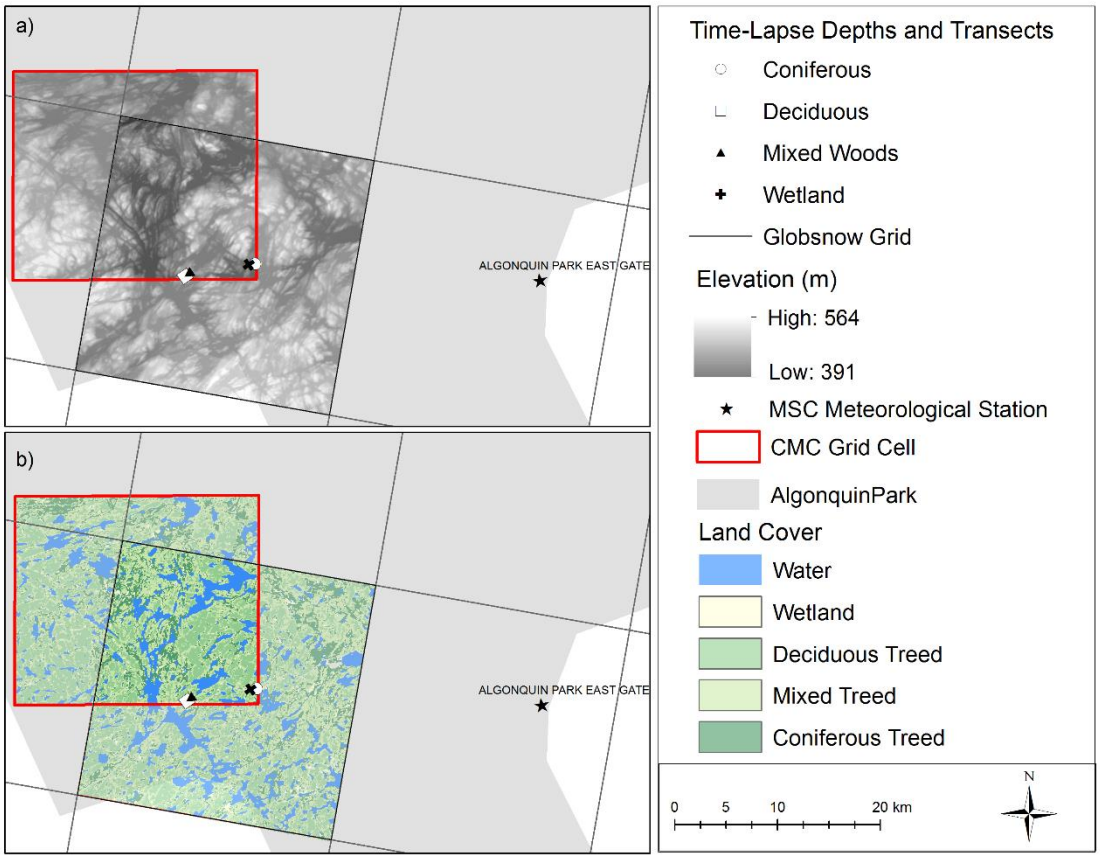

Figure 2.4: Canadian Meteorological Centre (CMC) and Globsnow grid cells, Meteorological Service of Canada climate station, study locations, grid cell elevations (a) and land cover classifications (b).

2.2.4 Measurement location and model grid attributes

A Phantom 3 Professional unmanned aerial system equipped with a 12 Megapixel camera with a 94° field of view and a 3.61 mm focal length was used to generate aerial photos over each site (Figure 2.2). Aerial photos were processed with Agisoft software to generate orthophotos. The orthophotos were used as inputs to an iso cluster unsupervised classification, which was then reclassified to create a binary vegetation/bare ground map. Fractional vegetation in an circular buffer with a 12 m radius surrounding each transect and TL measurement location was calculated (Table 2.1; Zheng *et al.*,

2018; Ullah *et al.*, 2019). Hemispheric photos at each TL location were taken to provide a view of the canopy (Figure 2.3). Locations of TL cameras and transect measurements were surveyed using a Trimble RTK and Nikon Total Station. Elevation and slope at the measurement locations and within model grid cells were derived from the PDEM (Table 2.1, Table 2.2; Ontario Ministry of Natural Resources and Forestry, 2018). Land cover percentages across the Globsnow and CMC model cells were calculated from the OLCC (Table 2.2; Ontario Ministry of Natural Resources and Forestry, 2014).

Table 2.2: Model grid elevation, slope, and land cover type for analysed gris cells.

	Land cover (%)				Elevation (m)†	Slope (degrees)†
	Coniferous	Mixed	Deciduous	Wetland/Open Water		
Globsnow	15	40	29	16	459, (391, 559)	5.4, (0 - 28.5)
Canadian Meteorological Centre	14	38	31	17	458, (398 - 564)	4.8, (3.7 - 26.3)

†mean, (min-max)

2.2.5 Analysis

The temporal scales evaluated in this study include sub-seasonal (accumulation and ablation) and winter (November 1st to May 15th, 2015/16, and 2016/17). The accumulation phase was defined as the period before peak depth or SWE and the ablation phase occurs after. Climate conditions over the two-year study period were compared to historic daily winter mean air temperature, total precipitation, and maximum snow depth using MSC East Gate Algonquin Park (WMO ID 71581) data from 2005-2018 (Figure 2.4).

Two measurement scales were defined for the purposes of evaluating process differences and bias across scale. The first is referred to as the TL scale and is defined by the mean and variability of three rulers captured by the TL photographs. The second was

defined by the mean and variability of the measurements along the 300 m transects and is referred to as the transect scale (Figure 2.2; Table 2.3). Two upscaled estimates of mean depth and SWE were calculated as a representation of aggregated grid scale mean and variability. One estimate was calculated by aggregating the TL scale means weighted by land cover percentages (Table 2.2) within the 625 km² Globsnow cell and the second by aggregating transect scale means weighted by the same land cover fractions. This method of aggregating snowpack estimates follows previous studies that demonstrated areal variations in snow cover are consistent with areal variations in landscape units driven by land cover (Steppuhn and Dyck, 1974; Adams, 1976) and has been used for estimating grid scale mean for comparison to model estimates (Derksen *et al.*, 2005a, 2005b). More robust methods of estimating regional scale snowpack have been demonstrated (Elder *et al.*, 1991) but require substantially increased work effort which limits frequency of sampling and the ability to evaluate temporal trends. Differences in land cover fractions between the CMC and Globsnow cells were negligible and produced upscaled estimates that were nearly identical. Lake and wetland classes were aggregated for calculation of land cover weights. The two model or grid scales evaluated in the study were the CMC snow depth and the Globsnow SWE products.

Process scale is frequently defined by correlation length, which represents the average distance over which a variable is correlated (Blöschl, 1999). Spatial autocorrelation is in part driven by the spatial structure of covariates that control physical processes and can be estimated by the range of an experimental variogram (Blöschl and Sivapalan, 1995). Correlation length was calculated for each transect to provide insight into the physical processes that govern snow distribution at the transect scale.

Differences in snowpack between land cover type at the TL scale were evaluated by calculating pairwise MADs in depth and SWE using TL data. Pairwise MADs in depth and SWE were calculated from transect mean values and statistically significant differences in means across land cover types for all survey dates were calculated using a Tukey Honest Significant Difference test with 95% confidence to understand the influence of vegetation on snowpack at the transect scale. A Bonferroni correction was applied to account for multiple comparisons (Tukey, 1949). Following methods outlined in previous studies (Blöschl, 1999; Molotch *et al.*, 2005; Meromy *et al.*, 2013), comparison of mean and variability across scales was made by calculating MAD, bias, mean bias (MB) and percent difference between scales. Influence of land cover on modelled product validation was assessed by calculating change in pairwise differences in MAD across land cover. Small pairwise differences suggest product validation is insensitive to the land cover class of the measurements. Variability was assessed using range and relative standard error (RSE), which normalizes variance by sample size and mean. Range is sensitive to extreme values that may skew the representation of variability but was chosen over more robust statistics such as standard deviation due to the small sample sizes at the TL scale.

Table 2.3: Scales of analysis investigated in this study.

	Scale	Support	Spacing	Extent	n
Measurement Scale	Time-lapse (TL)	12 cm*	~ 1m	~3m	3 per land cover type
	Transect	6 cm/30 cm²**	10 m/50 m***	300 m	31 per land cover type
Upscaled Estimates	Upscaled time-lapse points	6 cm/30 cm²**	~1m	625 km²	12
	Upscaled transects	6 cm/30 cm²**	10 m/50 m***	625 km²	124
Model Scale	Canadian Meteorological Centre Grid	24km	24km	576 km²	1
	Globsnow Grid	25km	25km	625 km²	1

*(width of snow ruler)
**(ESC 30 snow tube cutter diameter/ESC snow tube cutter area)
***(transect depth measurement spacing/transect snow water equivalent measurement spacing)

2.3 Results

2.3.1 Study period

There was a late start to the 2015/16 winter shown by the temperature fluctuations above 0 °C until late December and the lack of snow compared to average conditions during this period (Figure 2.5). Above normal winter mean air temperatures of −2.5°C and −2.9°C were observed in 2016 and 2017, respectively, compared to a 2005 to 2018 period of record (POR) average of −3.7°C (Table 2.2). Lowest daily minimum temperature for the POR (−31.2°C), however, was on February 14th during 2015/16 (Table 2.4). Above normal winter cumulative precipitation of 578 mm and 680 mm was observed in both seasons, respectively, compared to a POR average of 532 mm (Table 2.4). Cumulative precipitation was approximately normal in both seasons until early March when the amount increased above average (Figure 2.5). Peak snow depth in both seasons (80 cm and 71 cm, respectively) was larger than the average of peak depths over the POR (63 cm; Table 2.4). Peak depth in 2015/16 was the largest observed over the

13-year record (Figure 2.5). Dates of peak depth over the 13-year POR range from February 1st (in 2009) to March 28th (in 2014), with a mean peak date of February 28th. Peak dates observed within this study (March 5th, 2016 and February 14th, 2017) represent a late and early peak date, respectively (Figure 2.5).

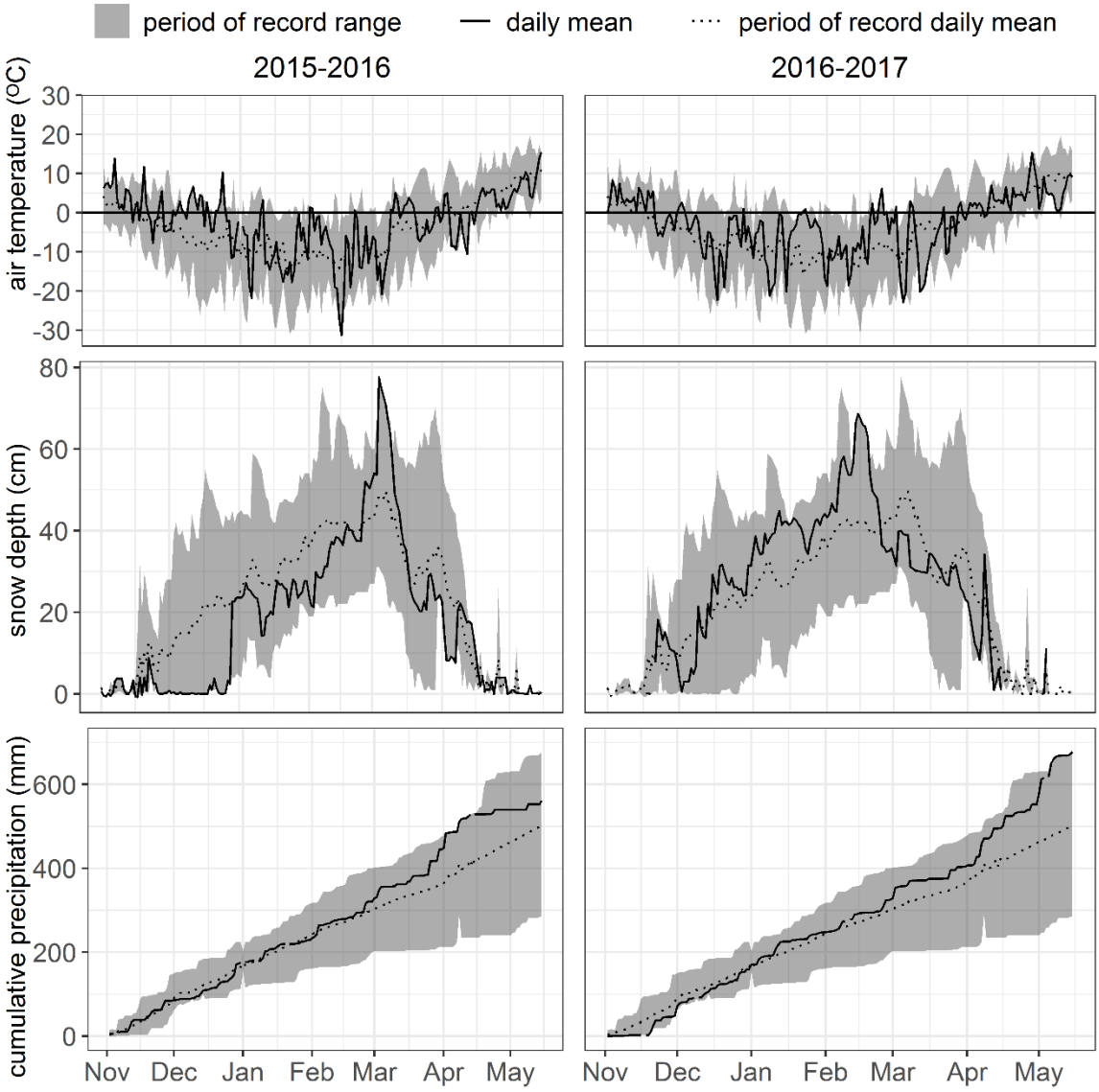

Figure 2.5: East Gate Algonquin climate station (WMO ID 71581) air temperature, snow depth and precipitation for the two study winter periods as well as the station period of record (2005 – 2018).

Table 2.4: Winter summary statistics at Meteorological Services Canada East Gate Algonquin climate station (WMO ID 71581) calculated from daily data.

	Minimum Temperature (^{O}C)	Mean Temperature (^{O}C)	Maximum Temperature (^{O}C)	Cumulative Precipitation (mm)	Peak Snow Depth (cm)
2015-2016	-31.2	-2.5	15.5	578	80
2016-2017	-22.8	-2.9	15.3	680	71
Period of Record (2005-2017) Average	-27	-3.7	16.3	532	63

2.3.2 Comparison of snow measurement and model data

2.3.2.1 Effects of land cover on snowpack across measurement scales

TL scale deciduous and mixed depth (except for 2015/16 mixed depth) and SWE values were consistently large while values in the coniferous land cover were consistently small until the last week of the season (Figure 2.6). This difference between coniferous and other forest types was not evident based on the mean transect data and calculation of significant differences (Table 2.5; Figure 2.7). Canopy cover (CC) percent at the coniferous TL land cover was substantially higher (70%) than the mixed and deciduous (16% and 12%, respectively; Table 2.1). Mean transect CC was larger at the coniferous (69%) versus other forested land covers (45% and 6% for mixed and deciduous, respectively; Table 2.1).

A difference in snowpack between the wetland and forested land covers was evident according to the transect data over both winters but not for the TL scale data during accumulation (Table 2.5; Figure 2.6 and Figure 2.7). Wetland TL scale depth and SWE tracked the coniferous cover and was closer during accumulation than ablation (Figure 2.6). This contrasts with the transect mean data (Figure 2.7) where wetland values were

substantially smaller than forested land covers over both accumulation and ablation. Tukey tests indicated that most pairwise comparisons for wetland-forest depth and SWE were significant (Table 2.5).

Calculated semi-variance was consistent across all lag distances (no correlation length) for all transects apart from the coniferous land cover with correlation lengths of approximately 50-70 m.

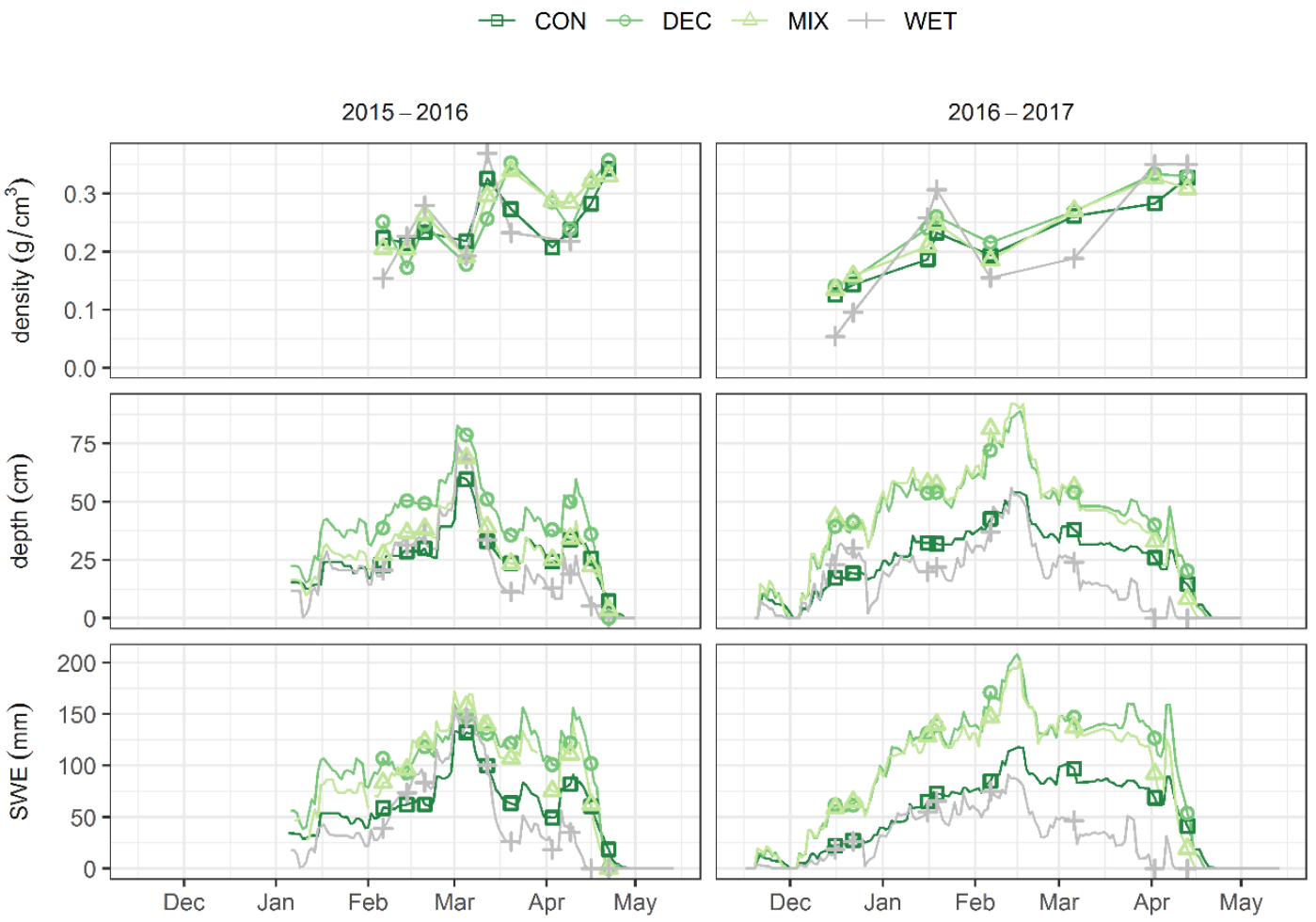

Figure 2.6: Daily snow depth, density, and snow water equivalent (SWE) within each land cover derived from daily time-lapse depth measurements and interpolated transect density measurements (DEC = deciduous, CON = coniferous, MIX = mixed woods, WET = wetland).

Table 2.5: Pairwise differences in winter depth and snow water equivalent across land cover type at the time-lapse (TL) and transect scale. Pairwise differences assessed using mean absolute difference (MAD) and the percentage of transects that had statistical differences.

	Coniferous-Deciduous		Coniferous-Mixed		Mixed-Deciduous		Wetland-Deciduous		Wetland-Mixed		Wetland-Coniferous	
Depth	2015/16	2016/17	2015/16	2016/17	2015/16	2016/17	2015/16	2016/17	2015/16	2016/17	2015/16	2016/17
TL points MAD (cm)	14.6	14.8	4.4	15.2	10.8	2.8	17.9	21.8	7.3	21.7	7.2	8.8
Transects MAD (cm)	9.5	4.8	8.7	4.1	4.3	2.0	31.7	33.5	29.0	32.0	31.7	32.4
% of transects with Significantly Different Means	60%	25%	50%	0%	0%	0%	90%	88%	90%	88%	100%	88%
	Coniferous-Deciduous		Coniferous-Mixed		Mixed-Deciduous		Wetland-Deciduous		Wetland-Mixed		Wetland-Coniferous	
Snow Water Equivalent	2015/16	2016/17	2015/16	2016/17	2015/16	2016/17	2015/16	2016/17	2015/16	2016/17	2015/16	2016/17
TL points MAD (mm)	39.4	38.4	31.7	34.7	16.9	15.6	52.0	59.9	41.7	54.9	23.5	22.6
Transects MAD (mm)	19.9	19.1	11.2	11.1	10.8	9.4	78.1	86.0	77.1	76.6	76.6	74.9
% of Surveys with Significantly Different Means	30%	63%	20%	0%	20%	10%	70%	88%	80%	75%	70%	75%

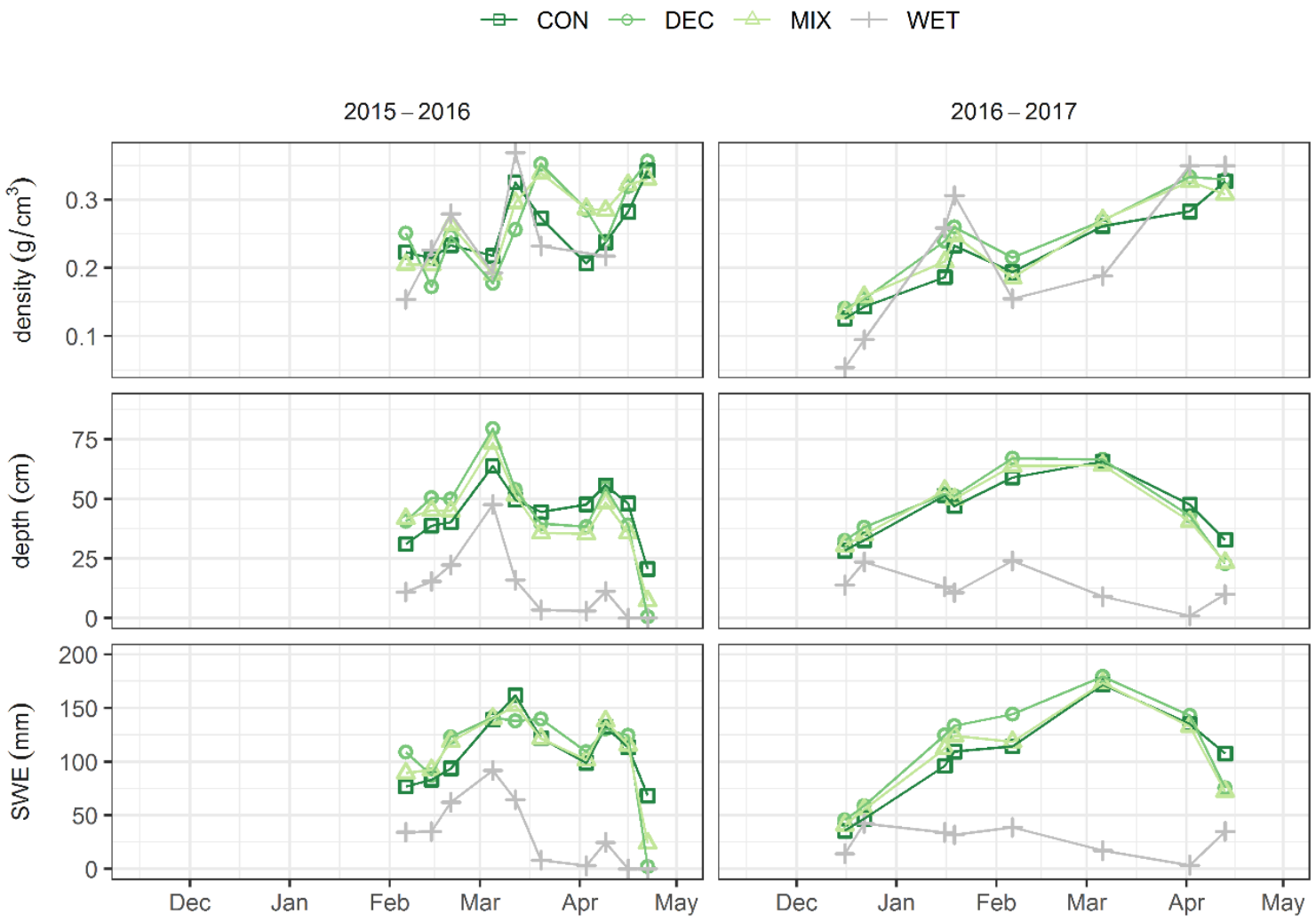

Figure 2.7: Mean snow density, depth, and snow water equivalent (SWE) across land cover types derived from transect measurements (DEC = deciduous, CON = coniferous, MIX = mixed woods, WET = wetland).

2.3.2.2 Bias across measurement scale

Coniferous TL scale mean depth and SWE values were negatively biased relative to coniferous transect medians over both years (Figure 2.8). Mean deciduous TL scale depth and SWE were mostly neutral or slightly negatively biased relative to the deciduous transect median in 2015/16 but in 2016/17 were positively biased during accumulation and negatively biased during ablation. The patterns of TL bias relative to the transect median in the mixed land cover were similar to the deciduous land cover. Wetland TL values had mostly positive bias relative to the transect median (Figure 2.8). The average percent difference between TL and transect scale means across all land cover types and both years was 42% for depth and 48% for SWE but was observed to be as large as 367% for depth and 936% for SWE during ablation.

Most mean TL scale values fell within the range of transect measurements. Mean TL scale values falling outside the lower and upper range were located at a cumulative frequency of 0 or 100, respectively (Figure 2.8). Land cover types that showed more than two TL scale mean values outside the transect range included the wetland depth and SWE values in 2015/16 (five values) and the coniferous depth and SWE values from 2016/17 (four values). TL scale values largely fell outside of the transect range during ablation.

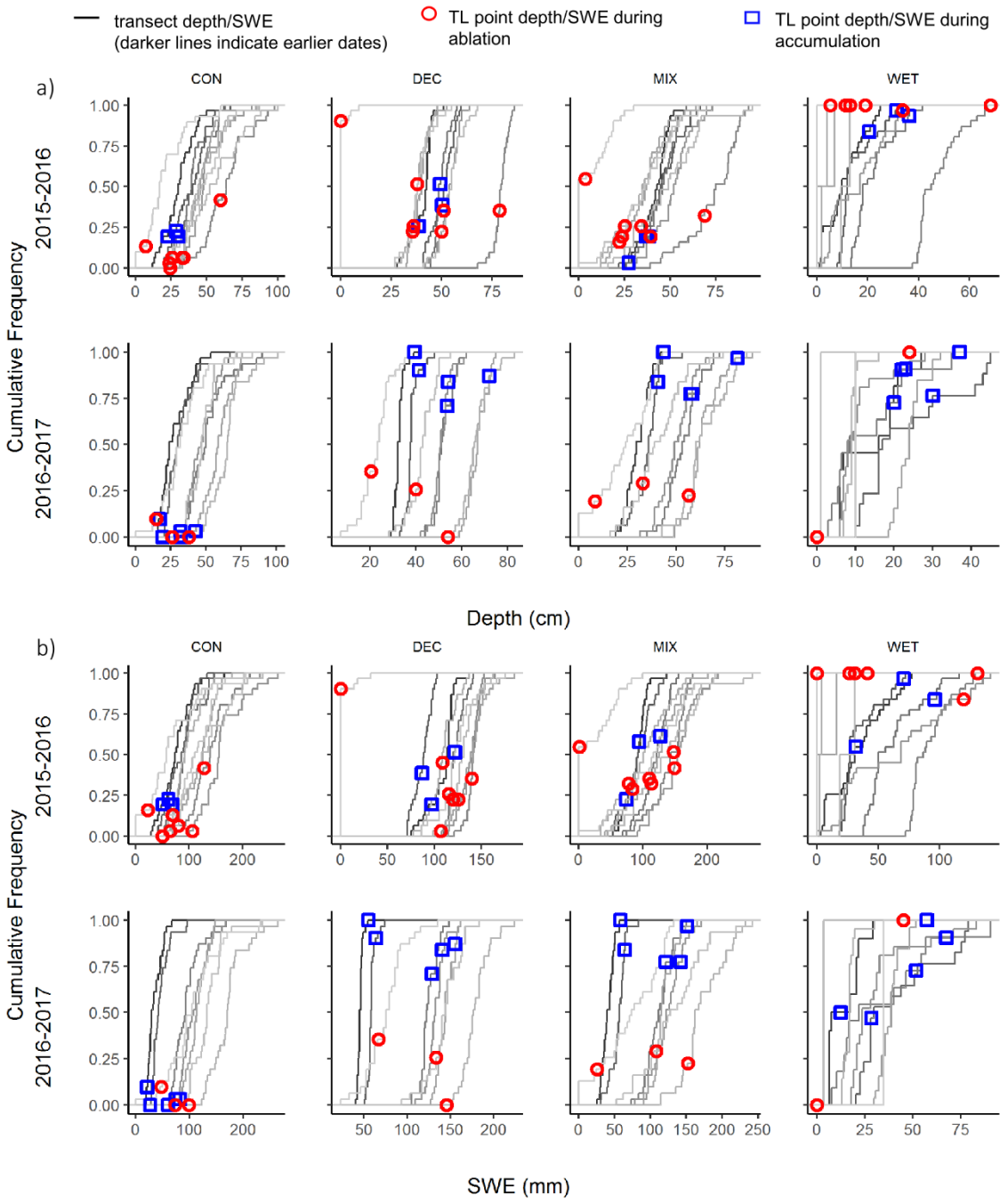

Figure 2.8: Frequency distribution of transect snow depth a) and snow water equivalent (SWE) measurements b). Mean depth and SWE derived from embedded time-lapse (TL) points within each transect plotted for each survey date (DEC = deciduous, CON = coniferous, MIX = mixed forest, WET = wetland. Shading of the lines represents the

snow survey date. Darker lines indicate snow surveys were taken earlier in the snow year and lighter lines indicate snow surveys were taken later in the snow year.

2.3.2.3 Bias across upscaled areal estimates and comparison of variability

The upscaled estimate from aggregating TL means across land cover types closely followed the patterns of the depth and SWE estimate from upscaling transects, with a MAD of 2.4 cm depth/7.3 mm SWE and 0.6 cm depth/10.0 mm SWE across 2015/16 and 2016/17, respectively (Figure 2.9). Bias between upscaled estimates for both depth and SWE was typically smaller and positive during accumulation (MB of 2.7 cm depth/5.8 mm SWE averaged over both years) and larger and negative during ablation (MB of -5.1 cm depth/-20.5 mm SWE).

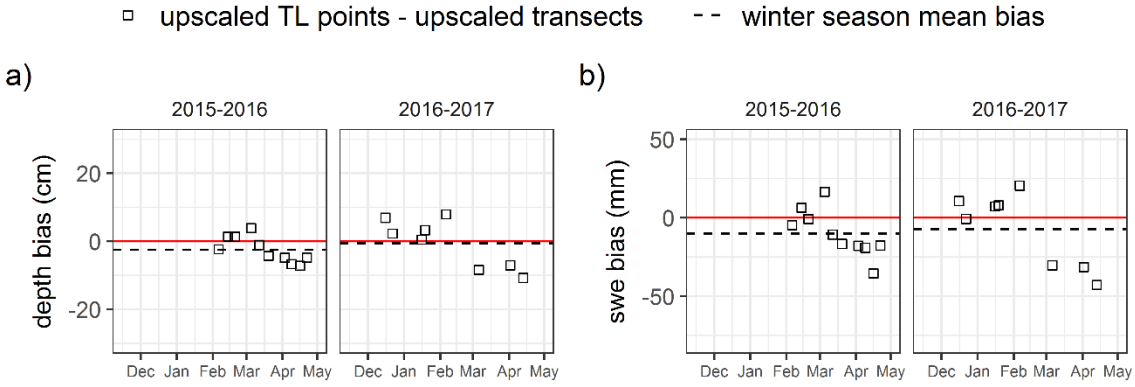

Figure 2.9: Difference between upscaled time-lapse (TL) points and upscaled transect measurements for snow depth (a) and snow water equivalent (SWE) (b).

The range of values across scales for each land cover type is shown in Figure 2.10. Areal estimate values were the same for each land cover type and are presented to illustrate relative values and patterns. The smallest range was seen between the TL points, but the ranges vary across land cover at this scale. The largest TL points range was observed in the mixed land cover (Figure 2.10). Transect ranges were smallest in

the deciduous and wetland land covers and were highest in the mixed and coniferous land covers (Figure 2.10). Transect ranges were smaller across all forested transects during accumulation than during ablation (Figure 2.10). Ranges in upscaled estimates mimicked the temporal trends of the TL points and transect ranges but were larger. RSE was low and consistent across all land cover types and scales but increased significantly at the beginning of accumulation and late in ablation.

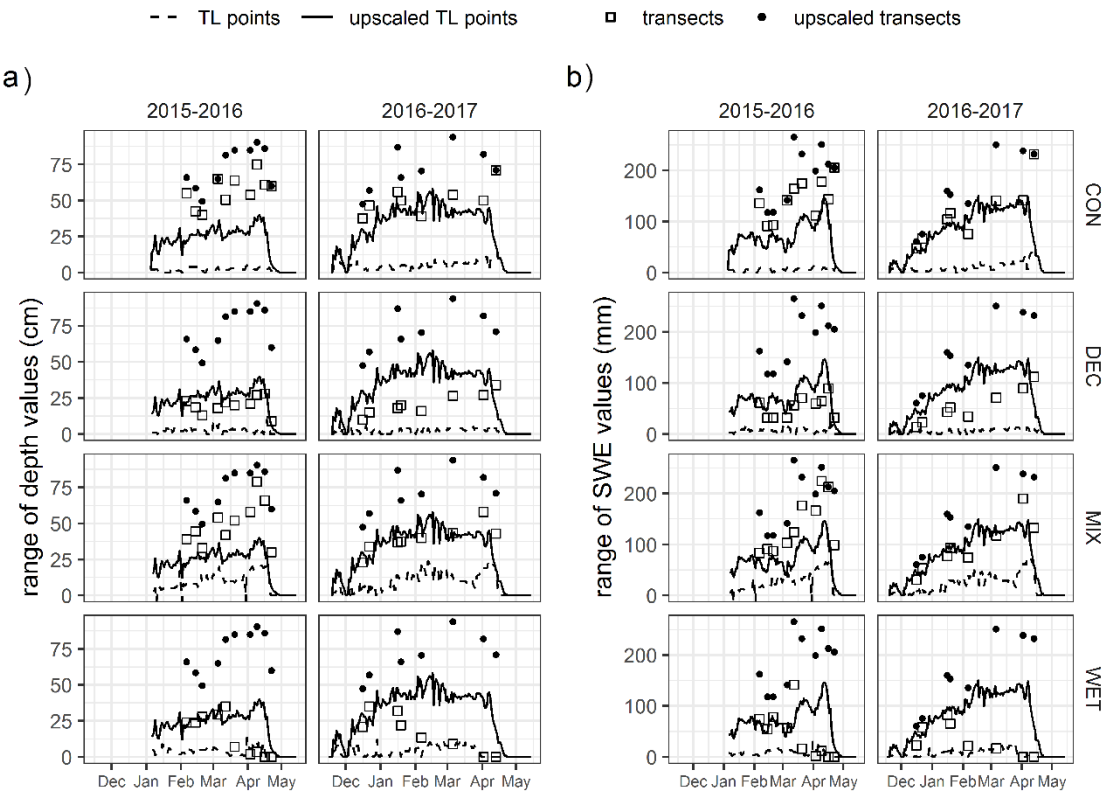

Figure 2.10: Range of snow depth (a) and range of snow water equivalent (SWE) values (b) across the time-lapse (TL) point scale, transect scale, upscaled TL points scale and the upscaled transects scale (DEC = deciduous, CON = coniferous, MIX = mixed woods, WET = wetland.

2.3.2.4 Comparison of multiscale means to gridded products

CMC grid cell land cover is predominantly mixed and deciduous with smaller amounts of coniferous and open water/wetland (Table 2.2; Figure 2.4). The cell has a range of elevations from 391 m to 559 m with a mean of 459 m (Table 2.2; Figure 2.4). Mean slope within the cell is 5.4 ° but ranges from 0 to 28.5° (Table 2.2). The sign of the CMC bias from TL scale measurements changed from accumulation to ablation in the coniferous land cover, was mostly negative at the mixed and deciduous land covers and mostly positive in the wetland (Figure 2.11a). The largest average winter CMC bias from the TL scale was at the wetland land cover with a positive MAD averaged over both years of 12.9 cm. CMC bias from transect measurements for forested land covers was consistently closer to measured depth during accumulation versus ablation, while bias remained consistently positive at the wetland land cover at this scale (Figure 2.11 a).

Globsnow grid cell land cover, slope and elevation are similar to the CMC attributes (Table 2.2). Globsnow bias in forested land covers from both the TL and transect measurements was mostly neutral or slightly negative during accumulation and negative during ablation. Bias magnitude was smaller during accumulation than ablation from both TL and transect measurements over both years (Figure 2.11b). Globsnow had mostly positive bias relative to the wetland TL and transect measurements (Figure 2.11 b).

Differences in pairwise mean winter MAD between scales indicated that bias was substantially larger when comparing products to TL points versus transect measurements

(Table 2.6 and Table 2.7). Maximum pairwise difference across forested land covers at the TL points scale was 14.7 cm depth/39.9 mm SWE (Table 2.6 and Figure 2.7). Forested pairwise differences at the transect scale were less than 2.7 cm depth/11.1 mm SWE. Pairwise differences between wetland-forest were as large as 37.0 cm depth/96.8 mm SWE (Table 2.6 and Figure 2.7).

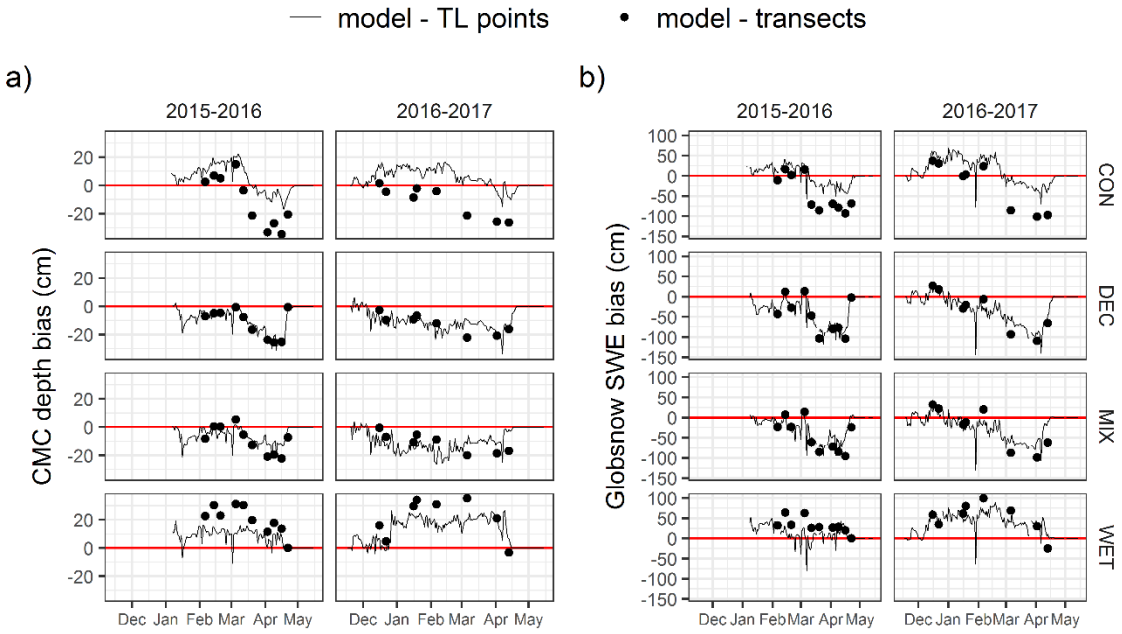

Figure 2.11: Canadian Meteorological Centre (CMC) snow depth (a) and Globsnow snow water equivalent (SWE) (b) bias from time-lapse (TL) scale and transect scale across land cover types (DEC = deciduous, CON = coniferous, MIX = mixed woods, WET = wetland).

All subsequent summary statistics presented in this section are an average over both study years. CMC depths were similar to upscaled estimates over the course of both years with a MAD of 4.4 cm and 7.9 cm for upscaled TL and transect measurements, respectively (Figure 2.12 a). There was smaller TL scale bias from CMC depth during accumulation (MB of −2.5 cm) than ablation (MB of −5.1 cm; Figure 2.12 a). There

were similar trends at the transect scale with MBs of −0.1 cm and −10.1 cm for accumulation and ablation, respectively. Globsnow bias from upscaled TL estimates during accumulation (MAD 11.9 mm, MB 1.8 mm) was smaller than ablation (MAD 28.9 mm, MB −25.1 mm; Figure 2.12 b). A similar pattern in bias was observed from upscaled transect estimates with MAD of 24.9 mm and MB of −0.9 mm during accumulation, and MAD of 62.1 mm and MB of −62.1 mm during ablation (Figure 2.12 b).

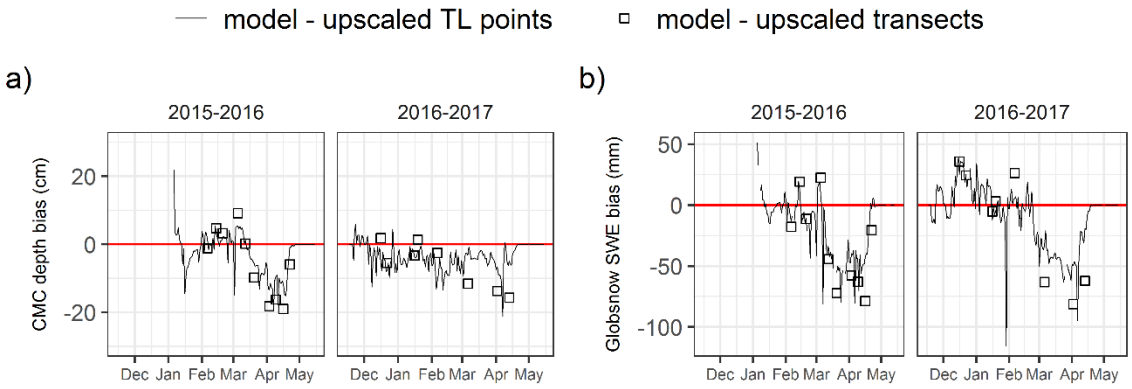

Figure 2.12: Canadian Meteorological Centre (CMC) snow depth a) and Globsnow snow water equivalent (SWE) (b) bias from upscaled time-lapse (TL) points scale and the upscaled transects scale.

Table 2.6: Pairwise differences in error across land cover between measured mean snow depth (at the time-lapse (TL) and transect scale) and modelled Canadian Meteorological Centre depth.

	Coniferous-Deciduous		Coniferous-Mixed		Mixed-Deciduous		Wetland-Deciduous		Wetland-Mixed		Wetland-Coniferous	
	2015/16	2016/17	2015/16	2016/17	2015/16	2016/17	2015/16	2016/17	2015/16	2016/17	2015/16	2016/17
Difference in error at TL point scale (cm)	14.7	14.6	11.6	14.6	3.2	0.0	19.2	24.2	16.0	24.3	4.4	9.7
Difference in error at transect scale (cm)	0.6	1.1	2.1	0.4	2.7	1.5	33.9	37.0	31.2	35.4	33.3	35.9

Table 2.7: Pairwise differences in error across land cover between measured mean snow water equivalent (at the time-lapse (TL) and transect scale) and modelled Globsnow snow water equivalent.

	Coniferous-Deciduous		Coniferous-Mixed		Mixed-Deciduous		Wetland-Deciduous		Wetland-Mixed		Wetland-Coniferous	
	2015/16	2016/17	2015/16	2016/17	2015/16	2016/17	2015/16	2016/17	2015/16	2016/17	2015/16	2016/17
Difference in error at TL point scale (mm)	38.9	39.9	30.6	33.1	8.2	6.8	53.9	69.9	45.7	63.0	15.1	29.9
Difference in error at transect scale (mm)	1.5	11.1	0.5	1.7	1.0	9.4	81.7	96.8	80.6	87.4	80.2	85.8

2.4 Discussion

2.4.1 Theoretical process representation of estimates across scale

Factors affecting the spatial variability of snowpack are hierarchically scale dependent (Blöschl, 1999; Clark *et al.*, 2011). In non-mountainous forested landscapes, topography and land cover are the physical characteristics that drive basin scale variability of SWE (Jiusto and Kaplan, 1972; Anderton *et al.*, 2004; Clark *et al.*, 2011). At the forest stand scale, vegetation structure plays the largest role along with slope and aspect (Metcalfe and Buttle, 1998; Jost *et al.*, 2007; Varhola *et al.*, 2010b). At the point scale, vegetation, micro-topography, and ground surface features such as boulders, branches, tree boles and ponded water are the physical factors that affect snow depth and SWE variability (López-Moreno *et al.*, 2011). Climate variability interacts with the physical factors described above to influence snow distribution across all scales (Rice and Bales, 2010; Sturm, 2015; Peters-Lidard *et al.*, 2017).

The single point measurements made by the rulers and snow corer captured processes that occurred at the scale of the support (area covered by the single measurement). Given that measurements within this study were stratified across land cover type and situated within areas of relatively homogeneous topography (Table 2.1; Figure 2.2), it is assumed that the physical factors affecting snow processes operating at the scale of the measurement support were primarily limited to vegetation, with micro-topography and ground surface features also playing a role. At the TL scale, mean and variability represent the integrated effect of stated support scale processes across the three ruler measurements.

The transect scale integrates processes observed at the support scale over a length defined by the extent (300 m) and may capture additional variability depending on the length and extent of the physical processes operating across the transect. Few observations (large spacing) over a long distance (large extent) may not capture fine scale processes along a transect but may capture spatial structure resulting from larger scale variability and processes. Conversely, measurements taken at a high spatial frequency (small spacing) across a shorter distance (small extent) may represent fine scale processes, but will not capture coarser scale variability and correlation lengths (Blöschl, 1999). The lack of correlation length identified by a semi-variogram range of 0 m along most of the transects within this study indicates that the sample design did not capture spatial structure (e.g., a change in slope or elevation along the transect) at a spacing greater than 10 m along the 300 m extent. The lack of correlation length also indicates that the transect measurements did not capture the spatial structure that would be introduced by fine scale effects such as the spatial autocorrelation introduced by individual tree crowns. Given the lack of observed correlation lengths, the statistical moments at the transect scale represent the integrated effect of support scale processes across the transect.

Upscaled mean and variability calculated by aggregating site and stand scale measurements represent the integrated effect of support scale processes across all sites and land cover types and all transects and land cover types, respectively, and may introduce additional variability due to differences in physiography between sites. Variability introduced by factors other than land cover (e.g., slope, aspect, elevation, and spatial variability in climate) that influence snowpack across the upscaled area was not

accounted for in these aggregates, resulting in potential deviation from the true statistical moments and processes within the grid element. The modelled products, in theory, integrate many processes that control variability across scales through modelling (CMC) or through remote sensing (Globsnow). This variability is integrated into a single value with a support defined by the grid element size.

2.4.2 Effects of land cover on snowpack across scales

According to the TL data, the greatest depth and SWE accumulation was in forested land cover types with less CC (deciduous and mixed). The smallest snowpack was in the coniferous land cover (larger CC) until the final week of ablation when the snowpack in the more open sites decreased below sites with denser canopy. This is consistent with literature where less snow is observed under denser canopies because of canopy interception and sublimation during accumulation, while snowpack remains under forests with larger canopy density during ablation due to reduced melt rates (Essery *et al.*, 2003; Ellis *et al.*, 2013). Within dense forest canopies, reduced melt rates are typically seen due to reduced solar radiation from canopy shading, combined with reduced wind and sensible heat flux from forest sheltering (Hedstrom and Pomeroy, 1998; Pomeroy *et al.*, 1998; Ellis *et al.*, 2013). While not observed in this study, previous research has shown that under conditions of high air temperature, high snow albedo and low wind speed, longwave radiation from dense vegetation can produce faster melt than a sparser vegetation emitting less longwave radiation (Yamazaki and Kondo, 1992; Metcalfe and Buttle, 1998)

Observed differences in snowpack between coniferous and other forested sites were less evident from the transect data where some differences were detected in 2015/16 but

most forest-forest comparisons for depth and SWE were insignificant. Variability in significant differences over time at the transect scale highlight the temporal variability of forest-snow interactions and the need for sub-seasonal sampling in order to obtain an accurate depiction of process at this scale. A larger mean CC was observed in the coniferous transects versus mixed and deciduous; however, the coniferous CC had a large range, including CC values that were smaller than some observed in the mixed transect (Table 2.1; Figure 2.2) The similarity in mean snowpack across all forested transects may reflect the complex and non-linear accumulated effect of CC on snow processes across transect measurements (Varhola *et al.*, 2010b) and/or the inability of CC to represent forest cover and capture snow-vegetation interactions adequately at this scale (Varhola *et al.*, 2010a). In depth investigation of forest metrics that control snow process in this study area are out of scope of this paper.

Wetland transects had consistently smaller snow depth and SWE than forested sites during both accumulation and ablation. During accumulation on the wetland, field observations and assessment of TL photos suggest the snowpack was incorporated into the ice due to freeze-thaw cycles and periodic flooding from ice cracking which led to a reduction of measurable snowpack. During ablation, snowpack rapidly decreased at the wetland versus forested sites, likely due to a lack of solar shading, melting of underlying ice and energy advection from exposed vegetation and open water. These observations are consistent with literature on snow processes over ice cover (Gray and Male, 1981). The TL data, however, suggest that the wetland data were closer to the coniferous stand during accumulation, but not ablation. Based on field observations and qualitative analysis of TL photos, the difference between the transect and TL wetland snowpack

may be due to differences in vegetation cover which affected snow retention across the wetland. The TL measurements were located in a vegetated area while several transect measurements were devoid of vegetation (Table 2.1; Figure 2.2).

2.4.3 Bias across measurement scale

Consistency in the difference between TL and transect scale values was observed when viewed within land cover type, year and during the accumulation and ablation phases (Figure 2.8). This implies that daily TL scale mean values could be bias corrected using a limited number of appropriately stratified transects to get a better representation of transect scale mean. Neumann et al. (2006) compared point scale depth and SWE measurements to transects over three years in a boreal forest during snow accumulation and found consistent bias that could be adjusted using scaling equations based on linear regression of means across scales. The findings of this study are consistent with Neumann et al. (2006) but also highlight that point to transect bias can vary between accumulation and ablation. These finding are of particular importance for this remote study region where obtaining frequent manual observations is a challenge.

While there was consistency of bias through time and across land cover type, some interannual differences in bias were observed (e.g., mixed, and deciduous in 2015/16 versus. 2016/17). Sturm and Wagner (2010) discuss fixed controls on snow processes (e.g., vegetation) that are relatively static versus dynamic controls (e.g., temperature, precipitation, etc.) that change more rapidly. They suggest that patterns in snow distribution through time are more consistent when fixed controls dominate (Sturm and Wagner, 2010). A deeper understanding of the factors that affect snow processes at a given location (e.g. forest structure) could help inform the temporal consistency (such as

interannual variability) of differences across scales and improve estimates of scaling coefficients (Varhola *et al.,* 2010a, 2014).

There were substantial differences between TL and transect depth and SWE with greater bias typically during ablation (Figure 2.8). Previous studies have also found that fine scale measurements are not necessarily representative of the surrounding area (Molotch *et al.,* 2005; Neumann *et al.,* 2006; Rice and Bales, 2010; López-Moreno *et al.*, 2011; Meromy *et al.*, 2013). Meromy et al. (2013) developed a binary regression tree model for estimating depth and SWE in a montane environment for 1, 4 and 16 km² grids. Approximately half of their sites had a percent bias greater than 10% during both accumulation and ablation and most point measurements deviated by more than 10% from the median spatially distributed value. These findings are comparable to the results of this study where the average percent bias across all land covers was ~ 40% for both depth and SWE. Using a similar method to Meromy et al. (2013), Molotch and Bales, (2005) also found point data were not representative of coarser scale SWE with observed differences as large as 200%. In our study, percent differences as large as 936% for SWE were observed, the result of conducting snow surveys during late melt when snowpack was low and relative differences were highly inflated. Magnitude of bias has been found to be greater during ablation across all scales, attributed to the introduction of additional variability due to melt processes (Molotch and Bales, 2005; Rice and Bales, 2010; Meromy *et al.*, 2013). Meromy et al. (2013) also found less bias across scales in sites that had smaller SWE variability and more uniform distributions. A smaller bias was observed across the deciduous transects that had smaller variability within this study.

These observations highlight the importance of understanding the impact of seasonality and data distributions on potential bias in snowpack across measurement scales.

Differences between TL and transect snowpack did not correspond to differences between TL and mean transect vegetative fraction. A wide range of vegetative fraction values were present across most transects. Investigation of snow-vegetation processes beyond the scope of this paper is required to decipher physiographic controls and the appropriate metrics to represent these processes (Varhola *et al.*, 2010b).

2.4.4 Bias across upscaled areal estimates and comparison of variability

Depth and SWE calculated by upscaling TL measurements were consistent with upscaled transects, although bias was greater during ablation. These results suggest that it may be appropriate to upscale point measurements instead of transects in remote basins (such as this study region) when resources are not available to obtain transect measurements. Rice and Bales (2010) used a binary regression tree model to distribute depth across a 1km² grid and then compared the model to 10-point measurements distributed across an embedded 0.4 ha area. They found that a single point measurement was not representative of the survey data but four or more point measurements substantially improved accuracy and estimated the mean within $\pm$ 25% (Rice and Bales, 2010). Other research has also found that approximately four measurements can substantially improve accuracy of estimating grid scale mean, with more than four measurements showing only marginal improvements in accuracy (Lundquist and Lott, 2010).

An understanding of range and how it differs over measurement scales is important as it can be used to understand and parameterize sub grid variability within models (Cline

et al., 1998; Blöschl, 1999). At the TL scale, the range in the mixed forest was substantially larger than for other land cover types. This might be attributed to the large degree of variability in forest floor structure at this site where downed trees and boulders were present (Figure 2.3; López-Moreno *et al.*, 2013). Within the transects, the largest ranges were seen in the coniferous and mixed forests. Stands with denser forest cover have been found to demonstrate larger variability in snowpack at the forest stand scale (Pomeroy *et al*., 1998). However, other studies have found little correlation between forest cover (defined by Leaf Area Index) and snowpack variability defined by the coefficient of variation and standard deviation (Pomeroy *et al.*, 2002).

Relatively small range was observed in the wetland transects, with larger range during accumulation when snowpack was present versus the ablation phase when little to no snowpack existed. The range of depth and SWE increased during the season and was larger during ablation than accumulation at all forested transects with the increases being more pronounced in the mixed and coniferous land covers. Larger differences in mean values and larger spatial variability exist as the season progresses and during ablation due to redistribution and the introduction of melt processes (Rice and Bales, 2010).

Range increased across scale and throughout the season with the smallest values at the TL scale (n = 3) and the largest within upscaled transects (n = 120). A consistently small RSE over most of the winter indicates that patterns in range were dependent on sample size and magnitude of depth/SWE. Substantial increases in RSE at the beginning and end of the winter were due to patchy snowpack with high spatial variability.

2.4.5 Comparison of multiscale means to gridded products

Bias between snow products and measurements will result from error in the model estimate and measurement data. Deviation of validation data from the true grid mean may contribute to bias from products, which may lead to misrepresentation of product accuracy. Comparisons of CMC depth and Globsnow SWE to *in situ* measurements indicated that the bias varied over land cover, measurement scale and time. Transect measurements in forested land cover types had similar bias for both depth and SWE (averaged over the winter) indicating that (for this grid cell) bias was independent of forested land cover type. Differences between accumulation and ablation were observed, indicating that forest cover type introduced bias at sub-seasonal timescales. This highlights the importance of validating products over both accumulation and ablation phases. There were large differences between forest-wetland bias at both scales due to the grid cell being predominantly forest covered. This highlights the importance of collecting validation data that are representative of grid cell physiography and heterogeneity. Large differences in TL scale bias across all land cover were introduced. TL scale measurements do not capture heterogeneity of the surrounding area and have a larger chance of differing from the grid mean. Spatial representativeness of *in-situ* measurements (during accumulation and ablation) and the processes those measurements represent should be considered when validating gridded snow products (Molotch and Bales, 2005; Neumann *et al.*, 2006; Meromy *et al.*, 2013; Mudryk *et al.*, 2015).

Despite the wide range in physiographic characteristics within the grid cells compared to the measurement locations, modelled depth averaged over either

accumulation, ablation or the winter season was within 10 cm of upscaled estimates. Modelled SWE was within 30 mm when averaged over accumulation or the winter season but Globsnow underestimated SWE by over 60 mm during ablation. These results indicate that a simple stratified sample within a grid cell can produce results comparable to model grid values, but that larger deviations may exist during ablation. The Globsnow estimate may integrate snowmelt variability into the grid cell mean value better than the aggregated measurements. For example, upscaled estimates do not account for variability due to slope and aspect, which could substantially increase melt rate, resulting in smaller SWE recorded by Globsnow during ablation (Anderson *et al.*, 1959; Murray and Buttle, 2003; Varhola *et al.*, 2010a). Alternatively, the Globsnow estimate may have been less than the true mean during melt. This is consistent with previous literature that has found that product estimates that assimilate point depths (such as Globsnow) typically underestimate depth and SWE, due to assimilation of point measurements in exposed areas (such as airports) that ablate more rapidly than the heterogeneous landscape (including forest cover) that the grid cell represents (Neumann *et al.*, 2006; Grünewald *et al.*, 2015; Brown *et al.*, 2018). Passive microwave SWE estimates have known error when liquid water is present in the snow pack (Dietz *et al.*, 2012). As a result, Globsnow heavily relies on assimilated snow depths during melt (Luojus *et al.*, 2010). Meromy et al. (2013) compared the National Operational Hydrologic Remote Sensing Centre gridded snow model to observed data across multiple scales and found that, in some cases, measurements were less accurate than the modelled values. They suggest either scaling assimilated measurements or omitting assimilation from the snow model under certain circumstances (Meromy *et al.*, 2013). This analysis

highlights important considerations when validating and applying modelled and remotely sensed snow products and assimilating data collected across different scales into these products.

2.5 Conclusion

Scaling issues in snow hydrology persist due to limitations in instrumentation and the inherent gap between sampled and true pattern and process across scales. The purpose of this study was to improve understanding of scaling issues in snow hydrology by assessing the difference in representation of snow processes and estimates of mean and variability across scales. Observed differences in snowpack between forested land cover types at the TL scale were attributed to differences in CC across the sites. Differences in forest snowpack across the transect scale were less evident while differences in mean transect CC were observed. This was attributed to the non-linear aggregation of complex snow processes across the transect and/or limitations in the study methodology. Semivariogram analysis indicated that no spatial structure was evident along the length of the transects. Differences in snowpack at the TL scale versus the transects within land cover types were observed but did not correspond with differences in TL and mean transect vegetative cover. This indicated that mean vegetative cover is not an effective metric for representing aggregate snow-vegetation processes over a transect and that more detailed analysis beyond the scope of this paper is required.

This study confirmed previous findings that point scale mean is not representative of the surrounding area, but bias can be consistent within homogeneous landscape units and time-periods. This study suggested that point scale mean snowpack from a Great Lakes-St. Lawrence environment could be bias corrected by scaling factors derived from

a limited number of transect measurements and also highlighted the influence of seasonality on bias. Consistency between upscaled estimates of depth and SWE using TL measurements and transect measurements suggested that four appropriately stratified point scale measurements may be a suitable replacement for transect scale mean when it is not possible to collect transect data. Differences in variability across scale was assessed and attributed to differences in microtopography, vegetative cover and sample size.

Comparison of modelled products (CMC depth and Globsnow SWE) to *in-situ* data indicated that bias depends on land cover type and measurement scale, and that the difference across land cover can vary by accumulation, ablation and across winters. These findings highlighted the importance of understanding the scale and processes that ground truth measurements and model estimates represent. Product snowpack compared well to both upscaled estimates with the exception of the Globsnow SWE during ablation. This may have been due to the better integration of the factors that affect SWE variability by the Globsnow product, or more likely was the result of assimilating data that were not representative of the grid scale mean due to the limitations of Globsnow during melt.

This study has improved understanding of the influence of scale on snow process and pattern. Rapidly improving technology that permits the deployment of inexpensive field-based measurement equipment and the rapidly evolving field of remote sensing will further our ability to explore these important research questions. This will in turn improve scientific inquiry that requires accurate estimates of distributed SWE including

assessment of water balance components in cold regions, ecosystem function and natural hazard risk (Sturm, 2015; Peters-Lidard *et al.*, 2017; Dong, 2018).

Chapter 3 Using field-based, photogrammetric point cloud, orthophoto and LiDAR-derived metrics to assess forest structure-snowpack relationships in the Great-Lakes St. Lawrence Forest region

Andy D. Beaton[1,2], Robert A. Metcalfe[1,3], James M. Buttle[4], Steven E. Franklin[4]

[1]Environment and Life Sciences, Trent University, 1600 West Bank Drive, Peterborough, ON, Canada, K9L 0G2

[2]Surface Water Monitoring Centre, Ministry of Natural Resources and Forestry, 300 Water Street, Peterborough, ON, Canada, K9J 8M5

[3]Aquatic Research and Monitoring Section, Ministry of Natural Resources and Forestry, c/o Trent University, 1600 West Bank Drive, Peterborough, ON, Canada, K9L 0G2.

[4]School of Environment, Trent University, 1600 West Bank Drive, Peterborough, ON, Canada, K9L 0G2

Unpublished Manuscript

*A.D. Beaton is the primary author of this paper. He designed the study, analyzed the data, and wrote the primary manuscript with guidance, input, and suggestions from coauthors.

Abstract

The efficacy of field-based, photogrammetric point cloud, orthophoto and light detection and ranging datasets to describe forest structure and resolve forest-snowpack relationships in a mixed forest region was evaluated over two years at the point and transect scales. Hemispheric photo-derived canopy metrics correlated well with remotely sensed metrics, but tree bole metrics were not effectively derived from remotely sensed data. Significant differences in melt rate and snow free date were found across forest type at the transect scale. Field and remotely sensed estimates of canopy cover were highly correlated with melt rate and snow free date at the point scale which aligns with previous literature and understanding of snowmelt processes. However, significant correlations were only present during the 2016 study year, which was attributed to canopy controlled solar radiation-driven melt in 2016 versus more spatially uniform turbulent flux-driven melt in 2017. Peak snow water equivalent metrics were not correlated well with canopy or tree height metrics, contrary to previous research. This was likely due to mid-winter melt events throughout both study years where a mix of accumulation and melt processes confounded forest-snowpack relationships. This study demonstrated that widely available remotely sensed data with a broad coverage can be used to: i) describe forest-snowpack relationships in mixed hardwood, coniferous forests and ii) elucidate the variability of forest-snowpack relationships under different climate conditions in this environment.

3.1 Introduction

Accurate representation of snow distribution is critical for understanding cold region hydrology (Barnett *et al.*, 2005). Forest structure controls snow accumulation and melt primarily through snow interception (Pomeroy *et al.*, 2002) and its influence on the energy balance (Gelfan *et al.*, 2004). Several previous studies focused on relationships between forest structure and snow accumulation metrics. Musselman et al. (2008) found that peak SWE was 47% less under a forest canopy compared to an adjacent open area. López-Moreno and Latron (2008) related individual point snow survey measurements to hemispheric photo-derived sky view factor and observed a strong relationship between SWE and canopy density with sky view factor explaining nearly 90% of the variance in peak SWE. Mean forest metrics from pine stand plots ranging from 100 to 800 m^2 were compared to plot mean snow survey data and strong relationships between LiDAR-derived metrics (forest cover and tree height) and peak SWE, and field-derived DBH and peak SWE were found (Varhola *et al.*, 2010a). Zheng et al. (2018) compared point snow depth sensor data to LiDAR-derived forest metrics calculated in circular areas ranging from 12 m^2 to 5000 m^2 surrounding the depth measurements. Canopy cover, LiDAR-derived tree heights and tree-height standard deviations controlled snow accumulation across eight locations (Zheng *et al.*, 2018).

Several studies have investigated the effect of forests on snow ablation. A meta-analysis of 33 snow studies primarily conducted in coniferous forests showed snowmelt rate decreases with increasing forest cover due to attenuated solar radiation from canopy shading, and decreased wind and sensible heat flux from forest sheltering (Varhola *et al.*, 2010b). Talbot et al. (2006) compared mean forest to snowpack metrics in 30 m by 30 m

plots and found tree height and light interception by the canopy had a significant impact on melt rate in a balsam fir forest in Quebec. Sky view factor, tree diameter at breast height (DBH) and basal area controlled SWE during melt based on the comparison of mean field-based forest metrics and snow surveys in 30 m x 30 m plots in a mixed forest in New Hampshire (Penn *et al.*, 2012). Metcalfe and Buttle, (1998) compared field-based gap fraction to snow wire-derived snowmelt at each measurement location and found melt in a boreal forest was primarily controlled by differences in canopy density represented as gap fractions. LiDAR-derived tree height standard deviation partially explained maximum snow ablation rate across 11 coniferous stands in British Columbia (Varhola *et al.*, 2010a). Varhola et al. (2010a) correlated forest metrics with snow ablation rates using different time periods and found the final ablation period (calculated as the difference between the last two consecutive surveys) had the strongest relationships. In contrast, Murray and Buttle, (2003) compared field-based gap fraction to snow wire-derived melt and found canopy density was not a good predictor of melt rate in deciduous forests in central Ontario.

Yamazaki and Kondo (1992) also observed that in general, snowmelt decreased with increasing forest cover, but observed that under conditions of high air temperature and snow albedo and weak wind the longwave radiation from a dense canopy produced faster melt than a sparser canopy with less longwave radiation. Sicart et al. (2003) confirmed that, in certain areas, increasing canopy density can show increased melt rates due to the increase in longwave radiation from the canopy.

Micro-scale vegetation properties such as directional distance from tree boles influence snow accumulation and melt at finer scales. Musselman et al. (2008) found

peak SWE occurred 21 days later on north versus south sides of trees. Faria et al. (2000) found that snow covered areas adjacent to tree wells with exposed leaf litter had higher melt rates due to advection from the exposed surface. Murray and Buttle, (2003) hypothesized inter-site differences in snowmelt in a deciduous stand were due to microtopography and proximity to tree trunks.

Field-based forest structure data for evaluating forest-snowpack relationships are time consuming to measure and difficult to distribute over larger areas (Varhola *et al.*, 2012; Moeser *et al.*, 2014). Spatially-distributed two-dimensional (2D) forest metrics have been derived from remotely sensed data and related to snowpack metrics (Metcalfe and Buttle, 1998; Essery *et al.*, 2008). More recently, three-dimensional (3D) forest metrics have been derived from light detection and ranging (LiDAR) data and photogrammetric point clouds (PPCs) (Pitt *et al.*, 2014; St-Onge *et al.*, 2015; White *et al.*, 2015; Stone *et al.*, 2016; Ullah *et al.*, 2019). These are considered the most useful form of remotely sensed data for describing forest characteristics and are an improvement over 2D forest metrics (Smith *et al.*, 2009; Dash *et al.*, 2016; Pearse *et al.*, 2018). Forest structure metrics derived from PPC approach the accuracy of airborne LiDAR-derived forest structure metrics (Baltsavias, 1999; Haala *et al.*, 2010; St-Onge *et al.*, 2015). Several studies have used LiDAR derived forest metrics to assess forest-snowpack relationships while use of PPC data for this purpose is limited (Morsdorf *et al.*, 2006; Essery *et al.*, 2008; Moeser *et al.*, 2015b; Zheng *et al.*, 2018).

The Ontario Imagery Program was established in 2011 with the purpose of collecting very high resolution, standardized data across southern and parts of central and northern Ontario on a predictable five-year repeat cycle. Orthophotos, PPCs and

derivative elevation products are generated and distributed by Land Information Ontario from the imagery acquisitions (Land Information Ontario, 2022a). The Ontario Airborne topographic LiDAR program has collected and disseminated LiDAR data across southern Ontario and parts of central and northern Ontario with plans to expand the acquisitions and continually update products (Land Information Ontario, 2022b).

The objective of this research was to evaluate the efficacy of the Ontario imagery and LiDAR data sets for describing forest-snowpack relationships and to improve our understanding of forest influences on snowpack characteristics in the Great Lakes-St. Lawrence Forest (GLSF) region by addressing the following questions:

- *How do forest metrics compare to peak snow water equivalent (SWE) and snowmelt rate magnitude and timing at the point and transect scales?*
- *How and why do relationships between forest structure and snowpack vary inter-annually?*

This comparison of field-based, 2D and 3D orthophoto- and LiDAR-derived metrics for the purposes of characterizing snowpack builds on previous studies, which typically have focused on a single remotely sensed data set to derive the required forest metrics (Varhola *et al.*, 2010a; Moeser *et al.*, 2015b). The present study also evaluated both field and remotely sensed canopy and tree bole characteristics whereas most previous studies focused on a single category of metrics. Previous studies have often been conducted in predominantly coniferous forests and alpine regions and evaluate forest-snowpack relationships at a single scale (Penn *et al.*, 2012), while this research was conducted in a non-mountain mixed hardwood and coniferous forest in the GLSF and evaluates relationships at different scales. The GLSF covers a broad swath of central Ontario and

southern Quebec and plays an important role in regulating water inputs to the Great Lakes, which contain nearly 20% of the earth's freshwater, are a vital source of drinking water, food, energy, transportation, and recreation, and support a diverse ecosystem (Ontario Ministry of the Environment, 2016). The GLSF's hydrology is dominated by a response to seasonal snow cover and improved understanding of SWE and melt processes is therefore critical to improve understanding of water inputs to the Great Lakes basin. Beaton et al. (2019) demonstrated that significant differences in snowpack across land cover in the GLSF were temporally variable and recommended more in-depth investigation of forest structure-snowpack relationships in this environment.

3.2 Materials and methods

3.2.1 Study area

The study area is in central Ontario, Canada in the GLSF, covers an area of ~13 km^2 (Figure 3.1) and is characterized by deciduous, coniferous, and mixed forests of uneven ages dominated by maple (*Acer*), oak (*Quercus*), birch (*Betula*), pine (*Pinus*), cedar (*Cedrus*), hemlock (*Tsuga*), balsam fir (*Abies balsamea*) and spruce (*Picea*) genera (Cumming, 2009). It is in the Canadian Shield physiographic region, which has a generally thin soil layer and glacial tills over Precambrian bedrock and many waterbodies and wetlands within the drainage networks (Singer and Cheng 2002). The study area is situated on the Algonquin dome topographic feature at an elevation of around 500 m above sea level (Cumming, 2009). This is one of the highest regions in Ontario and results in lower temperatures relative to the surrounding area. Monthly average temperatures range from −19.2 °C in January to 18.8 °C in July, and annual mean daily temperature for the year is 2 °C (Environment and Climate Change Canada, 2019). The

region has an average of 90 frost-free days per year. The study area is leeward of Georgian Bay, which influences the regional climate and results in lake-effect precipitation (Scott and Huff, 1996; Cumming, 2009). Higher elevations and lake-effect precipitation result in greater precipitation compared to the surrounding region, totaling 1,185 mm annually with 345 mm falling as snow. Mean March snow depth from 1981 to 2010 was 61 cm (Government of Canada, 2022).

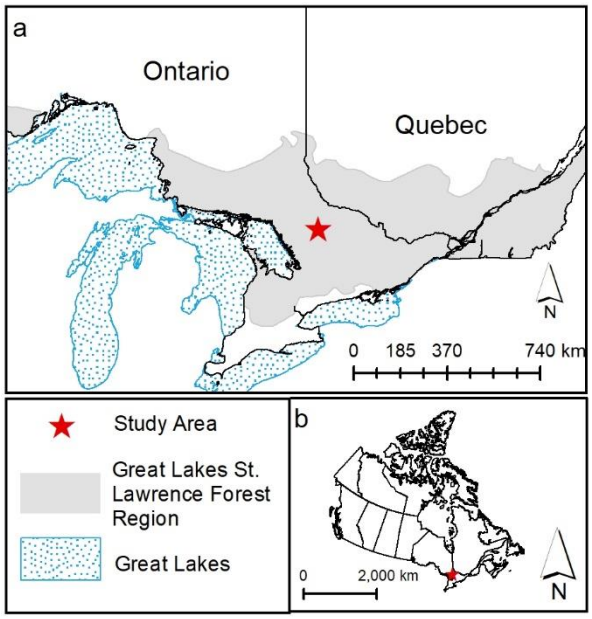

Figure 3.1:Location of study area within the context of Ontario (a) and Canada (b).

3.2.2 Data

3.2.2.1 Field data

SWE was measured along linear transects using an ESC-30 gravimetric sampler in relatively flat areas to focus on the structural factors influencing forest-snow interaction (Goodison *et al.*, 1987). Seven measurements spaced 50 m apart were taken in each of the three forest cover types, for a total of 21 measurements on each survey

date. Snow surveys were conducted over two winter seasons within coniferous, deciduous, and mixed wood forest types (Figure 3.2). Surveys were done February to April to capture peak SWE with 10 surveys in 2016 and 4 in 2017 snow seasons. Snowmelt was calculated from transects sampled in mid to late April. Snow measurements aggregated within each forest cover type are referred to as transect scale and represent a forest stand. Individual measurements at each of the snow core locations are referred to as point scale snowpack. Measurement sites were surveyed using a Nikon DTM-322 total station (Nikon, 2010). Locations were tied to Ontario geodetic benchmarks using a Trimble real-time-kinetic (RTK) Global Positioning System (GPS) (Land Information Ontario, 2020). Daily snow depth near the start of each of the three SWE transects was estimated from time-lapse cameras with snow rulers (Beaton *et al.*, 2019) and was used to assess snow accumulation and melt between surveys.

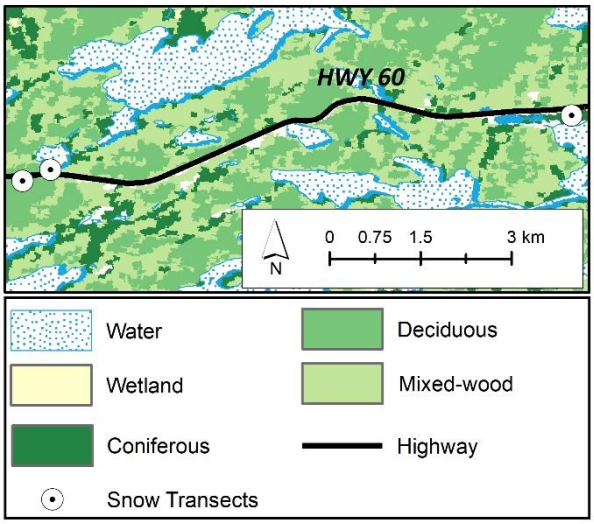

Figure 3.2: Snow survey locations and land cover types.

Upward facing hemispheric photos (HPs) of canopy were taken at each SWE measurement location (Figure 3.3) with a Nikon D7000 camera and a Sigma 4.5mm F2.8 EX DC HSM circular fisheye lens on a leveled tripod. HPs were taken during consistent

overcast conditions throughout late morning and early afternoon to minimize sun impacts including flares, shadows, and overexposure (Rich, 1990). Use of HPs for measuring field-based canopy characteristics and relating them to snowpack metrics is a well-established method (Morsdorf *et al.*, 2006; Musselman *et al.*, 2012; Zheng *et al.*, 2018). Distance to the closest tree bole and DBH of the closest tree in each cardinal direction were taken at each measurement location.

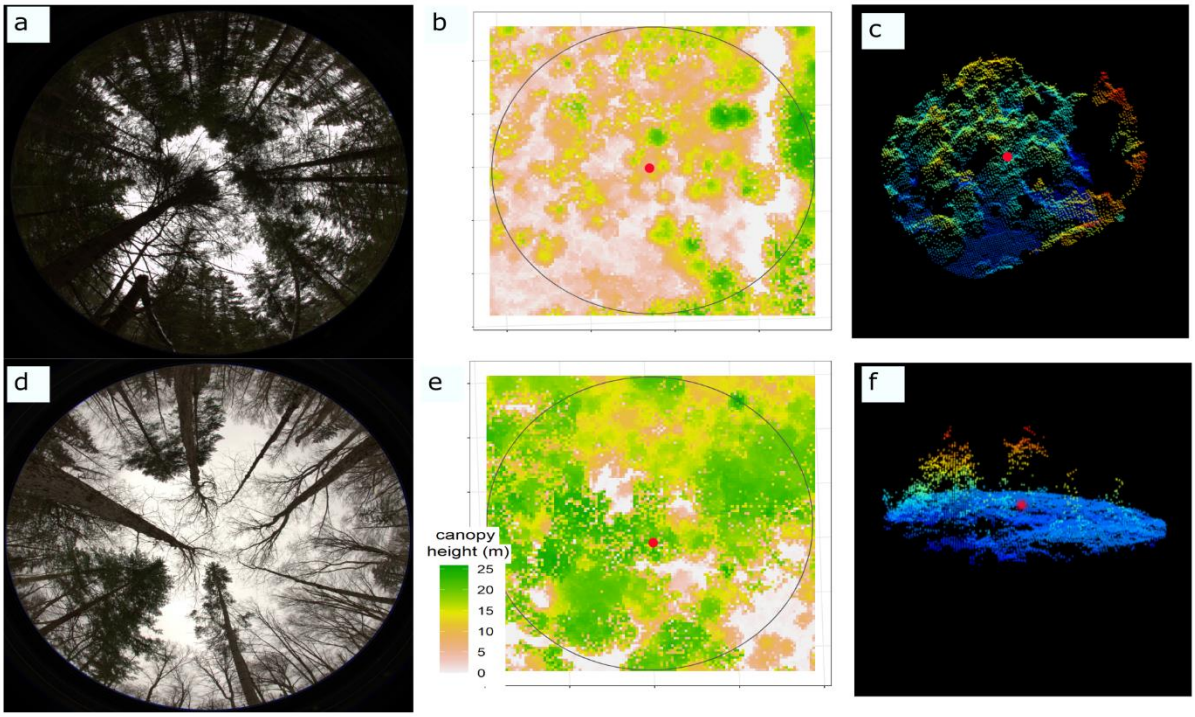

Figure 3.3: Hemispheric photos (left), LiDAR-derived canopy height model with 30 m buffer (middle) and South-Central Ontario Orthophoto (SCOOP) Photogrammetric Point Cloud (PPC) within a 30 m buffer (right) of the sample location at a predominantly coniferous stand (a, b, c) and a mixed wood stand (d, e, f). Dots at the centroid of canopy height model and PPC represent measurement locations.

3.2.2.2 Remotely sensed data

The South-Central Ontario Orthophoto Project (SCOOP) classified laser (LAS) and orthophoto data were used to quantify canopy cover. SCOOP data were acquired by an imagery contractor using an ADS80 Leica digital camera mounted on an airplane in spring of 2013 during leaf-off conditions. These data have a 20 cm resolution and geometric accuracy of 50 cm at 90% confidence (Figure 3.4). Red (604-664 nm), green (533-587 nm), blue (420-492 nm) and near infrared (833-920 nm) spectral bands were captured (Leica Geosystems, 2011). The Ontario Provincial Mapping Unit produced a 50 cm resolution point cloud from the orthophotos (Provincial Mapping Unit, 2020). The Algonquin Park LiDAR data were used to characterize canopy heights and detect trees. These data were acquired by an imagery contractor using a Leica SPL 100 mounted on an airplane during the summer of 2019 during leaf-on conditions with a 50% overlap to capture a minimum of 25 points/m^2 (I. Sinclair, personal communication, 2020).

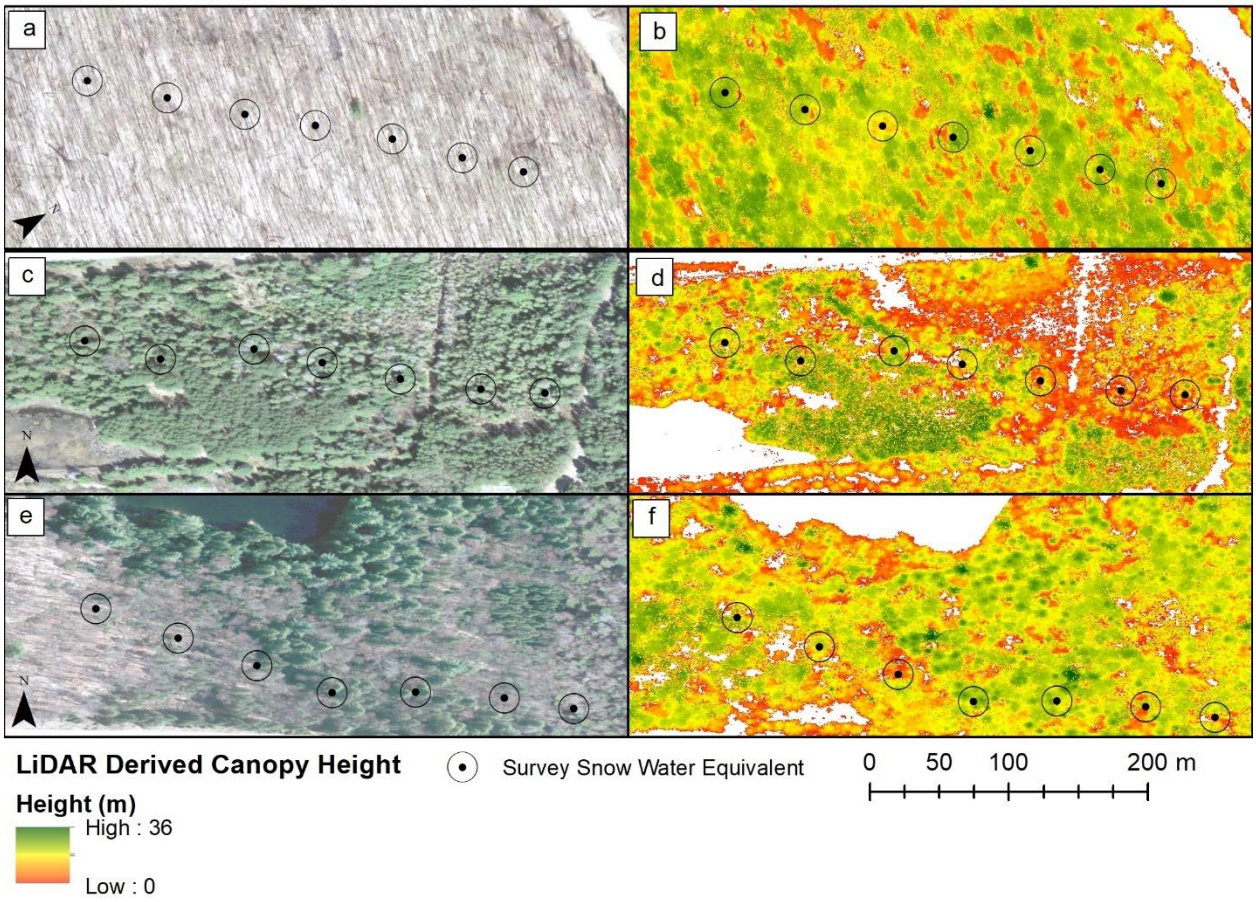

Figure 3.4: Orthophoto (left) and LiDAR-derived canopy height models (right) in a predominantly deciduous (a,b), coniferous (c,d) and mixed wood (e, f) stand.

3.2.2.3 Climate data

Inter-annual differences in climate and their effect on the forest structure-snowpack relationships were assessed. Temperature, precipitation, wind speed and relative humidity were measured at the Environment Canada Algonquin Park East Gate climate station (WMO ID 71581), 26 km east of the study area. Climate data were summarized for seven-day melt periods in 2016 and 2017 and were used to qualitatively evaluate interannual differences in energy flux. The melt period was from April 16th to April 22nd in 2016 and from April 7th to April 13th in 2017. Precipitation phase is

controlled by the energy balance of the falling hydrometeor which is dependent on several atmospheric variables (Harder and Pomeroy, 2013). Energy balance methods for determining precipitation phase are data intensive and temperature-based methods have been shown to provide reasonable estimates (Braun, 1991). Precipitation was partitioned into rain or snow using the two-parameter linear method (Equation 3.1).

$$\alpha_s = 0.5 + \frac{T_{trans} - T_{ave}}{\Delta T} \quad 3.1$$

where T_{ave} is the average daily temperature, T_{trans} is the rain/snow transition temperature, and ΔT is the range in air temperature along which the partitioning is applied to incoming precipitation. Parameters from a hydrologic model of the Petawawa basin located 50 km northeast of the study area were used. The model was calibrated to subbasin snow water equivalent and basin outlet discharge resulting in a T_{trans} and ΔT of -4.5 °C and 2.7 °C, respectively.

The Modern-Era Retrospective Analysis, version 2 (MERRA-2) hourly shortwave irradiance is a National Aeronautics and Space Administration (NASA) generated atmospheric re-analysis product and was used to evaluate interannual differences in solar radiation reaching the canopy (Gelaro *et al.*, 2017). The product accounts for differences in radiation due to cloud cover. MERRA-2 radiation data have been successfully used in energy balance based snow modelling and were shown to be a good estimate of shortwave radiation (Massmann, 2019).

3.2.2.4 Snowpack and forest metrics

A list of all metrics and their definitions is provided in (Table 3.1). Snowmelt rate (SMR) was calculated during the final stages of spring snowmelt as the difference in SWE between the last two sample dates where snow was observed (i.e. not snow free), divided by the number of days between measurements following equation 3.2 (Varhola *et al.*, 2010a):

$$\mathrm{SMR} = \frac{\mathrm{SWE}_i - \mathrm{SWE}_f}{\mathrm{P}} \quad 3.2$$

where SWE_i and SWE_f are initial and final SWE, and P is the number of intervening days. A snowfall event was detected in the time-lapse camera derived snow depth data at the beginning of the melt period in 2017. The event accumulation (5 cm in the coniferous stand, 10 cm in the deciduous and mixed stands) was added to the survey SWE. A snow density of 0.1 g/cm^3 was assumed following standard practice, given typical ranges of fresh snowfall density of 0.07 g/cm^3 to 0.15 g/cm^3 (Dingman, 2015). Analysis was conducted with and without the event compensation and the impacts were negligible. Where the snow free date (SF_{doy}) was not recorded by the survey, SWE was extrapolated to an assumed snow free date based on the calculated melt rate.

Metrics describing canopy structure (height and cover) and tree bole characteristics (distance to bole and bole diameter) were calculated within a 30 m circular trap around each sample point. Trap size is the area around the sample location where a metric is assumed to affect snowpack (Lovell *et al.*, 2003; Morsdorf *et al.*, 2006). Within the context of HPs the trap size is the assumed distance the camera can "see" and is derived from literature or determined through calibration (Lovell *et al.*, 2003). Influence

of trap size is dependent on heterogeneity of the forest structure surrounding the measurement location (Morsdorf *et al.*, 2006). Correlations between forest and snowpack metrics for trap sizes from 5 to 60 m were calculated and a circular trap with a 30 m radius (consistent with values found in the literature e.g. Moeser *et al.*, 2014) was found to be optimal, although relationships were generally insensitive to changes in trap size.

Table 3.1 Data source, abbreviation and description of calculated snow and forest metrics.

Data Source	Abbreviation	Description [unit]
Snow Measurement	SWE_{peak}	Maximum SWE within each year [mm]
	$PEAK_{doy}$	Maximum SWE day of year for each year
	SMR	Snowmelt rate [mm day^{-1}]
	SF_{doy}	Snow free day of year
Forest Measurements	GF_{55}	Hemispheric photo derived gap fraction at a 55-degree zenith angle [sky pixels/total pixels]
	DTB_{field}	Distance to closest tree bole [m]
	DBH_{max}	Maximum diameter at breast height within 5 m of site [m]
Photogrammetric Point Cloud	$PGRND_{PPC}$	Percentage of points that reach the ground [ground returns/total returns]
LiDAR Point Cloud	$zmax_{LiDAR}$	Maximum point cloud heights [m]
	$zmean_{LiDAR}$	Mean of point cloud heights [m]
	zsd_{LiDAR}	Standard deviation of point cloud heights [m]
	DTB_{LiDAR}	Distance to closest tree bole [m]
Orthophoto	NDVI	Normalized Difference Vegetation Index [dimensionless]

Gap fraction (GF) is the ratio of sky to vegetation pixels across concentric circles from a specified angle of view from the zenith toward the horizon (Varhola and Coops, 2013). HPs were processed using R Hemiphot to calculate gap fraction at each site across zenith angles from 0 to 90° (R Development Core Team, 2011; ter Steege, 2018).

Moeser et al. (2014) compared the strength of the relationship between HP and LiDAR-derived canopy closure across zenith angles from 30° to 90° and found them to be insensitive to zenith angle, especially at lower trap sizes. López-Moreno and Latron, (2008) found zenith angles between 35° and 55° were relevant to maximum SWE with 55° showing the strongest correlation. Zenith angles from 0° to 90° were tested by correlating HP GF to $PGRND_{SCOOP}$ (the ratio of PPC ground returns to total returns) and HP GF to snow metrics. The optimal zenith angle was 55°; therefore, GFs were calculated from cumulative field of view up to a zenith angle of 55° (GF_{55}).

$PGRND_{PPC}$ was calculated from the leaf-off SCOOP PPC as the ratio of photogrammetric points that reach the ground, similar to the forest cover (fCover) metric used to describe canopy-snowpack relationships in several previous studies (Morsdorf *et al.*, 2006; Solberg *et al.*, 2009; Solberg, 2010; Moeser *et al.*, 2014). The Cartesian method was used as it yielded consistent and accurate results in previous studies when compared to coordinate transformation (Morsdorf *et al.*, 2006; Essery *et al.*, 2008; Solberg *et al.*, 2009). For each measurement location, the range of PPC heights was divided into 10 equal intervals and the percentage of points reaching each interval was calculated to evaluate the relationship between snowpack and forest vertical structure (Woods *et al.*, 2008). There were no improvements in correlations between PPC height deciles and snowpack metrics compared to $PGRND_{PPC}$, so they were not included in the analysis. Tree heights were calculated from the leaf-on LiDAR point cloud by subtracting the height of points classified as vegetation from LiDAR derived bare earth (Varhola *et al.*, 2010a). Non-ground points were filtered and the maximum, mean, and standard deviation of tree heights were calculated within each circular trap. Both

SCOOP PPC and LiDAR-derived point clouds were processed using the R lidR package (Rousse and Auty, 2020). PPC-derived tree heights were evaluated but the leaf-off point cloud was unable to resolve deciduous tree heights, so these metrics were omitted from further analysis.

The Normalized Difference Vegetation Index (NDVI; equation 3.3) proposed by Rouse et al. (1973) has been used to describe forest structure for snow hydrology applications (Azar *et al.*, 2008; Essery *et al.*, 2008; Varhola and Coops, 2013). NDVI derived from orthophotography approximates values calculated from satellite data (Erlandsson *et al.*, 2019). The Normalized Difference Vegetation Index (NDVI; equation 3.3) was calculated from the SCOOP imagery:

$$\mathrm{NDVI} = \frac{\mathrm{NIR} - \mathrm{Red}}{\mathrm{NIR} + \mathrm{Red}} \tag{3.3}$$

where NIR and Red represent reflectance in the near infrared and red bands respectively. Additional spectral metrics included in Varhola and Coops (2013), such as Enhanced Vegetation Index and Green-Red Vegetation Index, were also tested but were statistically redundant and thus were not included in the analysis.

Distance to the closest tree bole in each cardinal direction was measured in the field (DTB_{field}). Trees with smaller boles (< 20 cm DBH) were not measured. An area with several boles smaller than 20 cm DBH will not be captured by the DTB_{field} metric but would influence snow accumulation and melt. Measurement locations in this study were generally not characterized by small dense trees, justifying use of the 20 cm DBH threshold. Directional DTB did not produce interpretable results so minimum DTB at each site was used as a metric for distance from tree boles. Point cloud data can be used

to detect individual trees (Zhen *et al.*, 2016) and have been used to calculate DTB for evaluating forest-snowpack relationships (Zheng *et al.*, 2018). The highest point of each crown is typically located near the tree's center and was used as a proxy for tree bole location (Lu *et al.*, 2014). In stands affected by wind damage, treetops may be displaced several meters off of the tree trunk (Lu *et al.*, 2014; Zhen *et al.*, 2016). The study area forests were relatively unaffected by strong wind damage, so the approximation was considered valid. The lidR R package was used to detect treetops (Rousse and Auty, 2020) using a local maxima filter algorithm as per Popescu and Wynne, (2004). The detected treetops were used to estimate the distance to the nearest tree bole from the LiDAR data (DTB_{LiDAR}).

DBH of trees in each cardinal direction within 10 m of the snow sample locations were measured. These directional data did not produce meaningful results in this study and consequently the DBH data were summarized as the maximum value at each measurement location.

Statistical differences in mean transect forest metrics were calculated to evaluate characteristics driving differences in mean transect snowpack metrics across forest stands. Differences in mean transect snowpack metrics were calculated to evaluate forest effects on snowpack as this scale. Correlation between forest metrics at each measurement point was calculated to validate remotely sensed metrics with field estimates and to highlight colinear variables. Forest metrics and snowpack variables were correlated at each measurement point to evaluate forest-snowpack relationships at this scale. The Shapiro Wilks test (Shapiro and Wilk, 1965) was used to determine if distributions were normal and the Levene's test (Levene, 1960) was used to assess

homogeneity of variance. Tukey Honest Significant Difference (Tukey, 1949) tests were used for determining pairwise differences for parametric data and Dunn's test (Dunn, 1964) was used for non-parametric data. Pearson's correlation coefficient (r) was calculated to evaluate relationships between forest metrics and snowpack variables at the point scale (Table 3.1). An $r \geq 0.65$ was considered a moderate to strong correlation, ≥ 0.45 $r < 0.65$ a weak to moderate correlation and < 0.45 was considered uncorrelated. Correlations were considered significant where $p < 0.05$. A Bonferroni correction was applied given the large number of comparisons.

3.3 Results

3.3.1 Interannual climate differences

Figure 3.5 shows temperature and precipitation over both winter seasons for the purpose of qualitatively identifying climate conditions that may influence peak SWE metrics. Peak SWE date ranged from March 6th to April 17th with a mean of March 22nd in 2016 and ranged from January 19th to April 3rd with a mean of March 6th in 2017 (Figure 3.5). Daily maximum temperatures rose above 0 °C several times throughout the 2016 and 2017 winter seasons. Positive temperatures coincided with precipitation prior to peak SWE occurrences likely resulting in rain on snow and potential melt events (Figure 3.5).

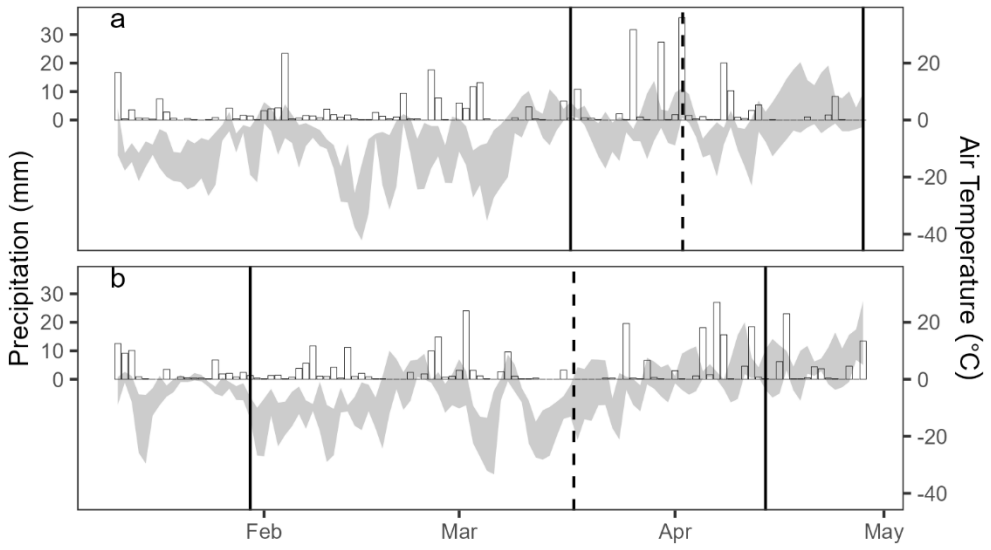

Figure 3.5: Daily precipitation (bar), daily minimum and maximum air temperature range (grey ribbon), mean peak date (dashed vertical line), minimum and maximum peak dates (solid vertical line) for 2016 (a) and 2017 (b).

Figure 3.6 shows climate variables for the seven-day melt period analyzed to qualitatively relate the climate conditions to the snow energy balance. Mean solar irradiance for the analyzed period was larger in 2016 (240 W/m^2) than 2017 (194 W/m^2) (Figure 3.6). More days in 2017 had attenuated solar irradiance compared to 2016. Diurnal temperature fluctuations were more distinct and nocturnal sub-zero temperatures were more frequent during melt in 2016 than 2017 (Figure 3.6). Wind speeds were variable in both years, but mean values were slightly higher in 2017 than 2016. Mean relative humidity was larger in 2017 than 2016 and there were two rain events in 2017 where relative humidity remained around 75% for several days. There was little rain in 2016 (2.9 mm) but a substantial amount in 2017 (66.5 mm). There was negligible snowfall in both years (Figure 3.6).

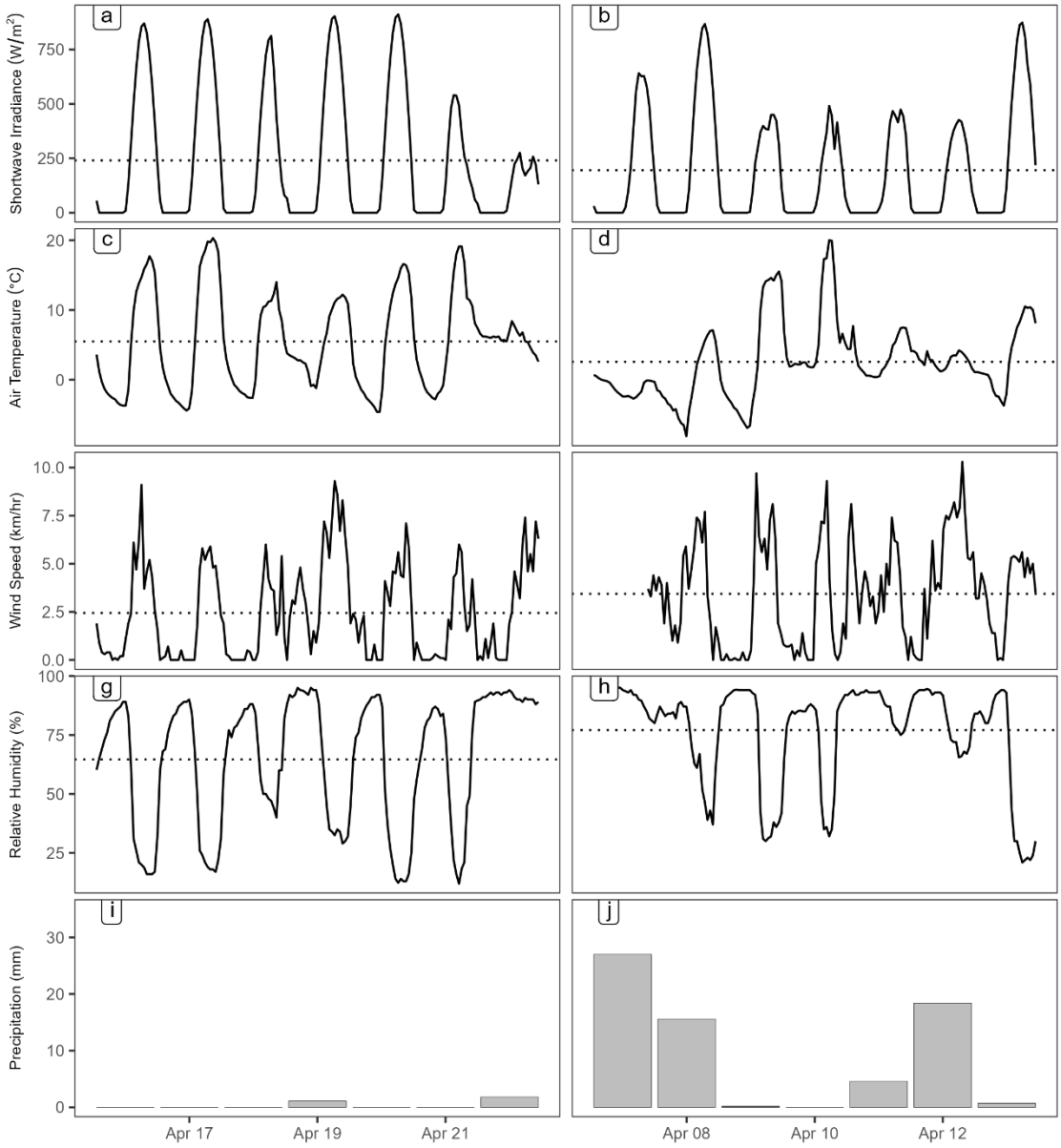

Figure 3.6: Climate data for 2016 (left) and 2017 (right). Hourly shortwave irradiance (a, b), hourly air temperature (c, d), hourly wind speed (e, f), hourly relative humidity (g, h) and daily precipitation (i, j). All precipitation during this period was partitioned into rain. Dotted horizontal lines are melt-period means.

3.3.2 Forest metrics

GF_{55} ranged from 14% open to 80% open and mean transect values were much smaller in the coniferous stand than the deciduous stand (statistically significant) with a greater range of values in the mixed wood stand (Figure 3.7). $PGRND_{PPC}$ followed a similar pattern to GF_{55} but with less variability in the mixed forest. Mean transect coniferous versus deciduous $PGRND_{PPC}$ differences and deciduous versus mixed forest $PGRND_{PPC}$ differences were significant. Mean transect NDVI was much smaller in the deciduous stand than coniferous and mixed stands and these differences were statistically significant. $zmean_{LiDAR}$ ranged from 6 m to 18 m with smaller mean and maximum tree heights in the coniferous stand than mixed and deciduous stands. All mean transect pairwise differences for $zmean_{LiDAR}$ were statistically significant. Forest stands had similar variability in tree heights (zsd_{LiDAR}). DTB_{field} ranged from 0.5 m to 3.8 m and was smaller in the coniferous stand than deciduous and mixed stands while DTB_{LiDAR} was similar across forest stands and larger than DTB_{field}. DBH_{max} ranged from 5 cm to 65 cm and was smaller in the coniferous stand than the deciduous and mixed stands. Mean transect differences across forest stands for DTB_{field}, DTB_{LiDAR} and DBH_{max} were not significant.

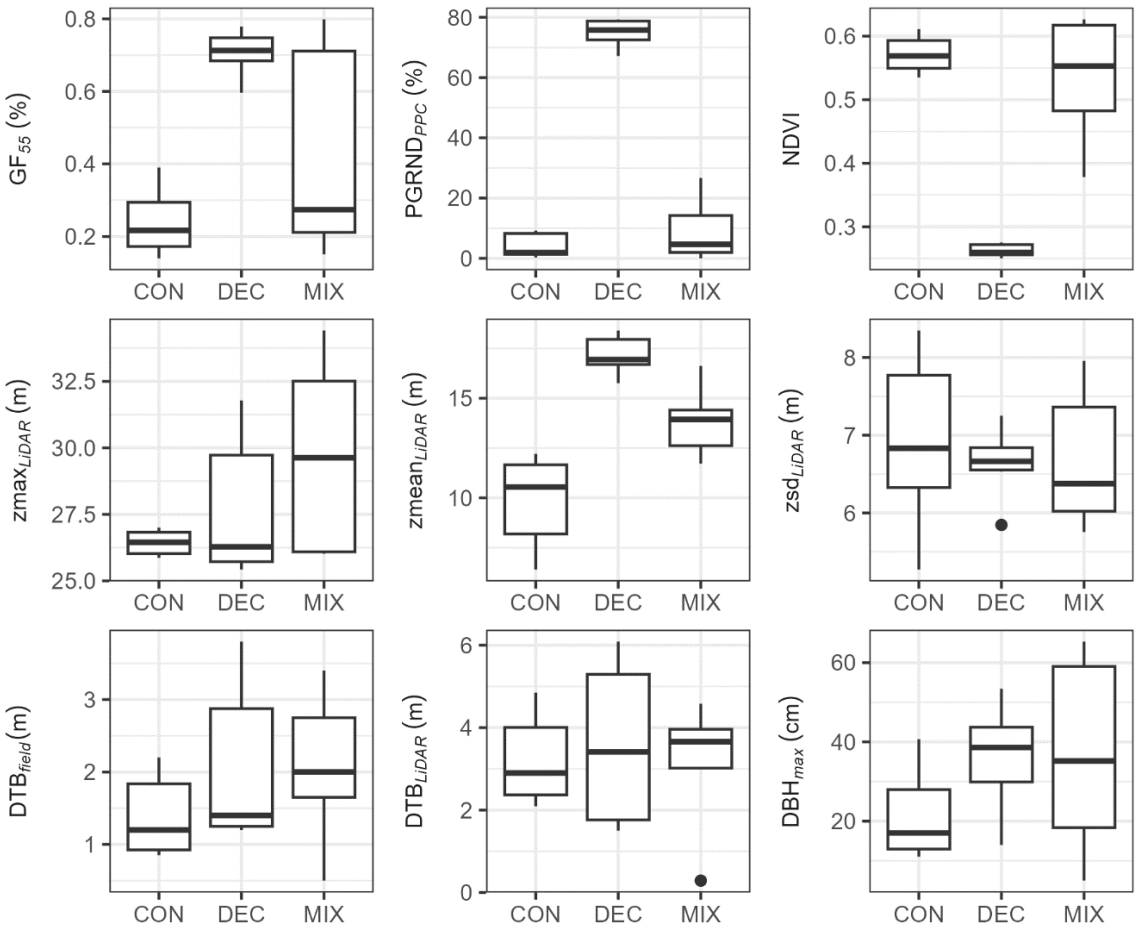

Figure 3.7: Forest metrics within the coniferous (CON), deciduous (DEC) and mixed wood forest (MIX). GF*55* is the hemispheric photo derived gap fraction at a 55 degree zenith angle; $PGRND_{PPC}$ is the percentage of photogrammetric cloud points that reach the ground; NDVI is the Normalized Difference Vegetation Index; $zmax_{LiDAR}$ $zmean_{LiDAR}$, and zsd_{LiDAR} are the maximum, mean and standard deviation of LiDAR point cloud heights; DTB_{field} and DTB_{LiDAR} are the distance to closest tree bole derived from field-based measurements and LiDAR, respectively; DBH_{max} is the field-based maximum diameter at breast height within 5 m of the measurement location. The boxes represent the 25th and 75th percentiles of the distributions, the horizontal lines in the boxes represent the median and the dots represent outliers.

At the point scale, there were moderate to strong significant correlations between canopy cover metrics (GF_{55}, NDVI, $PGRND_{PPC}$). Strong significant correlations between $zmean_{LiDAR}$ and NDVI, and $zmean_{LiDAR}$ and $PGRND_{PPC}$ were found. There was insignificant moderate correlation between $zmean_{LiDAR}$ and GF_{55}. DTB_{field} and DTB_{LiDAR} were uncorrelated (Table 3.2).

Table 3.2: Correlation matrix of forest structure metrics. GF*55* is the hemispheric photo derived gap fraction at a 55 degree zenith angle; $PGRND_{PPC}$ is the percentage of photogrammetric cloud points that reach the ground; NDVI is the Normalized Difference Vegetation Index; $zmax_{LiDAR}$ $zmean_{LiDAR}$, and zsd_{LiDAR} are the maximum, mean and standard deviation of LiDAR point cloud heights; DTB_{field} and DTB_{LiDAR} are the distance to closest tree bole derived from field-based measurement and LiDAR, respectively; DBH_{max} is the field-based maximum diameter at breast height within 5 m of the measurement location.

	DBH_{max}	DTB_{field}	$PGRND_{PPC}$	$zmax_{LiDAR}$	$zmean_{LiDAR}$	zsd_{LiDAR}	GF_{55}	NDVI	DTB_{LiDAR}
DBH_{max}	1								
DTB_{field}	**0.74**	1							
$PGRND_{PPC}$	0.21	0.2	1						
$zmax_{LiDAR}$	0.14	0.09	-0.11	1					
$zmean_{LiDAR}$	0.48	0.29	**0.72**	0.23	1				
zsd_{LiDAR}	0.07	0.12	-0.04	-0.22	-0.02	1			
GF_{55}	0.2	0.31	**0.77**	0.05	0.52	0.03	1		
NDVI	-0.14	-0.14	**-0.98**	0.17	**-0.68**	0.01	**-0.78**	1	
DTB_{LiDAR}	-0.11	0.16	0.08	0.03	0.27	0.01	-0.08	-0.04	1

bold if $r \geq 0.65$; highlighted if $p < 0.0014$

3.3.3 Snowpack versus forest metrics

Mean SWE_{peak} averaged across all forest cover types was larger in 2017 than 2016. Coniferous SWE_{peak} was generally larger than for deciduous and mixed stands in 2016 (transect mean differences not significant) but not 2017 (Figure 3.8). $Peak_{doy}$ mostly occurred in March but ranged from January to mid-April and was later in 2016 than 2017. $Peak_{doy}$ was generally later in the coniferous versus the deciduous and mixed forests, but the differences in transect means were not statistically significant (Figure 3.8).

SMR in 2016 was substantially larger than 2017. In 2016, the coniferous stand had a smaller mean transect SMR (statistically significant) compared to the deciduous stand and smaller, but not significant mean transect SMR compared to the mixed forest. Mean transect SMR in the coniferous stand was smaller than that for the deciduous stand in 2017 (not significant) and the SMR in the mixed forest was highly variable (Figure 3.8). SF_{doy} ranged from late April to early May and on average was slightly later in 2016 than 2017. Mean transect SF_{doy} in the coniferous stand was later than for the deciduous stand in 2016 (statistically significant). Mean transect SF_{doy} in the coniferous stand was later than the mixed forest in the 2016 and 2017 but the differences where not statistically significant (Figure 3.8).

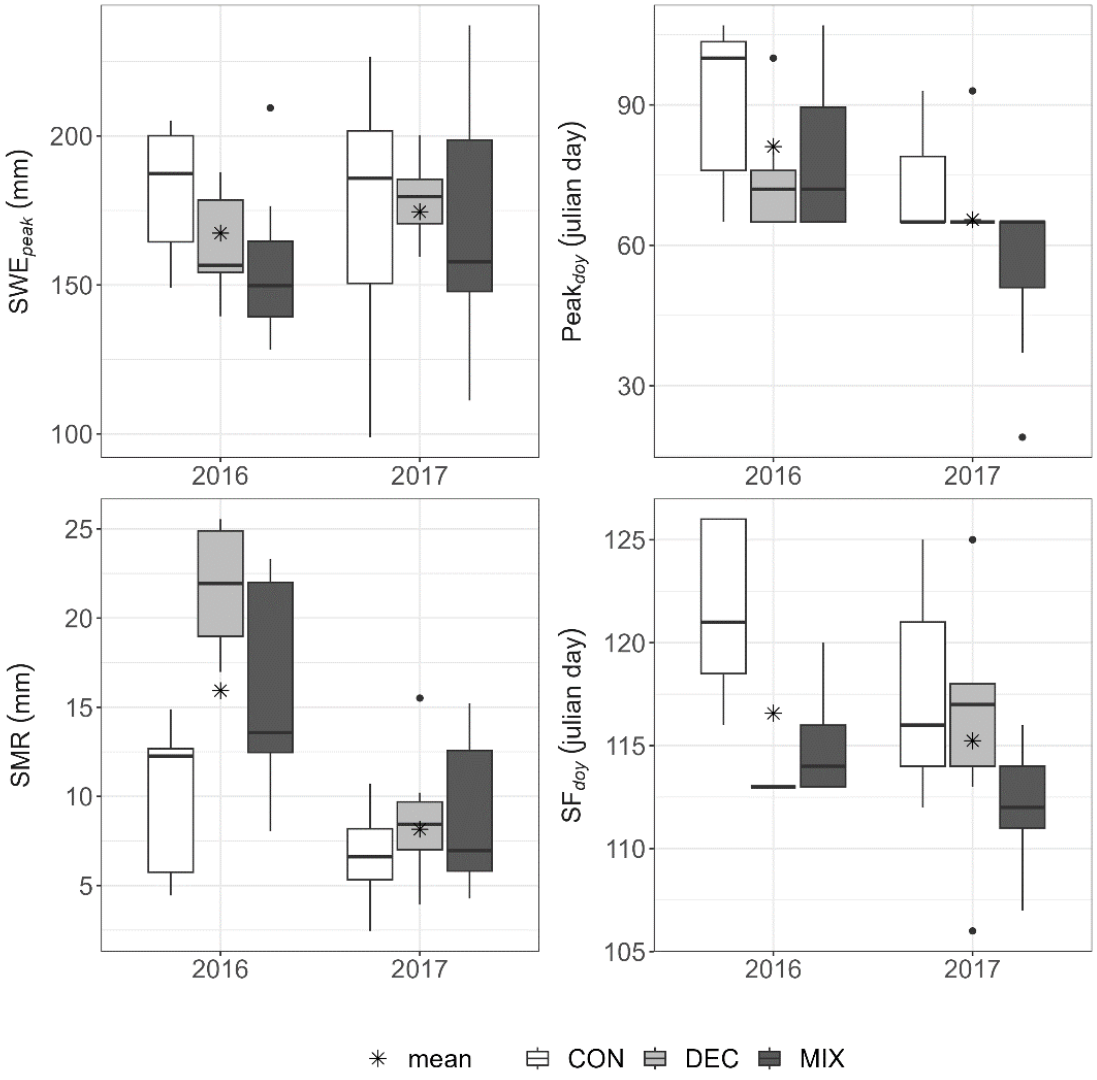

Figure 3.8: Range of snowpack metrics within the coniferous (CON), deciduous (DEC) and mixed wood forest (MIX) in 2016 and 2017 snow seasons. SWE_{peak} and $PEAK_{doy}$ are the maximum SWE magnitude and timing, respectively; SMR is the snowmelt rate and SF_{doy} is the snow free day of year. The boxes represent the 25th and 75th percentiles of the distributions, the horizontal lines in the boxes represent the median and the dots represent outliers. The asterisk represents the annual mean summarized across all forest types.

At the point scale, $zmean_{LiDAR}$ had a significant, negative correlation with SF_{doy} 2016. SWE_{peak} and $PEAK_{doy}$ were generally uncorrelated with forest metrics (Table 3.3; Figure 3.9). A significant correlation between $PEAK_{doy}$ and DTB_{field} in 2016 indicated that SWE measurements closer to tree boles had a later peak SWE in that year. Weak to moderate but statistically insignificant negative correlations between DBH_{max} and SWE_{peak} in both years and $PEAK_{doy}$ in 2016 suggests a weak relationship between measurement locations with larger DBH and a smaller and later peak SWE (Table 3.3; Figure 3.9). Moderate to strong significant relationships between SMR, SF_{doy} and forest structure metrics ($PGRND_{PPC}$, GF_{55}, NDVI) were observed in 2016 but not 2017 indicating sites with open canopies had larger melt rates and earlier snow free dates (Table 3.3; Figure 3.9).

Table 3.3: Correlation coefficients for relationships between snowpack and forest structure metrics. GF*55* is the hemispheric photo derived gap fraction at a 55 degree zenith angle; $PGRND_{PPC}$ is the percentage of photogrammetric cloud points that reach the ground; NDVI is the Normalized Difference Vegetation Index; $zmax_{LiDAR}$ $zmean_{LiDAR}$, and zsd_{LiDAR} are the maximum, mean and standard deviation of LiDAR point cloud heights; DTB_{field} and DTB_{LiDAR} are the distance to closest tree bole derived from field-based measurements and LiDAR, respectively; DBH_{max} is the field-based maximum diameter at breast height within 5 m of the measurement location; SWE_{peak} and $PEAK_{doy}$ are the maximum SWE magnitude and timing, respectively; SMR is the snowmelt rate and SF_{doy} is the snow free day of year.

	SMR		SF_{doy}		SWE_{peak}		$PEAK_{doy}$	
	2016	2017	2016	2017	2016	2017	2016	2017
DBH_{max}	0.18	-0.21	-0.53	-0.06	-0.54	-0.44	-0.55	-0.06
DTB_{field}	0.18	-0.1	-0.42	-0.01	-0.3	-0.24	**-0.69**	0.09
$PGRND_{PPC}$	**0.65**	0.1	-0.57	0.15	-0.09	0.05	-0.29	0.03
$zmax_{LiDAR}$	0.25	0.07	-0.19	-0.03	-0.09	0.26	-0.16	0.21
$zmean_{LiDAR}$	0.58	0.06	**-0.69**	-0.1	-0.4	-0.07	-0.41	-0.03
zsd_{LiDAR}	-0.01	-0.06	0.11	0.2	0.05	-0.23	-0.26	-0.17
GF_{55}	**0.69**	0.35	**-0.65**	-0.05	-0.28	0.08	-0.46	-0.23
NDVI	**-0.66**	-0.13	0.58	-0.1	0.07	0.02	0.22	0.11
DTB_{LiDAR}	0	-0.12	0.01	0.02	0.19	-0.1	-0.07	0.19

bold if r >= ±0.65; highlighted if p < 0.000694

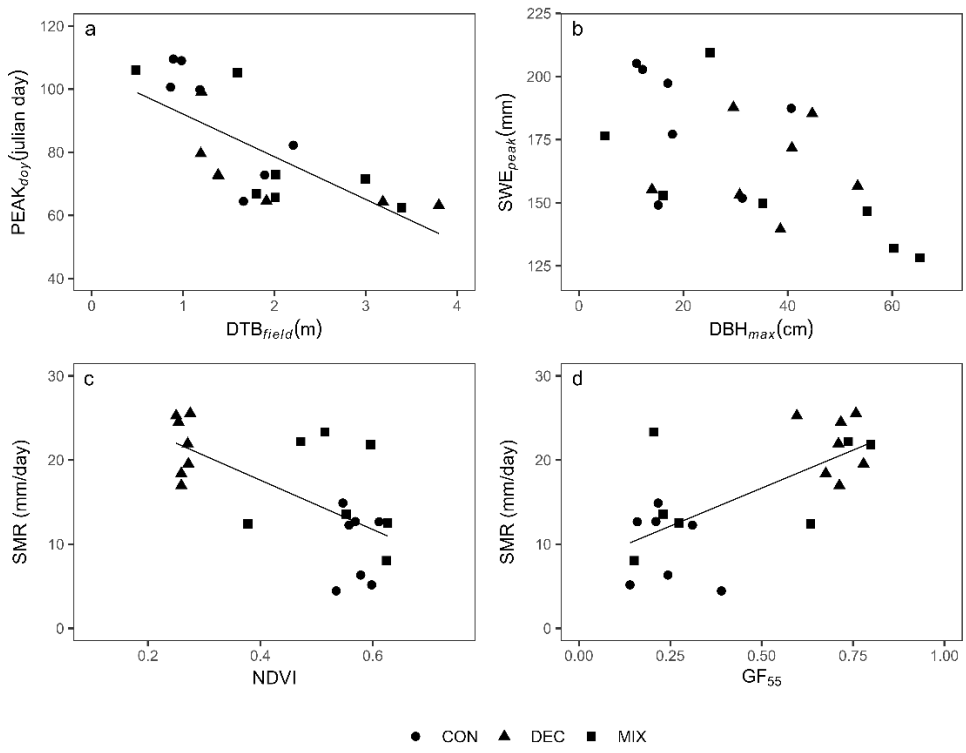

Figure 3.9: Scatterplots and statistically significant linear relationships (lines) between snowpack and forest structure metrics for different forest types in 2016. SWE$_{peak}$ and PEAK$_{doy}$ are the maximum SWE magnitude and timing, respectively; SMR is the snowmelt rate; DTB$_{field}$ is the distance to the closest tree bole derived from field-based measurements; DBH$_{max}$ is the field-based maximum diameter at breast height within 5 m of the measurement location; NDVI is the Normalized Difference Vegetation Index; GF*55* is the hemispheric photo derived gap fraction at a 55-degree zenith angle.

3.4 Discussion

3.4.1 Field-based verification of remotely sensed forest metrics

Remotely sensed canopy cover metrics agreed with field-based measurements providing confidence in the PPC- and orthophoto-derived estimates. The strong correlations found in this study (GF_{55} versus $PGRND_{PPC}$ = 0.77, GF_{55} versus NDVI = -0.78) are comparable to those from the literature. Morsdorf et al. (2006) and Moeser et al. (2014) compared HP estimates of canopy cover to LiDAR-derived estimates calculated as the ratio of canopy to total returns (similar to $PGRND_{PPC}$ metric) and both found a correlation coefficient of 0.85. Contrasts between field and remotely sensed canopy estimates were attributed to differences in viewing geometry. Downward looking LiDAR and PPCs are biased towards detecting elements in the upper canopy. Conversely, the upward looking HPs will be biased towards detecting understory and tree stems (Morsdorf *et al.*, 2006; Varhola *et al.*, 2012). Contrary to the findings of Smith et al. (2009) relationships between field-derived and remotely sensed canopy closure were not improved using 3D ($PGRND_{PPC}$) versus 2D data (NDVI). This may be due to differences in study area forest structure and methods between the present study and that work (Smith *et al.*, 2009).

Lack of correlation between field and remote sensing derived DTB estimates indicates that point cloud tree delineation could not be used to derive an accurate representation of this metric within these sites. Generally, tree detection is more successful in softwood forests of homogeneous age and spacing (Zhen *et al.*, 2016), attributes not characteristic of this study area. Integration of spectral data with point

cloud data may improve the accuracy of tree detection and should be considered in future studies (Breidenbach *et al.*, 2010; Heinzel and Koch, 2012).

3.4.2 Correlation of snowpack and forest metrics

Significant differences in transect scale snowmelt rate and timing across forest types indicate that forests are an important driver of snow process at this scale. Differences in canopy cover metrics across forest stands were found to drive this difference given their statistically significant difference across forest types. Hydrologic models developed in this region should consider forest cover in their discretization to obtain an accurate representation of melt. Forest cover discretization may be less important for applications focused on modelling peak SWE as significant differences across forest type were not found.

Significant relationships between SMR, SF_{doy} and canopy closure metrics (GF_{55}, $PGRND_{PPC}$ and NDVI) at the point scale are consistent with previous observations of smaller melt rates in areas with denser canopies and more canopy shading (Metcalfe and Buttle, 1995, 1998; Davis *et al.*, 1997; Varhola *et al.*, 2014). The significant, negative relationship between tree height and snow free date is counter-intuitive and was attributed to the clustering of smaller trees in the closed canopy coniferous stand and larger trees in the open deciduous stands as opposed to effects of the tree height.

Differential forest effects on SMR and SF_{doy} were observed between 2016 and 2017. Inter-annual differences in canopy-snowmelt relationships may be due to contrasts in climate conditions and resulting energy flux to the snowpack which includes net solar radiation, net longwave radiation, turbulent fluxes (latent and sensible heat), ground heat, and energy delivered to the snowpack by rainfall. Net radiation is generally the most

important component of the energy balance in forests followed by turbulent heat flux, though the relative importance of these drivers can be highly variable (Kuusisto, 1986). Turbulent fluxes are a function of wind speed, air temperature and relative humidity. Warm, humid conditions result in the transfer of latent heat to the snowpack, increasing with larger wind speeds (known as condensation melt). These conditions are less influenced by slope, aspect, and forest cover than radiation-driven melt (Dingman, 2015).

Larger shortwave irradiance in 2016 possibly promoted more radiation-driven melt, while more rain and higher humidity, in 2017 may have increased condensation melt. Inter-annual difference in the relationship between SMR, SF_{doy} and canopy structure may reflect greater canopy control on melt variability during radiation-driven melt in 2016 compared with smaller canopy influences on the larger turbulent flux contributions to melt in 2017. Nocturnal energy losses may have been greater during melt in 2016 due to the higher frequency of night-time sub-zero temperatures. Such losses are regulated by forests through reduction of wind speed and associated turbulent fluxes and longwave radiation fluxes from the canopy to the snowpack (Dingman 2015). These differences in nocturnal energy losses in 2016 relative to 2017 may have increased variations in SMR across sites and improved the forest-SMR relationship compared to 2017 with less frequent sub-zero temperatures. Metcalfe and Buttle (1998) found the form of the relationship between GF and melt varied inter-annually depending on meteorological conditions primarily due to canopy influences on penetration of solar radiation, turbulent fluxes, and nocturnal energy losses from the snowpack. Musselman et al. (2012) found that the relationship between canopy metrics and SMR was heavily dependent on contrasts in seasonal meteorology between years (e.g., differences in the degree of cloud

cover), which supports our interpretations. The magnitude of SMR was substantially larger in 2016 than 2017. The effect of forest structure on SMR may be more pronounced at higher melt rate magnitudes.

The poor relationship between canopy and peak SWE metrics found here is not consistent with some previous studies. López-Moreno and Latron (2008) found an r of 0.94 between HP-derived GF and SWE max at a 55° zenith angle, while Varhola et al., (2010a) found correlations between peak SWE and field and LiDAR-derived forest structure metrics including LiDAR-derived mean height. Previous findings of strong peak SWE, canopy cover relationships were obtained in environments with a more consistent accumulation period and fewer melt events prior to peak SWE. For example, López-Moreno and Latron (2008) conducted their study in an environment where annual SWE can reach 600 mm, over three times the typical SWE of the current study area. Open areas accumulate more snow due to less canopy interception, but also ablate snow more rapidly due to less canopy shading, reduced attenuation of winds and increased advection. As a result, the relationship between peak SWE and canopy during winters with more intermittent melt may be confounded, such as occurred here. Snow event air temperature, the intensity, frequency and duration of snow events and redistribution by wind can also complicate the relationship between canopy structure, interception, snow accumulation and peak SWE. Winters with many large snowfall events exceeding canopy interception capacities may result in poor relationships between forests and snow accumulation (Boon, 2007), which may have also contributed to the lack of correlation.

The observation that close, larger diameter trees were associated with smaller and later peak SWE is consistent with both previous literature and our understanding of the

relevant physical processes. Tree boles may influence solar shading resulting in reduced melt, and later peak SWE. Snow redistribution and longwave radiation to the snowpack may be influenced by tree boles, affecting peak SWE. Musselman et al. (2008) found snow depth peak was strongly influenced by the presence of tree boles and that depth increased non-linearly outward from the boles. Varhola et al. (2010a) found that DBH was inversely related to peak SWE.

Moderate to strong and significant correlations between field (GF_{55}) and remotely sensed metrics ($PGRND_{PPC}$ and NDVI) of forest structure indicate that SCOOP PPC data or digital orthophotography can be used to derive an adequate representation of canopy openness in this environment. Correlations between PPC- and orthophoto-derived canopy metrics and snowpack were comparable within this study. PPC data are more complex and computationally intensive to process compared to orthophotography and may not provide an advantage over using less complex orthophoto-derived spectral metrics for the applications examined here. However, spectral methods of deriving canopy closure are sensitive to subcanopy herbaceous evergreen vegetation (Smith *et al.*, 2009). In study environments where this is present, 3D datasets may be superior at resolving canopy closure. This distinction between ground cover and canopy may have important implications for snow processes warranting the use of 3D forest structure metrics for describing forest-snowpack relationships in this type of environment.

3.4.3 Limitations

Forest gaps and distance to canopy edge correlate well with snowpack characteristics (Broxton *et al.*, 2015; Moeser *et al.*, 2015a; Huerta *et al.*, 2019; Mazzotti *et al.*, 2019) but were not included within this study. This analysis focused on forest

structure factors and does not account for the contributions of slope and aspect to SWE and melt variability. While these factors were controlled for in the study design, they may still influence melt. Changes in forest structure between the time of the snow measurements (2016 and 2017) and the data acquisition (2013 SCOOP, 2019 LiDAR) may have impacted the accuracy of relationships presented here, although the differences between field and remotely sensed data acquisition timing are within the range of similar studies (Morsdorf *et al.*, 2006; Moeser *et al.*, 2014, 2015b). The strength of relationships between forest structure and snowpack characteristics has been found to vary based on the number of sample locations as lower sample sizes may not capture the range of variability of forest structure and snow metrics. This study was conducted over a limited number of study years and study locations, so conclusions may not be broadly applicable.

3.5 Conclusion

Relationships between forest structure and snowpack characteristics were examined over two winters in the Great Lakes-St. Lawrence Forest Region of Ontario using field and remotely sensed estimates of the tree canopy and boles. Comparisons between field and remotely sensed forest structure and peak SWE, peak SWE timing, snowmelt rate and snow free date were made. Orthophotography-derived 2D spectral metrics and photogrammetric point cloud 3D metrics correlated well with field estimates of canopy density derived from hemispheric photos while tree bole metrics were not successfully derived from LiDAR data. Significant differences in transect scale snowmelt rate and timing across forest types in 2016 indicate that forests can be a significant driver of snow process at this scale. The differences in melt across forest type suggest semi-distributed hydrologic models in this region should consider inclusion of forest cover in model

discretization to obtain an accurate representation of melt. Moderate to strong significant correlations were found at the point scale between snowmelt rate, snow free date and canopy density metrics derived from both field and remotely sensed data. Inter-annual differences in the snowmelt-forest structure relationship were attributed to contrasts in seasonal weather between years where canopy controlled solar radiation likely dominated melt in 2016 versus more spatially uniform turbulent flux-driven melt in 2017. Canopy metrics were not correlated with peak SWE and peak SWE timing, whereas tree bole characteristics were. This is contrary to several previous studies that found stronger correlations between peak SWE and canopy structure and may be explained by a more consistent accumulation period and less mid-winter melt in those studies. Three-dimensional forest structure data derived from photogrammetric point clouds, and LiDAR data and simple orthophoto-derived spectral metrics were highly colinear. This was attributed to the characteristics of this study area and may not be generally applicable.

This study confirmed that widely available remotely sensed data with a broad coverage and frequent acquisition can be used to describe forest-snowpack relationships in Great Lakes-St. Lawrence Forest Region mixed wood, hardwood, and coniferous stands. The successful application of Ontario Imagery Program spectral and point cloud data should encourage future uses of these data to explore forest-snowpack relationships in other regions or investigate the impacts of forest change on snowpack as the imagery are acquired every five years. Future research should evaluate the implications of climate variability on forest-snowpack relationships at more study locations and across a greater range of forest structure and climate conditions.

Chapter 4 Assessing the impact of subbasin SWE calibration and Copernicus SWE assimilation on modelled SWE and flow using the Raven Modelling Framework

Andy D. Beaton[1,2], Ming Han[3], Bryan A. Tolson[3], James M. Buttle[4], Robert A. Metcalfe[1,5]

[1]Environmenal and Life Sciences, Trent University, 1600 West Bank Drive, Peterborough, ON, Canada, K9L 0G2

[2]Surface Water Monitoring Centre, Ministry of Natural Resources and Forestry, 300 Water Street, Peterborough, ON, Canada, K9J 8M5

[3]Department of Civil and Environmental Engineering, University of Waterloo, 200 University Ave W, Waterloo, ON, Canada, N2L 3G1.

[4]School of Environment, Trent University, 1600 West Bank Drive, Peterborough, ON, Canada, K9L 0G2

[5]Aquatic Research and Monitoring Section, Ministry of Natural Resources and Forestry, c/o Trent University, 1600 West Bank Drive, Peterborough, ON, Canada, K9L 0G2.

Unpublished Manuscript

*A.D. Beaton is the primary author of this paper. He designed the study, analyzed the data, and wrote the primary manuscript with guidance, input, and suggestions from coauthors. Ming Han developed the baseline model used in this study and provided assistance with model discretization and calibration.

Abstract

Accuracy of the Copernicus snow water equivalent (SWE) product and the impact of SWE calibration and assimilation on modelled SWE and streamflow was evaluated in this study. Daily snowpack measurements were made at 12 locations from 2016 to 2019 across a 4104 km² mixed-forest basin in the Great Lakes region of central Ontario, Canada. Daily SWE from these sites was used to calibrate a baseline model previously calibrated to lake levels and basin outflow discharge. Daily basin average SWE was calculated from the measured data and compared to bias corrected Copernicus SWE. Bias corrected Copernicus SWE was then assimilated into the model calibrated to subbasin SWE.

The bias corrected Copernicus product agreed well with measured data and provided a good estimate of mean basin SWE. This study demonstrates that the product shows promise for hydrology applications including flood forecasting and water management within the study region.

Calibration to subbasin SWE substantially improved the basin scale SWE estimate, demonstrating the value of including SWE in a multi-objective calibration formulation. Assimilating Copernicus SWE did not improve SWE performance compared to the model calibrated with subbasin SWE, indicating that assimilation of Copernicus SWE may provide little advantage over a well calibrated model. However, when subbasin SWE is not available for model calibration, Copernicus assimilation will likely result in better performance of modelled SWE.

All models had similar streamflow performance. This demonstrates that basin outlet streamflow can be accurately estimated using a model with a poor representation

of distributed SWE. This may be sufficient for applications where estimating flow is the primary water management objective. However, in applications where understanding the physical processes of snow accumulation, melt and streamflow generation are important, such as assessing the impact of climate change on water resources, accurate representations of SWE are required and can be improved via multi-objective calibration or data assimilation, as demonstrated in this study.

4.1 Introduction

Knowledge of the temporal and spatial variability of snow water equivalent (SWE) is important for understanding the Earth's water and energy balance, ecosystem function, and hydrologic processes (Barnett *et al.*, 2005; Riggs and Hall, 2011; Kinar and Pomeroy, 2015). Assessing flood risk, hydropower potential, aquatic ecosystems, water supply and the impacts of climate change on water resources requires accurate estimates of streamflow (Barnett *et al*., 2005; Beaton and Bradford, 2013; Musselman *et al*., 2018). Hydrologic models are valuable tools for estimating SWE and streamflow and can facilitate planning, prediction and decision making (Luce *et al.*, 1998; Jenicek *et al.*, 2016; Hammond *et al.*, 2018).

SWE is typically a state variable within hydrologic models that can be improved by calibrating to observed snowpack measurements. Commonly applied optimization algorithms for automatic calibration of hydrologic models include Simulated Annealing, Genetic Algorithms, Shuffled Complex Evolution, Particle Swarm Optimization and Dynamically Dimensioned Search algorithms (DDS) (Kirkpatrick *et al.*, 1983; Duan *et al.*, 1993; Kennedy and Eberhart, 1995; Tolson and Shoemaker, 2007; Katoch *et al.*, 2021). DSS is a simple and efficient optimization method that searches for an acceptable solution using one tuning parameter and a user defined number of function evaluations. DDS has been shown to perform well relative to other optimization algorithms when applied to hydrologic models (Tolson and Shoemaker, 2007; Arsenault *et al.*, 2014; Yen *et al.*, 2015). Multi-objective calibration is carried out when a model is fit to two or more variables, and when formulated as a multi-objective optimization problem, the resulting solution is a set of non-dominated, Pareto-optimal solutions where one objective function

value cannot be improved without degrading another. The Pareto Archived Dynamically Dimensioned Search (PA-DDS) algorithm is a multi-objective version of DDS and has been successfully applied within many hydrologic modelling studies (e.g. Asadzadeh and Tolson, 2012, 2013; Yang *et al.*, 2017; He *et al.*, 2020).

Multi-objective model calibration has been used to constrain hydrologic models with remotely sensed snow covered area (SCA) and discharge observations (e.g. Parajka *et al.*, 2007; Parajka and Blöschl, 2008; Finger *et al.*, 2011, 2015; Franz and Karsten, 2013; Duethmann *et al.*, 2014; Bennett *et al.*, 2019; Riboust *et al.*, 2019). Bennett et al. (2019) calibrated a SNOW-17 model to MODIS SCA in five basins and found improved snow depletion timing but only moderate improvement in streamflow skill. They found basins with fewer streamflow observations had larger increases in simulated streamflow performance. Finger et al. (2015) tested calibration of the HBV-light model using glacier mass balance, SCA and streamflow and found that calibration only to streamflow resulted in implausible melt rates. They also suggested that calibration to internal state variables may be more important than complexity of process representation and spatial discretization for developing realistic models.

Fewer studies have incorporated SWE into multi-objective calibration (Gao et al., 2017; Tuo et al., 2018; Nemri and Kinnard, 2020). Nemri and Kinnard, (2020) evaluated four calibration strategies using a combination of streamflow and SWE in 12 subbasins across southern Quebec, Canada. Multi-objective calibration to SWE and streamflow improved modelled SWE without significantly degrading simulated streamflow. They found differences in performance across subbasins related to spatial representativeness of point snow measurements, where calibrating to observations in forests did not effectively

define snow parameters in agricultural landscapes. Tuo et al. (2018) tested single and multi-objective calibration to snow observations and discharge using the Soil and Water Assessment Tool in the Italian Alps. A more accurate set of model parameters was identified using multi-objective calibration resulting in better model performance across elevation bands, SWE magnitudes and over both calibration and validation periods.

Another method of improving SWE performance in hydrologic models is assimilation of measured or modelled and remotely sensed SWE products. Widely used data assimilation methods include direct insertion, Kalman and particle filtering (Andreadis and Lettenmaier, 2006; Vuyovich and Jacobs, 2011; Fletcher *et al.*, 2012; Magnusson *et al.*, 2014, 2017; Smyth *et al.*, 2020). With direct insertion model states are replaced with observed values (Liston *et al.*, 1999; Fletcher *et al.*, 2012). This method is limited as it ignores observation and model uncertainties and can lead to extreme corrections in the output (Magnusson *et al.*, 2017). Filter methods explicitly address model and observation uncertainty by perturbing model forcings and/or parameters and generating a probability density of the system state variables. The ensemble of simulations have unique parameter sets for each assimilated value corrected towards observed data providing potential advantages over standard single-set calibration (Smyth *et al.*, 2019)**.** Particle filtering is more flexible as it does not require a parametric form like the Kalman filter (Moradkhani, 2008; Van Leeuwen, 2009) and was found to predict SWE better than ensemble Kalman filtering (Leisenring and Moradkhani, 2011) . An ensemble of model simulations (particles) is generated for each time-step. These are then filtered based on a probabilistic deviation from the observed state variable value and propagated forward to the next time-step (Moradkhani *et al.*, 2005).

Many studies have investigated assimilation of SCA into hydrologic models to improve simulations for practical applications and to explore processes (e.g. Clark *et al.*, 2006; Udnæs *et al.*, 2007; Roy *et al.*, 2010; Yatheendradas *et al.*, 2012; Liu *et al.*, 2013; Thirel, Salamon, Burek, 2015; Stigter *et al.*, 2017). Assimilation of SCA is limited when SWE is a variable of interest and can be restricted to late season melt when bare ground is exposed. Accuracy of SCA assimilation is also limited by the lag time between snowmelt and SCA depletion (Clark *et al*., 2006). Several studies have assimilated SWE observations, SWE products or a combination of both into hydrologic models (e.g. Vuyovich and Jacobs, 2011; Bergeron *et al*., 2016; Dziubanski and Franz, 2016; Griessinger *et al*., 2016; Huang *et al*., 2017a, 2017b; Leach *et al*., 2018; Zahmatkesh *et al*., 2019; Micheletty *et al*., 2021). Assimilation of snowpack data generally improves simulated SWE and SCA but has variable effects on modelled discharge, which has been found to be the result of several factors. Variable effects of snowpack data assimilation on streamflow was found to be dependent on the magnitude of SWE, where locations and years with larger SWE resulted in increases in modelled streamflow skill (Udnæs *et al.*, 2007; Dziubanski and Franz, 2016; Griessinger *et al*., 2016). Griessinger et al. (2016) assessed assimilation of snow measurements into the HBV-light hydrologic model in 20 catchments in Switzerland and found that simulated runoff was improved at higher elevations, especially in years with large snow accumulations. Dziubanski and Franz, (2016) assimilated bias corrected AMSR-E SWE in a coupled SNOW17-Sacramento Soil Moisture Accounting (SACSMA) model using an Ensemble Kalman Filter and found streamflow skill increased in basins with higher discharge magnitudes and melt runoff. Previous research has found that the accuracy of assimilated data impacts modelled

streamflow skill where larger error in assimilated SWE resulted in degraded streamflow simulations (Dressler *et al*., 2006; Yatheendradas *et al*., 2012; Liu *et al*., 2013; Thirel *et al*., 2013; Dziubanski and Franz, 2016; Micheletty *et al*., 2021). Yatheendradas et al. (2012) used direct insertion to assimilate MODIS SCA and found streamflow skill decreased in densely forested areas where SCA is poorly represented by the optical remotely sensed data. Dressler et al. (2006) assimilated blended observed and remote-sensed SWE into the precipitation-runoff modelling system (PRMS) using direct replacement in two study basins. They found streamflow skill decreased in one basin and attributed this to larger assimilated SWE error in the poorer performing basin. Quality of the original (open loop) model including calibration methods, model forcings, and streamflow data has been found to effect assimilation performance (Huang *et al*., 2017b; Micheletty *et al*., 2021). Data assimilation methods (Thirel *et al*., 2015) and parameterization of the assimilation algorithm may also affect SWE and streamflow skill (Huang *et al*., 2017a; Micheletty *et al*., 2021).

Observed SWE data are rarely available as SWE is labor intensive and expensive to measure in the field. Field-based measurement of SWE typically captures less than 1% of a basin's snowpack and spatially distributed measurements are infrequent (Sturm, 2015). Remotely sensed and modelled gridded SWE products provide estimates across larger extents and at higher frequencies than can feasibly be measured. Several modelled (e.g. GLDAS, ERA-Interim/Land, and MERRA), remotely sensed (e.g. NASA AMSR-E, JAXA AMSR-2) and data assimilated (e.g. Copernicus, ESA Globsnow, SNODAS and CMC Analysis) daily gridded SWE datasets generated by government and academia are available at various spatial and temporal resolutions (Brown *et al*., 2003; Rodell *et al*.,

2004; Kelly, 2009; Rienecker *et al*., 2011; Takala *et al*., 2011; Balsamo *et al*., 2015; Luojus *et al.,* 2017). Copernicus is a daily 5 km resolution SWE product that has data from 2006 up to near real time. It is distributed by the European Commission for use by government, research institutions and the hydropower industry for runoff modelling and flood forecasting, planning for hydropower generation, agriculture, forestry, water supply and climate change modelling (Luojus *et al*., 2017; European Commission Joint Research Centre, 2022).

While previous research has focused on multi-objective calibration using SWE or SWE assimilation, the comparative effect of these two approaches on model performance remains unresolved. The objectives of this study are to: 1) estimate daily, basin average SWE from distributed subbasin measurements of snow depth and density; 2) compare measured basin average SWE to the Copernicus SWE product; 3) calibrate and validate a baseline hydrologic model developed by Han et al. (2021) using subbasin SWE measurements; 4) assimilate Copernicus SWE into the model using a particle filter; and 5) evaluate and compare the performance of the following three models to ascertain the effect of calibrating to subbasin SWE and assimilating Copernicus SWE on model performance using:

i) A baseline model calibrated to lake levels and basin outlet discharge

ii) Model (i) calibrated to subbasin SWE

iii) Copernicus SWE assimilated into model (ii) using a particle filter.

To the author's knowledge this is the first study to validate Copernicus SWE at the basin scale, assimilate Copernicus SWE into a hydrologic model, and assimilate SWE using the Raven hydrologic modelling framework. This study contributes to snow

hydrology science by elucidating the accuracy and value of a readily available, spatially distributed SWE dataset for hydrologic modelling at the basin scale in a mixed forest region and the relative impact of SWE calibration and SWE data assimilation on model performance. In addition, this study contributes to our knowledge of the effects of climate change on water availability and hazard risk in nival basins. Change to snow processes is one of the earliest and most significant impacts of a changing climate on basin hydrology, and building hydrologic models that more accurately represent snow, snow processes, and the movement of meltwater will allow us to better understand the hydrologic consequences of these potential changes. This study was conducted in a basin situated in the Great Lakes drainage area, which contain nearly 20% of the earth's freshwater. Great Lakes hydrology is dominated by a response to seasonal snow cover. Understanding SWE and streamflow processes in this geography will help protect this vital source of drinking water, food, energy, transportation, recreation, and its diverse ecosystem (Ontario Ministry of the Environment, 2016).

4.2 Methods

4.2.1 Study area

The Petawawa basin, situated in central Ontario, has a drainage area of 4104 km^2, and a mean elevation of 356.11 masl. The basin is topographically defined by the Precambrian Upland (the Algonquin dome) in the west and the Ottawa Lowlands in the east (Cumming, 2009). Elevations on the Algonquin dome reach up to 560 masl, whereas elevations in the Ottawa Lowlands range from 180-300 masl (Cumming, 2009; Figure 4.1). The elevation difference and lake effect from Georgian Bay have a combined influence on basin climate, producing lower temperatures and higher

precipitation on the dome. The frost free period varies from 90 days in the uplands to 130 days in the lowlands and annual total precipitation ranges from over 1100 mm in the west of the basin to less than 750 mm in the east (Cumming, 2009). The cooler, wetter uplands are predominantly covered by tolerant hardwoods and hemlock with white and red pine, poplar and white birch in the warmer, drier lowlands (Cumming, 2009). The basin is almost entirely situated within Algonquin Provincial Park and is largely inaccessible during the winter. A Water Survey of Canada water level and streamflow gauge (Petawawa River Near Petawawa (02KB001)) is located at the basin outlet (Figure 4.1).

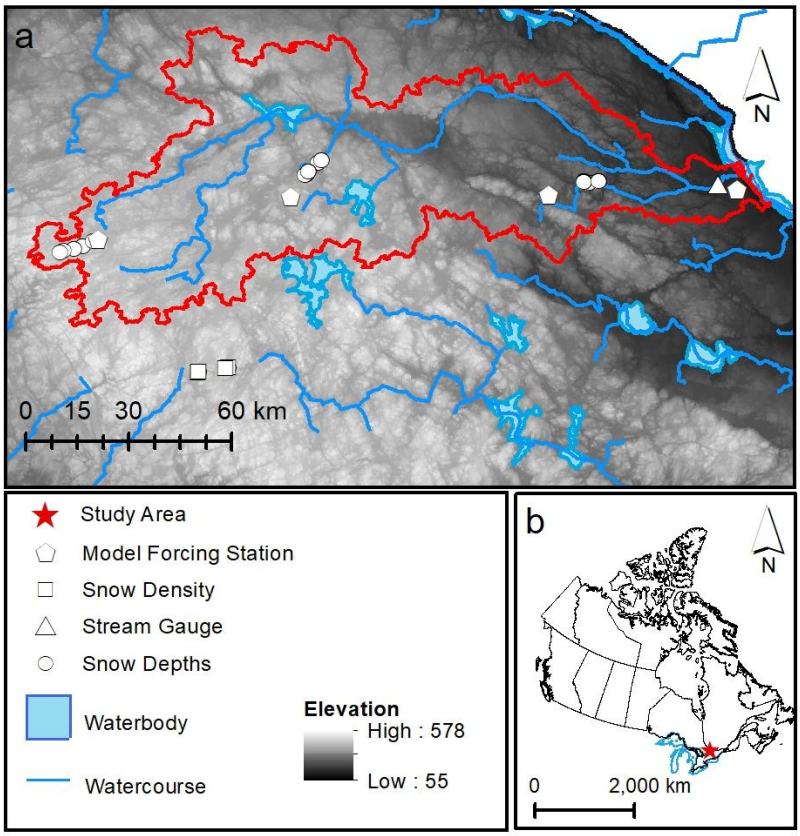

Figure 4.1: Study area map with snow depth, snow density and streamflow measurement locations, locations where model forcings (temperature and precipitation) are measured, elevations, and the hydrographic network.

4.2.2 SWE estimation from measurements

A stratified sampling approach was used to measure SWE based on the assumptions that SWE is controlled by 1) a west to east precipitation gradient resulting from lake effect snow from the Georgian Bay and Lake Huron (Suriano and Leathers, 2017); 2) the Algonquin dome effect on temperature and precipitation (Cumming, 2009); and 3) land cover control on snow interception and energy balance during accumulation and ablation (Adams, 1976).

Field measurements were made over four winters during the 2016 to 2019 water years. Snow measurements were made in three regions created by dividing the basin into

three zones of equal area (west, central, and east) and stratified using criteria one and two above. Within each region, daily snow depth was measured in four land cover types (wetland, coniferous, deciduous, and mixed woods forest; Figure 4.1). Sites were located using the Algonquin Forest Resource Inventory and Ontario Land Cover Compilation (Ontario Ministry of Natural Resources and Forestry, 2007, 2014). Site suitability was verified in the field prior to establishing each sample location. Snow depths were measured using an array of time-lapse cameras and rulers secured into the ground as shown in Figure 4.2. Three rulers were spaced approximately 1 m to 2 m apart in front of each time-lapse camera to capture fine scale variability. This is a cost-effective method of automatically measuring daily, spatially distributed snow depths in a remote basin such as the Petawawa (Kim *et al.*, 2007; Parajka *et al.*, 2012; Hedrick and Marshall, 2014; Fortin *et al.*, 2015; Lundberg *et al.*, 2016).

Figure 4.2: Example of trail camera and rulers for measuring snow depth at the deciduous site in the east region.

Snow depth at each site was calculated from the mean of the three rulers. Due to access restrictions, snow density was measured at a location adjacent to the basin along Highway 60 (HWY60) across the four land cover types (Figure 4.1). Snow density was linearly interpolated between 10, 8, 5 and 7 measurement dates in the 2016, 2017, 2018 and 2019 water years, respectively, to create a daily snow density time series for each land cover type. Linearly interpolated daily snow density from the HYW60 sites and daily snow depths were used to calculate daily SWE within each of the four land covers within each of the three regions in the basin (Equation 4.1).

$$SWE_l = \Theta_l \overline{d_{ru}} * 10 \quad 4.1$$

where SWE_l (mm) is the SWE for land cover *l*, Θ_l (g/cm^3) is the HWY60 snow density for land cover *l*, and $\overline{d_{ru}}$ (cm) is the mean snow depth at ruler set *ru*. Yao et al. (2018) demonstrated the applicability of the regression-based method of McCreight and Small (2014) for estimating snow density from depth in a similar study environment. Linear interpolation of snow density produced more accurate estimates of SWE than the McCreight and Small method based on tests using daily SWE and depth calibration data for the study period at a station 85 km soutwest of the center of the basin and data from within the basin but outside the study period. Land cover weighted mean SWE was calculated for each region (Equation 4.2).

$$SWE_R = \sum_{l=1}^{N=4} w_l SWE_l \quad 4.2$$

where SWE_R (mm) is the SWE in each region R, w_l is the weight for each land cover type l, SWE_l (mm) is the SWE at each land cover type l and N is the number of land cover types in each region. Daily mean basin SWE was calculated as the average of the regional SWE values.

$$SWE_b = \overline{SWE_R} \quad 4.3$$

where SWE_b (mm) is mean basin SWE, and SWE_R (mm) is the SWE for each region R. Snow cores using an ESC-30 gravimetric sampler were taken at each site in February or March of 2016, 2017 and 2019 to verify the trail camera SWE estimates (Goodison *et al.*, 1987).

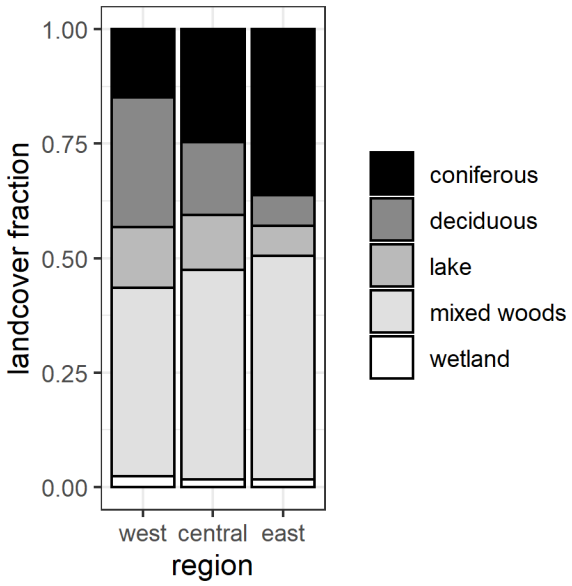

Figure 4.3: Land cover fraction for each basin region.

4.2.3 Copernicus SWE

Copernicus applies the emission model inversion methodology developed by Pulliainen (2006) and refined by Takala et al. (2011). The algorithm assimilates a

background field of kriged snow depth observations into the 25 km resolution passive microwave depth estimate from the Special Sensor Microwave Imager/Sounder (SSMIS). A constant snow density of 0.24 g/cm^3 is used to calculate SWE (Luojus *et al.*, 2017). The 25 km SWE estimate is resampled to 5 km using the 5 km ESA Globsnow Visible Infrared Imaging Radiometer (VIIRS) product and NOAA Ice Mapping System (IMS) optical remote sensing to identify snow free areas.

Daily Copernicus SWE was downloaded from the Finnish Meteorological Institute in NetCDF format and averaged over the Petawawa basin area to produce a daily SWE time series using R statistical computing software (R Development Core Team, 2011). Mean error between basin average trail camera and Copernicus SWE was calculated from March 15th to June 1st and values from 2016 and 2017 were used to bias correct the raw product for known issues during melt (Beaton *et al.*, 2019). Mean bias subtraction was used as it has been shown to produce reasonable results for correcting snow products (Dziubanski and Franz, 2016; King *et al.*, 2020)

4.2.4 Hydrologic model

Han et al. (2021) developed a hydrologic model for the Petawawa basin using the Raven Hydrologic Modelling Framework (Craig et al., 2020) and extensively calibrated it to a network of natural lake levels and discharge at the basin outlet. This model was discretized into 521 subbasins characterized by channel properties and connectivity to adjacent subbasins, and 890 hydrologic response units (HRUs) discretized by unique combinations of land use, vegetation, terrain and soils classes using the BasinMaker GIS toolbox (Han *et al.*, 2022). The Han et al. (2021) model HRUs were divided into forest, open and lake land covers. For the current study, the model was modified to include five

land classes - lake, wetland, coniferous, deciduous, and mixed woods – resulting in 2733 HRUs (but the same original 521 subbasins). This is henceforth referred to as the baseline (BL) model. This model uses daily precipitation, minimum and maximum air temperature forcings from four meteorological stations (Figure 4.1).

Model processes and parameters are described below, and calibrated parameters are summarized in Table 4.1. Precipitation is partitioned into rain or snow using the two-parameter linear method from the HBV model. A parameter establishes the rain/snow transition temperature, and another sets the range in air temperature along which the partitioning is applied to incoming precipitation. Snow accumulates into the SNOW storage compartment unless it is intercepted by the canopy which is a linear function of leaf area index (LAI) and stem area index and is limited by the maximum interception capacity. Snow is sublimated from the canopy at a rate determined by the potential evapotranspiration (PET) and the forest cover. Potential melt is calculated using the HBV corrected degree day approach which is driven by air temperature and day angle with corrections made for forest cover, slope, and aspect. Melted snow moves to the SNOW_LIQ compartment. Liquid snow can move back to the SNOW compartment based on air temperature and a refreeze factor parameter or to the PONDED_WATER storage compartment based on the maximum liquid snow water content parameter (Raven : User's and Developer's Manual v3.6).

PET is calculated with the Penman Monteith method that is driven by atmospheric variables including net radiation and vapor pressure gradient (both estimated from forcings) and the vegetative variables leaf conductance and LAI (Raven : User's and Developer's Manual v3.6; Dingman, 2015). There are three soil layers: forest floor (top),

ablation till (middle) and basal till (bottom). The Green-Ampt method is used to calculate infiltration from PONDED_WATER into the soil layers and water percolates to the second and third soil layer using the GAWSER linear method where percolation is dependent on a maximum percolation rate parameter, soil field capacity and water content. Soil evaporation from the forest floor is driven by PET and is linearly proportional to soil saturation. Baseflow is generated from all soil layers using the threshold base power law method where the rate is non-linearly proportional to soil water storage and commences once the soil layer exceeds a threshold saturation (Raven : User's and Developer's Manual v3.6). Capillary rise can occur from basal till to the ablation till and is linearly proportional to the ablation till saturation and is constrained by a maximum interflow rate parameter.

Hydrologic routing to the subbasin channels is calculated using a triangular unit hydrograph based on time to peak and time of concentration estimated from subbasin properties. In channel, lake and reservoir routing is based on an iterative level-pool approach, with lake outlets modelled as having a broad crested weir and is parametrized by channel characteristics. Lake crest widths (i.e., broad crested weir width) were either calibrated directly for monitored lakes or calculated using the following equation for all other simulated, but unmonitored, lakes.

$$w_i = \alpha * (DA_i)^n \quad 4.4$$

where w_i is the crest width of lake *i*, DA_i is the drainage area of lake *i* in km^2, and α and *n* are coefficient parameters (Han *et al.*, 2021).

Table 4.1: Calibrated model parameters, ranges, and optimal values for the baseline model calibrated to lake levels and flow (BL) and the BL model calibrated to subbasin SWE (BLS). Darker shading of the "Percent difference BL-BLS (%)" column indicates larger percent differences.

process	parameter	description	minimum	maximum	BL value	BLS value	Percent difference BL-BLS (%)	units
snow-rain partitioning	RAINSNOW_DELTA	range of values over which linear transition is applied	0	6	1.42	2.74	64	°C
	RAINSNOW_TEMP	rain-snow transition temperature	-4.5	2	-1.98	-4.50	78	°C
snowmelt and refreeze	MLT_F	snowmelt factor	1	9	6.62	3.00	75	mm/d/°C
	HBV_MLT_A_C	aspect snowmelt correction	0.1	1	0.91	0.12	152	none
	Rfrez_F	liquid water refreeze factor	0	4	0.12	0.00	200	mm/d/°C
	MELT_FOR_CORR_WET	wetland melt correction factor	0.8	1	1.00	1.00	0	none
	MELT_FOR_CORR_DEC	deciduous forest melt correction factor	0.7	1	0.72	0.76	6	none
	MELT_FOR_CORR_MIX	mixed forest melt correction factor	0.6	1	0.97	0.75	26	none
	MELT_FOR_CORR_CON	coniferous forest melt correction factor	0.5	1	0.51	0.75	39	none
vegetation	SRL_WET	wetland leaf area index correction factor	0.1	0.3	0.14	0.29	66	none
	SRL_DEC	deciduous forest leaf area index correction factor	0.1	0.5	0.11	0.23	70	none
	SRL_MIX	mixed forest leaf area index correction factor	0.3	0.8	0.80	0.80	0	none
	SRL_CON	coniferous forest leaf area index correction	0.8	1	0.91	1.00	10	none
snow interception	SNOW_ICEPT_FACT_WET	wetland snow interception correction factor	0.1	0.3	0.26	0.30	15	none
	SNOW_ICEPT_FACT_DEC	deciduous snow interception correction factor	0.1	0.3	0.30	0.25	17	none

	SNOW_ICEPT_FACT_MIX	mixed forest snow interception correction factor	0.1	0.5	0.10	0.38	114	none
	SNOW_ICEPT_FACT_CON	coniferous snow interception correction factor	0.2	0.6	0.40	0.47	16	none
	MAX_SNOW_CAPACITY	maximum canopy snow storage	3	30	3.44	27.10	155	mm
soil	D_FF	vertical depth of forest floor layer	0.1	0.5	0.17	0.30	58	m
	D_AT	vertical depth of ablation till layer	0.1	2	1.36	1.08	23	m
	WFPS	wetting front PSI	0.9	27	11.20	10.90	3	mm
	HYD_COND_FF	hydraulic conductivity	10	1000	717	342	71	mm/d
	FC_FF	field capacity of the forest floor	0.1	0.7	0.25	0.14	60	none
	FC_AT	field capacity of the ablation till	0.1	0.7	0.18	0.12	34	none
	FC_BT	field capacity of the basal till	0.5	0.99	0.51	0.56	8	none
	MABASEFLOW_RATE_FF	maximum baseflow rate at the forest floor	10	1000	643	31	182	mm/d
	MABASEFLOW_RATE_AT	maximum baseflow rate at the ablation till	10	1000	295	974	107	mm/d
	MABASEFLOW_RATE_BT	maximum baseflow rate at the basal till	10	1000	206	162	24	mm/d
	BASEFLOW_N_FF	baseflow parameter n for the forest floor	0.1	4	2.81	0.14	181	none
	BASEFLOW_N_AT	baseflow parameter n for the ablation till	0.1	4	3.92	3.28	18	none
	BASEFLOW_N_BN	baseflow parameter n for the basal till	0.1	4	4.38	5.08	15	none
	MAPERC_RATE_FF	maximum percolation rate at the forest floor	10	1000	24	347	174	mm/d
	MAPERC_RATE_AT	maximum percolation rate at the ablation till	10	1000	97.07	10.00	163	mm/d
	MACAP_RISE_RATE	maximum capillary rise	10	1000	218	988	128	mm/d
potential evaporation	LAKE_PE_CORR	lake potential evaporation correction factor	0.5	1.5	1.40	1.21	14	none
	PE_CORR	potential evaporation correction factor	0.5	1.5	1.12	0.96	15	none

	N_MULTI	Manning's n correction factor	0.54	3.28	2.28	0.67	109	none
	W_A0	alpha coefficient parameter for crest width equation*	0.1	0.8	0.52	0.24	73	none
	W_N0	n coefficient parameter for crest width equation*	0.1	0.8	0.11	0.31	93	none
	W_CEDAR	crest width at Cedar Lake outlet	0.1	100	46.64	48.30	3	m
	W_BIG_TROUT	crest width at Big Trout Lake outlet	0.1	100	17.82	19.10	7	m
	W_GRAND	crest width at Grand Lake outlet	0.1	100	16.22	21.50	28	m
	W_LAVIELLE	crest width at Lavielle Lake outlet	0.1	100	16.76	16.50	2	m
	W_MISTY	crest width at Misty Lake outlet	0.1	100	7.07	6.23	13	m
routing	W_ANIMOOSH	crest width at Animoosh Lake outlet	0.1	100	6.42	4.54	34	m
	W_TRAVERSE	crest width at Traverse Lake outlet	0.1	100	27.70	26.00	6	m
	W_BURNTROOT	crest width at Burntroot Lake outlet	0.1	100	19.07	20.00	5	m
	W_LA_MUIR	crest width at La Muir Lake outlet	0.1	100	3.75	5.07	30	m
	W_NARROWBAG	crest width at Narrowbag Lake outlet	0.1	100	8.47	10.90	25	m
	W_LITTLE_CAUCHON	crest width at Little Cauchon Lake outlet	0.1	100	10.51	10.60	1	m
	W_HOGAN	crest width at Hogan Lake outlet	0.1	100	10.12	10.10	0	m
	W_NORTHDEPOT	crest width at North Depot Lake outlet	0.1	100	14.13	12.30	14	m
	W_RADIANT	crest width at Radiant Lake outlet	0.1	100	21.20	24.10	13	m
	W_LOONTAIL	crest width at Loontail outlet	0.1	100	2.03	1.15	55	m

* See equation 4.4

The BL model was automatically calibrated using DDS (Tolson and Shoemaker, 2007). The DDS objective function was an aggregate of Kling Gupta Efficiency (KGE) values using lake levels and discharge at the basin outlet (Han *et al.*, 2021). KGE is an aggregate of linear correlation, bias and variance and is commonly applied in hydrologic modeling (Equation 4.5 ; Gupta *et al.*, 2009):

$$KGE = 1 - \sqrt{(1-r)^2 + \left(\frac{\sigma_{sim}}{\sigma_{obs}} - 1\right)^2 + \left(\frac{\mu_{sim}}{\mu_{obs}} - 1\right)^2} \quad 4.5$$

where r is the linear correlation between observed and simulated values, σ_{sim} and σ_{obs} are the standard deviations of the observations and simulations, respectively, and μ_{sim} and μ_{obs} are the observation and simulation means, respectively. The KGE for discharge was calculated using equation 4.5 with daily observed values at the Water Survey of Canada Petawawa River Near Petawawa (02KB001) gauge. Lakes were incorporated into the objective function using a relative deviation KGE (Equation 4.6; Han *et al.*, 2021):

$$KGED = 1 - \sqrt{(1 - r(N(sim_l), N(obs_l)))^2 + \left(\frac{\sigma_{N(sim_l)}}{\sigma_{N(obs_l)}} - 1\right)^2} \quad 4.6$$

where r is the linear correlation between normalized observed $N(obs_l)$ and normalized simulated $N(sim_l)$ lake water levels, and $\sigma_{N(sim_l)}$ and $\sigma_{N(obs_l)}$ are the standard deviations of normalized lake level observations and simulations, respectively. The overall objective function for DDS calibration of the BL model (OF_{Q+LAKE}) was the sum

of the discharge KGE and the unweighted averaged KGED of 15 lake level gauges within the basin (Equation 4.7; Han *et al.*, 2021):

$$OF_{Q+LAKE} = KGE_Q + \overline{KGE_{LAKE}^{15}} \quad 4.7$$

OF_{Q+LAKE} has a maximum value of 2.0 with KGE_Q and $\overline{KGE_{LAKE}^{15}}$ both having maximum values of 1.0.

A second model, henceforth referred to as the baseline SWE (BLS) model, was the BL model with additional calibration to SWE at each of the 12 snow measurement locations**.** The BLS model was automatically calibrated using PA-DDS (Asadzadeh and Tolson, 2013)**.** Two objective functions were defined for calibrating the model to lake level, discharge and subbasin SWE. The objective function from the BL calibration (OF_{Q+LAKE}) was used in addition to a second objective function for SWE that was a landscape-weighted average of KGE values across the wetland, coniferous, deciduous, and mixed forest trail camera measurement locations:

$$OF_{SWE} = (\sum_{s=1}^{N=12} w_s * KGE_s) \quad 4.8$$

where w_s is the basin landscape area of site *s* and, KGE_s is the KGE at site *s*. The maximum value of OF_{SWE} was 1.0.

The output of PA-DDS is a set of calibration solutions that describes the tradeoff between the two objective functions (i.e., non-dominated solutions). Model parameters from a non-dominated solution that balanced the two objectives were selected as the

deterministic calibrated model. BL DDS and BLS PA-DDS were run with 5000 iterations using the Ostrich model calibration software (Shawn Matott, 2017). Models were calibrated in 2016, 2017 and validated in 2018, 2019. Calibration was run multiple times to verify consistency in the selected solutions.

4.2.5 Data assimilation

A particle filter was run from November 1st, 2015, to July 1st, 2019, using BLS and propagating 100 particles per day. Filter results typically stabilize when propagating 100 or more particles (Magnusson *et al.*, 2017). A warm-up period from January 1st, 2014, was run to initialize state variables prior to data assimilation. Simulations were varied to reflect model uncertainty by perturbing forcings at each meteorological station, and by perturbing selected snow related parameters. Following Smyth et al. (2020) forcings were perturbed by adding random noise from a uniform distribution bound by ±50% of the forcing value. A qualitative sensitivity analysis was conducted by running the model with a limited number of particles and over select time periods to determine snow related parameters to perturb within the particle filter. Each particle's parameter value was randomly selected from a uniform distribution within a range of plausible values. Parameter ranges from the Raven Hydrologic Modelling Framework manual (Raven : User's and Developer's Manual v3.6) were used, with some modifications based on manual calibration (Table 4.1). For each simulation day, a distribution of 100 potential SWE and flow estimates was generated by running the BLS model with perturbed forcings and parameter values. Particles were then filtered based on assigned weights following Smyth et al. (2020) with initial particle weights set to 1/number of particles = 0.01. Weights were multiplied by the previous time-step's weights to decrease the

likelihood of selecting particles that diverge from the observed values over several consecutive days (Smyth *et al*. 2020):

$$w_k^i = w_{k-1}^i \, p\left(z_k \middle| x_k^i\right) \tag{4.9}$$

where w_k^i is the weight of particle *i* at time-step *k*, z_k is the observed SWE at time-step *k*, $x_k^i$is the modelled SWE for particle *i*, at time-step *k* and $p\left(z_k \middle| x_k^i\right)$ is the probability of observing z_k given x_k^i. Weights were assigned to each particle based on a normally distributed likelihood function. The likelihood function assigns lower weights to modelled values that have larger differences from the observed value (Equation 4.10; modified from Smyth *et al*. 2020):

$$p\left(z_k \middle| x_k^i\right) = \frac{1}{\sqrt{2\pi * SD}} e^{\left[-\frac{1}{2}\left(\frac{z_k - x_k^i}{SD}\right)^2\right]} \tag{4.10}$$

where SD is the standard deviation of the likelihood function distribution. The SD parameter was set to 5% of SWE with a minimum value of 5 mm. The weights were normalized to sum to 1, then particles were filtered using stochastic universal sampling (Kitagawa, 1996). A cumulative distribution function was created from the particle weights and a random number between 1 and 1/number of particles (0.01) was generated. The particle associated with the location that the random value lands on the cumulative distribution function was selected, another random number within the stated range was generated, added to the previous random number and the particle associated with this value of the distribution was selected. This process continued for the selection of 100 particles. This method generally selects particles with higher weights but introduces

stochastic variability into the selection. Selected particle model states were used for the next time-steps model runs. The particle filter was coded within the R statistical computing software with the Raven executable called within R. Perturbations to forcings and parameters were made by modified Raven input files within R before each model run (R Development Core Team, 2011). The particle filter model is referred to as PF throughout the paper.

4.2.6 Evaluation metrics

Snow core SWE was compared to trail camera SWE using Pearson's r, mean absolute error (MAE) and percent bias (PBIAS) to evaluate the accuracy of the SWE estimate from the trail camera depths and interpolated snow density. Daily trail camera SWE was compared to raw and bias corrected Copernicus SWE to evaluate product accuracy using KGE and bias.

KGE and the difference in KGE between models was calculated to evaluate the performance of the three models during model calibration (2016, 2017) and validation (2018, 2019). SWE simulations were compared to the trail camera estimate and flow simulations were compared to observed basin outlet discharge. Model and Copernicus SWE performance was assessed using the following criteria applied to KGE; poor performance ($-\infty$ to 0.48), medium performance (0.48 to 0.65), good performance (0.65 to 0.83), excellent performance (0.83 to 1.0) (Mai *et al.*, 2022). SWE statistics were calculated during the snow season (November 1st to May 1st) and flow statistics were calculated from April 1st to July 1st to evaluate the rising limb, peak, and recession of the melt hydrograph. The difference between BL and BLS KGE was calculated to evaluate

the effect of the SWE calibration on model performance. The PF-BL and PF-BLS KGE differences were compared to evaluate the benefit of assimilating Copernicus SWE.

4.3 Results

4.3.1 Evaluation of measured and Copernicus SWE

The trail cameras were reliable for the majority of days with only 8.2% of the data missing due to camera malfunction or poor ruler visibility. Trail camera SWE compared well with snow core SWE with Pearson's r of 0.80 and a land cover weighted MAE of 24.9 mm. The trail camera SWE estimate was larger than snow core SWE with a land cover weighted percent bias of 12.5 % (Figure 4.4). All land cover types had similar correlations between snow core and trail camera SWE.

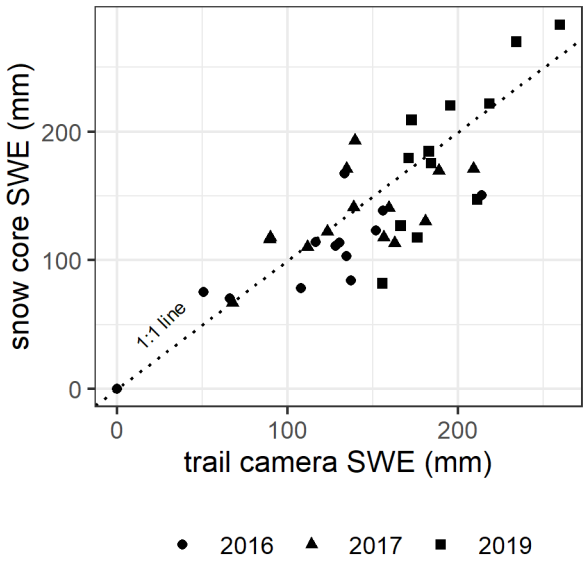

Figure 4.4: Snow core SWE versus trail camera SWE.

Basin average raw (not biased corrected) Copernicus KGE ranged from good (three of the four study years) to excellent with a mean annual bias of -6.4 mm and a mean bias during accumulation and ablation of 4.9 mm and -33.8 mm (Table 4.2) when compared with the trail camera-derived basin average. Mean bias during model calibration years

(2016, 2017) was -26.8 mm. Copernicus SWE was bias corrected by adding 26.8 mm during ablation (March 15 to June) for each year, when snow was present. Bias corrected KGE performance was excellent for all years except 2018. Correction reduced annual bias to 0.8 mm, accumulation bias was not affected, and mean ablation bias was reduced to -7.6 mm (Table 4.2; Figure 4.5).

Table 4.2: Goodness of fit statistics for SWE estimates from the trail camera versus the raw and bias corrected Copernicus SWE. KGE values are coloured by performance classification where good = green (0.65 to 0.83) and excellent = blue (0.83 to 1.0).

	Annual KGE		Annual Bias (mm)		Accumulation Bias (mm)		Ablation Bias (mm)	
	raw	corrected	raw	corrected	raw	corrected	raw	corrected
2016	0.79	0.93	-11.5	-3.6	-1.1	-1.1	-30.5	-8.1
2017	0.85	0.94	-6.4	0.1	-0.7	-0.7	-23.1	2.5
2018	0.67	0.73	2.9	9.5	12.2	12.2	-20.5	4.2
2019	0.77	0.88	-10.3	-2.6	9.2	9.2	-61.0	-29.2
mean	0.77	0.87	-6.4	0.8	4.9	4.9	-33.8	-7.6

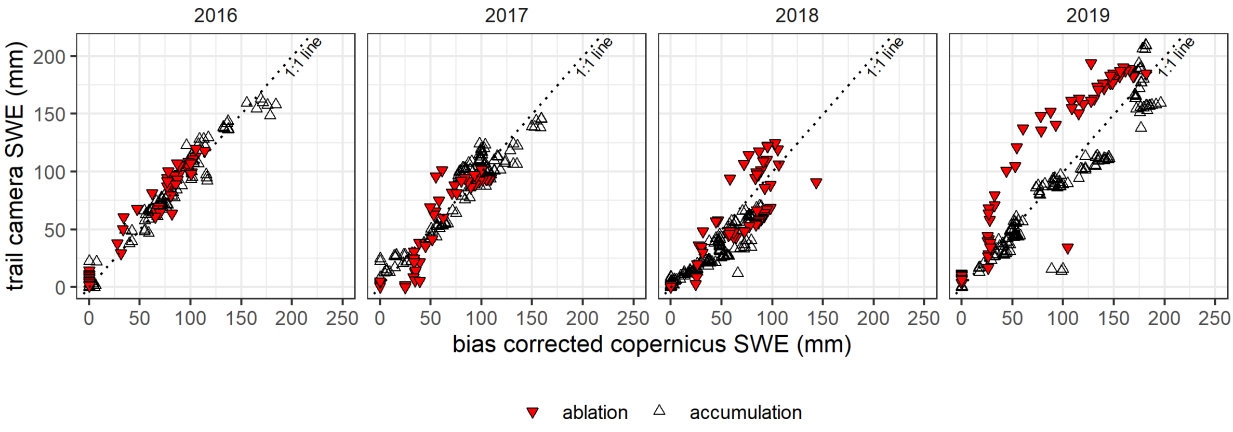

Figure 4.5: Scatterplot of basin average SWE estimate from trail camera versus bias corrected Copernicus SWE during accumulation (November to March) and ablation (March 15 to June).

4.3.2 Subbasin scale calibration and validation

BL DDS calibration yielded an OF_{Q+LAKE} equal to 1.86. This BL calibration yielded an OF_{SWE} equal to -0.24 (Figure 4.6). A non-dominated solution of the PA-DDS was selected with an OF_{Q+LAKE} of 1.83 and an OF_{SWE} of 0.70 (Figure 4.6). The range of OF_{SWE} was low (Figure 4.6) but there was variability in the dominated solutions and repeated runs of PA-DDS also produced small OF_{SWE} ranges.

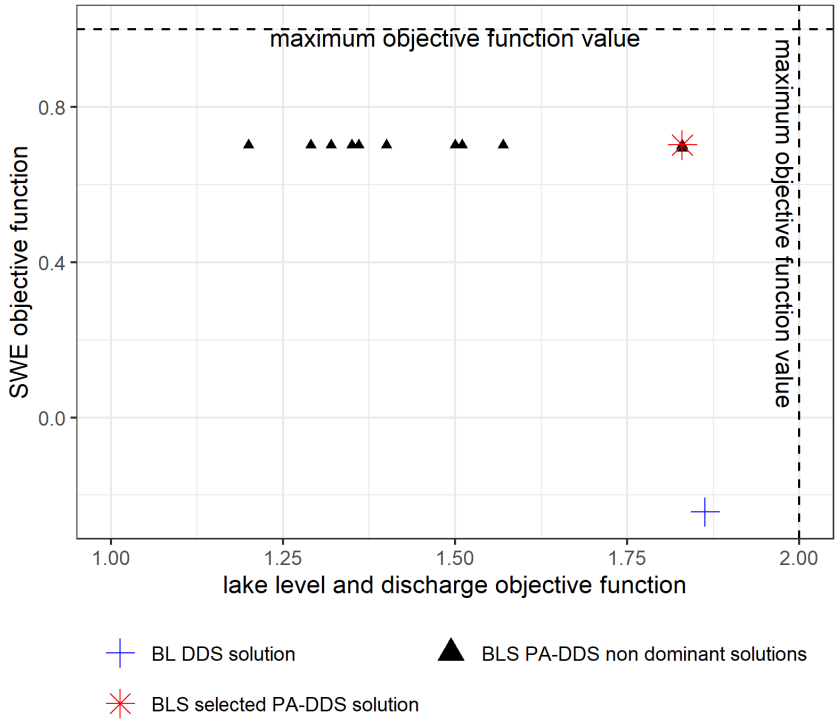

Figure 4.6: Baseline model calibrated to lake levels and flow (BL) DDS calibration solution and the BL model calibrated to subbasin SWE (BLS) PA-DDS calibration non-dominated and selected solutions. Non-dominated solutions are a set of solutions in the objective space that cannot be improved without degrading at least one of the other objectives. The maximum objective function value was 1.0 for BLS PA-DDS and 2.0 for the BL DDS objective function.

There were differences in most snow related parameters between BL and BLS. The melt factor in BL was more than twice that of BLS:, 6.62 mm/d/°C and 3.0 mm/d/°C, respectively. Model correction factors scale parameters by the factor's value. Melt correction factor by land cover ranged from 0.51 (coniferous) to 1.0 for the wetland in the BL and were consistent across forest type but larger in the wetland in BLS. LAI and snow interception correction factors were generally larger for coniferous HRUs and progressively smaller for mixed, deciduous and wetland HRUs, respectively. The maximum canopy snow storage was an order of magnitude higher in BLS versus BL. Both BL and BLS rain-snow partitioning temperatures were negative with the BLS threshold value of -4.5 ℃ (Table 4.1).

Hydraulic conductivity and baseflow rate in the upper soil zone parameters were substantially larger in BL than BLS. PET correction factors on both lake and land were larger for BL than BLS. Manning's n correction factor was larger for BL and crest width coefficient correction factors resulted in smaller crest widths for BLS, depending on the subbasin drainage area (Table 4.1).

BL substantially overestimated SWE (Figure 4.7) and had poor SWE performance across all sites during both calibration and validation except for the eastern region validation period (Table 4.3). BLS SWE KGE was larger than that of the BL model at each of the 12 sites. BLS generally followed trail camera estimated SWE time series and aligned with snow survey mean values except for the forested sites in the west in 2019 (Figure 4.7). BLS SWE KGE values were in the upper range of medium performance or higher for most sites during calibration and validation. BLS SWE model performance

was similar during calibration and validation. There were no overall observed trends in model performance across land cover type or region (Table 4.3).

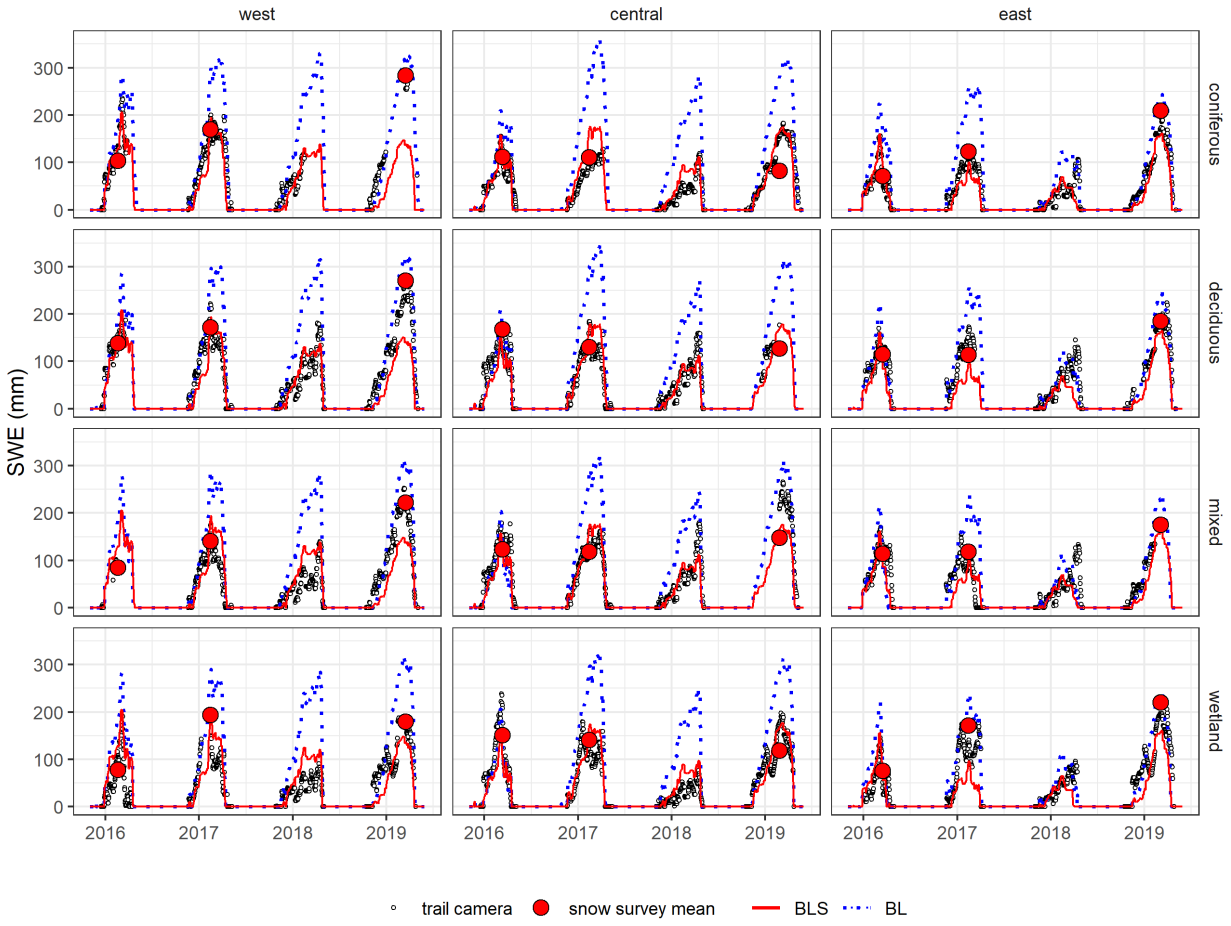

Figure 4.7: SWE time series for a baseline model calibrated to lake levels and flow (BL), the BL model calibrated to subbasin SWE (BLS), estimated SWE using trail cameras and snow survey mean SWE for each study site during calibration (2016, 2017) and validation (2018, 2019).

Table 4.3: SWE KGE values for the baseline model calibrated to lake levels and flow (BL), the BL model calibrated to subbasin SWE (BLS) for the calibration period (2016, 2017) and the validation period (2018, 2019) across land cover type and region. Values are coloured by performance classification where poor = light red (-∞ to 0.48), medium = yellow (0.48 to 0.65), good = green (0.65 to 0.83) and excellent = blue (0.83 to 1.0).

	west				central				east			
	calibration		validation		calibration		validation		calibration		validation	
	BL	BLS	BL	BLS	BL	BLS	BL	BLS	BL	BLS	BL	BLS
coniferous	0.10	0.84	0.24	0.46	-1.42	0.40	-0.70	0.85	-0.70	0.80	0.31	0.78
deciduous	0.16	0.83	0.11	0.59	-0.31	0.81	-0.41	0.78	0.24	0.57	0.66	0.64
mixed	-0.45	0.57	-0.05	0.64	-0.09	0.85	0.29	0.64	-0.07	0.53	0.63	0.62
wetland	-0.60	0.37	-0.95	0.62	-0.02	0.77	-0.68	0.81	0.24	0.37	0.68	0.59

4.3.3 Basin scale model evaluation

BL simulated daily basin average SWE poorly for all years (Table 4.4), substantially overestimating SWE at the basin scale (Figure 4.8; Figure 4.9). Basin mean BLS and PF SWE performance was good to excellent during calibration and validation (Table 4.4). Performance of all models was good to excellent for flow.

Table 4.4: Goodness of fit statistics comparing basin average trail camera SWE and basin outlet observed flow to a baseline model calibrated to lake levels and flow (BL), the BL model calibrated to subbasin SWE (BLS) and a particle filter model assimilating Copernicus SWE (PF) into BLS. Values are coloured by performance classification where poor = light red (-∞ to 0.48), medium = yellow (0.48 to 0.65), good = green (0.65 to 0.83) and excellent = blue (0.83 to 1.0).

		SWE KGE			Flow KGE		
		BL	BLS	PF	BL	BLS	PF
calibration	2016	0.37	0.85	0.88	0.86	0.79	0.80
	2017	-0.53	0.86	0.68	0.77	0.81	0.82
	2016-2017	*-0.29*	*0.86*	*0.77*	*0.81*	*0.85*	*0.88*
validation	2018	-0.79	0.77	0.67	0.74	0.67	0.67
	2019	-0.24	0.83	0.85	0.74	0.83	0.68
	2018-2019	*-0.34*	*0.89*	*0.83*	*0.74*	*0.77*	*0.68*
	2016-2019	*-0.28*	*0.89*	*0.83*	*0.79*	*0.82*	*0.78*

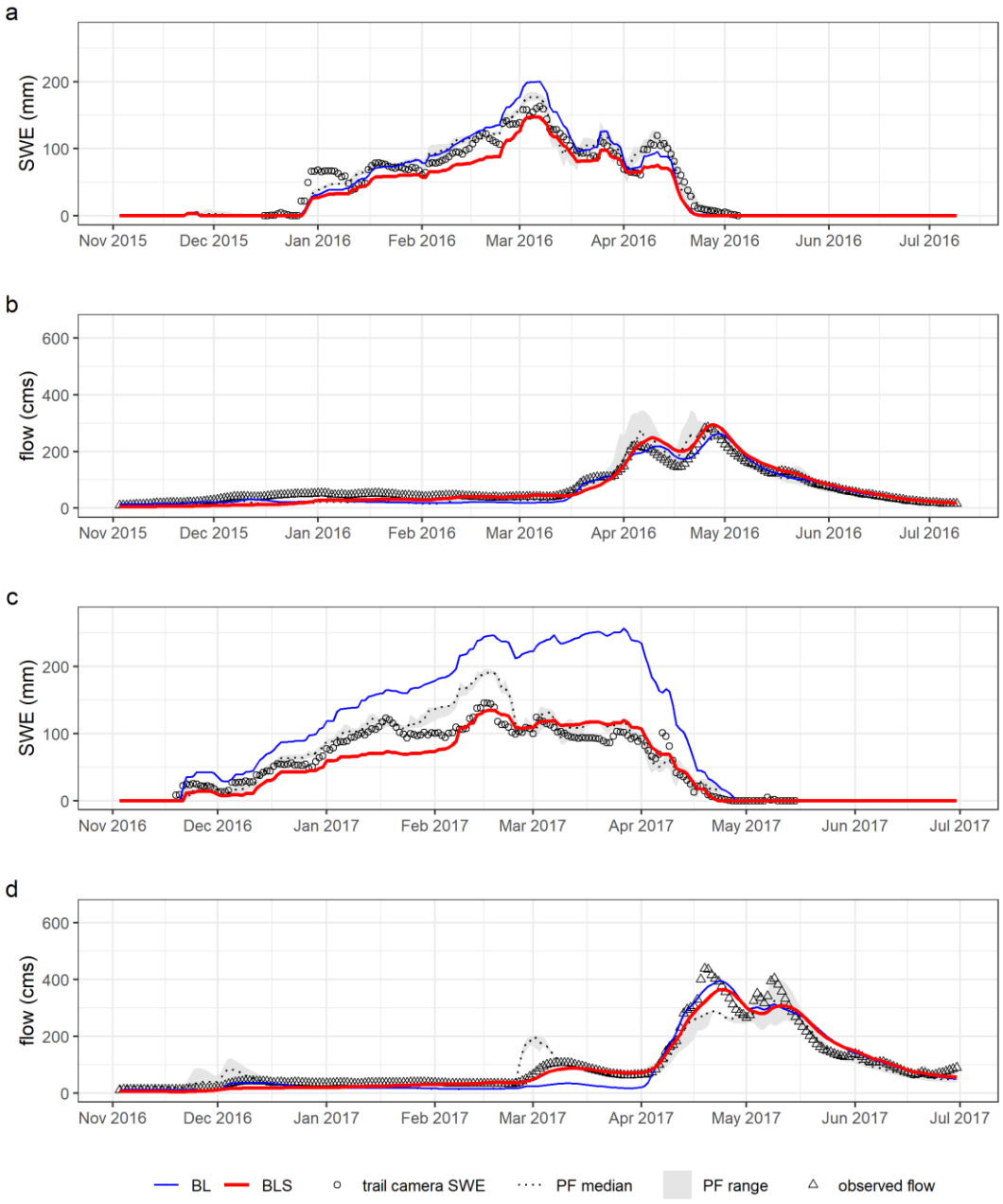

Figure 4.8: Calibration period time series data for a baseline model calibrated to lake levels and flow (BL), the BL model calibrated to subbasin SWE (BLS), a particle filter model assimilating Copernicus SWE (PF) into BLS, measured SWE using trail cameras and observed flow for 2016 water year (a, b) and 2017 water year (c, d).

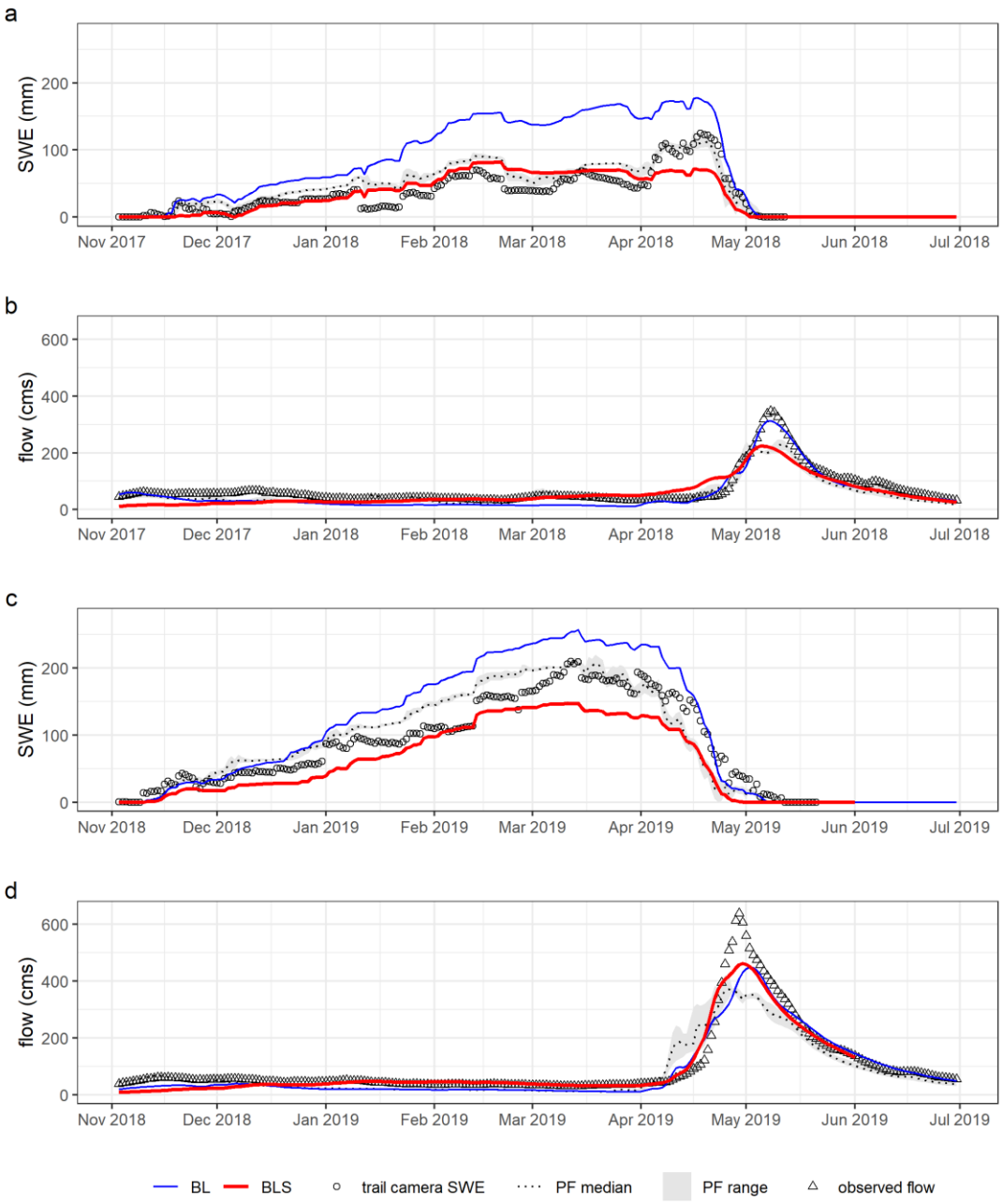

Figure 4.9: Validation period time series data for a baseline model calibrated to lake levels and flow (BL), the BL model calibrated to subbasin SWE (BLS), a particle filter model assimilating Copernicus SWE (PF) into BLS, measured SWE using trail cameras and observed flow for 2018 water year (a, b) and 2019 water year (c, d).

Calibrating to subbasin SWE substantially improved SWE simulation. Mean BLS SWE KGE over the four years was 1.13 larger than BL (Figure 4.10). The PF modelled SWE substantially better than BL. PF SWE KGE was 1.07 greater than BL averaged over the study period. The PF and BLS SWE KGE were very similar with an average difference over the study period of -0.06. All flow KGE differentials across all study years were near 0. BL modelled flow slightly better than BLS and PF with a larger mean KGE over the study period of 0.06 and 0.16, respectively (Figure 4.10). The BLS and PF underestimated spring flow peaks in all years except 2016 (Figure 4.8, Figure 4.9)

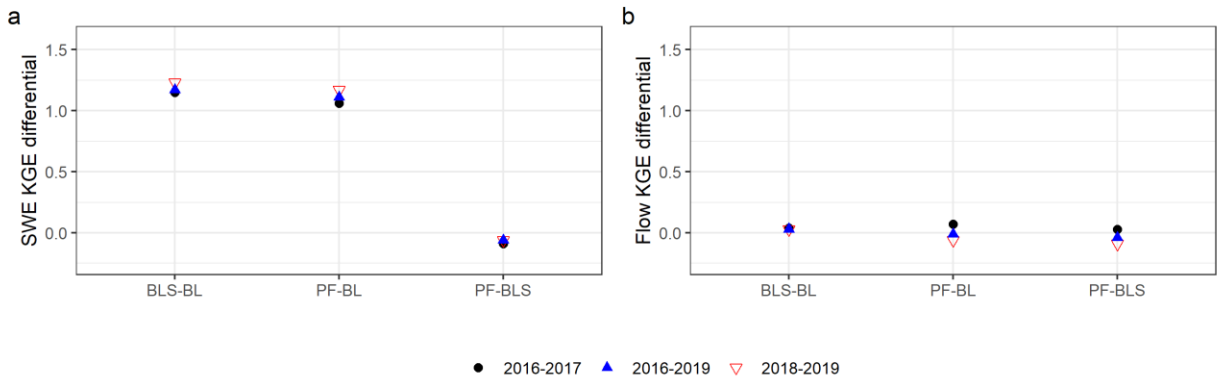

Figure 4.10: Calibration (2016-2017), validation (2017-2018) and study period (2016-2019) KGE differential between the baseline model calibrated to lake levels and flow (BL), the BL model calibrated to subbasin SWE (BLS) and a particle filter model assimilating Copernicus SWE (PF) into BLS for modelled SWE (a) and flow (b).

4.4 Discussion

4.4.1 Evaluation of Copernicus SWE

Bias corrected Copernicus SWE is suitable for assimilation into hydrologic models in this landscape given the large KGE and low bias when compared with measured data

(trail camera SWE). Interannual differences between Copernicus and the trail camera SWE were likely due to interannual differences in climatic variables driving melt between the basin and stations assimilated into the Copernicus product. Passive microwave derived SWE is sensitive to differences in snow structure which may vary with climate and also result in interannual differences in error (Dong, 2018). The assimilation of snow depths into Copernicus and the simple method of converting depth to SWE using a constant density may lead to product error where processes such as decreases in density from fresh snowfall, or increases in density from snow compaction, ripening, and rain on snow may be misrepresented (Dingman, 2015). For example, anomalous climate variability with several melt, refreeze and rain on snow events in 2018 led to abnormal patterns in snow accumulation and ablation likely leading to a poorer relationship with observed values during this year.

Both Copernicus (via snow depth assimilation) and the trail camera SWE rely heavily on snow depth for their estimates which may result in a strong agreement between the values but a misrepresentation of SWE due the factors mentioned above. While limited in number, agreement of trail camera derived SWE with site specific snow surveys provides some confidence in the estimated SWE and the Copernicus product. Comparison of Copernicus SWE to other SWE measurements and/or products to further investigate the limitations discussed above is recommended.

4.4.2 Subbasin scale calibration and validation

The BLS modelled subbasin SWE well during calibration and validation, indicating a robust model structure and parameter set. Consistency of KGE across site and region during validation indicated little spatial bias in the models. Auto-calibrated vegetation-

related snow model parameters were consistent with our understanding of physical process with larger LAI and snow interception and smaller melt rates in coniferous forest versus mixed and deciduous stands. An exception was the BLS melt correction factors that had small variability (Varhola *et al.*, 2010; Table 4.1). SWE was substantially overestimated in BL. The significantly larger BLS maximum canopy snow storage and lower precipitation partitioning thresholds likely contributed to decreased SWE in BLS.

The BLS precipitation partitioning threshold value was lower than that typically found in the literature (Jennings *et al.*, 2018). This was possibly due to the model partitioning precipitation based on daily average temperature values, which may not have accurately represented the actual temperature during a precipitation event (Harder and Pomeroy, 2013). Partitioning based on surface air temperature is a simplification of the more complex processes controlling precipitation phase transitions including vertical air mass boundaries, falling snow grain size and earth surface properties (Harder and Pomeroy, 2013; Feiccabrino *et al.*, 2015). Large bodies of open water are known to affect precipitation partitioning thresholds (Feiccabrino *et al.*, 2015) and maintain temperatures around 0 °C where precipitation phase is difficult to resolve (Mekis *et al.*, 2020). The influence of Georgian Bay on the partitioning thresholds in the western versus the unaffected eastern basin may create spatial variability in thresholds. Temporal variability in the threshold may result from the open versus frozen state of the lake throughout the winter. This was not accounted for in the model, which used static values for partitioning parameters (Raven : User's and Developer's Manual v3.6).

Larger variability of the land cover-based melt correction factor in BL compared to BLS may have resulted in higher spatial variability of melt patterns in BL. Subbasin

evaluation of the processes governing storage and routing of melt and streamflow is beyond the scope of this paper but is recommended for future research.

4.4.3 Basin scale model evaluation

At the basin scale, BLS modelled SWE better than BL, indicating that calibrating a model to subbasin SWE may improve the accuracy of simulated basin scale SWE. This finding is consistent with Mai et al. (2022), who found a model calibrated to streamflow only cannot adequately resolve the parameters required to estimate snow accumulation and ablation accurately in forested environments of the Great Lakes Basin. It also agrees with several previous multi-objective calibration study results (Parajka and Blöschl, 2008; Franz and Karsten, 2013; Bennett *et al.*, 2019; Nemri and Kinnard, 2020).

PF modelled SWE better than BL. Copernicus was assimilated into BLS so the increased performance may be due to subbasin SWE calibration. However, Copernicus SWE was a better estimate than BL SWE, so assimilating Copernicus would likely improve SWE performance when observed SWE data are not available for model calibration. Further research assimilating Copernicus into BL would be required to confirm this finding.

BLS and PF simulated SWE with comparable skill, demonstrating that a well calibrated model may be sufficient and assimilating Copernicus SWE may be unnecessary. However, model forcings, structure and parameterization do not capture the complexity of scaling, weather patterns and physical processes driving snow accumulation and melt (Beven, 2012). The snow depth and density measurements were point scale estimates with potential human, scaling and methodological error in converting depth and density to SWE (Blöschl, 1999). While not captured in the

performance assessment of this study, in theory the PF balances model and observation error and may be a more representative estimate of the true mean basin SWE (Blöschl, 1999; Moradkhani *et al.*, 2005).

Despite improved SWE skill in the BLS and PF compared to BL, all models had similar flow simulation performance. This finding is consistent with several previous multi-objective calibration and data assimilation studies (Dressler *et al.*, 2006; Parajka and Blöschl, 2008; Franz and Karsten, 2013; Dziubanski and Franz, 2016). Good BL streamflow performance without an accurate representation of SWE was possibly because the model was calibrated to a network of lakes and the basin outlet discharge that spatially integrated hydrologically significant processes including upstream melt dynamics. The effect of SWE calibration or assimilation on modelled flow performance will be dependent on the quality of the original model and its calibration. In this study, the original model (BL) was a very well-constructed, extensively calibrated model. SWE calibration and data assimilation may improve flow simulations if a poorer original model with fewer calibration data were used. Previous studies assimilating SWE into hydrologic models have led researchers to conclude that recalibration of their original models was required (Dziubanski and Franz, 2016).

Larger SWE in BL versus BLS but similar streamflow simulations indicates a difference in snow ablation and delivery of water to the basin outlet between the two models. A full assessment of water budgets and flow generation parameter sensitivities, beyond the scope of this paper, is required to investigate the differences in the delivery of the excess SWE to the basin outlet. However, a preliminary assessment of the parameter differences between BL and BLS suggests that BL melted snow at twice the rate of BLS,

thus adding more simulated input to the catchment. Based on the parameter differences, BL infiltrated water from the surface and discharged baseflow at a higher rate, and then conveyed this water through channels and reservoirs at a slower rate than BLS. Both lake and land surface evaporation corrections led to higher water loss to the atmosphere in BL compared to BLS. Therefore, excess water in the BL model was likely held in storage and lost to the atmosphere from the soil and lakes. Improvement of both SWE and flow-related process representation and parameterization should be explored as they will be important for assessing the impact of a changing climate on snow, water availability, and water related hazards.

4.5 Conclusion

The bias corrected Copernicus product provided a good estimate of mean basin SWE in the Petawawa River basin and shows promise for supporting water management decisions. Potential limitations in the product related to the conversion of assimilated snow depths to SWE were highlighted and should be further explored. Snow related hydrologic model parameters (except for precipitation partitioning thresholds) were generally consistent with current understanding of physical process. Precipitation partitioning was identified as a challenge within other modelling studies in the Great Lakes Region and warrants additional research (Mai *et al.*, 2022).

Calibration to subbasin SWE substantially improved the basin scale SWE estimate. Copernicus SWE was a much better estimate than the baseline model, so assimilation would likely improve SWE skill when subbasin SWE are not available for calibration. Assimilating Copernicus SWE did not improve SWE performance compared to the model calibrated with subbasin SWE, demonstrating that assimilation of

Copernicus SWE may provide little advantage over a well calibrated model. However, the particle filter balances model and measurement error. While not reflected in the model performance statistics, PF may be a better representation of the true mean basin SWE.

All models had similar streamflow performance. This demonstrates that streamflow can be accurately estimated using a model with a poor representation of SWE. This may be sufficient for applications where estimating flow is the primary objective. However, applications where understanding the physical processes of snow accumulation, melt and streamflow generation are important, such as assessing the impact of climate change on water resources, require accurate representations of SWE. In this case, calibration to subbasin SWE and assimilation of Copernicus SWE can substantially improve modelled SWE, as shown in this study. Exploration of flow process representation and parameterization to determine why improving SWE accuracy in the model did not improve performance of simulated flow is recommended for future research.

Chapter 5 Summary, conclusions, and future work

This thesis investigated three primary objectives. Snowpack scaling issues were addressed in Chapter 2, forest-snowpack relationships in Chapter 3 and methods of integrating SWE into a hydrologic model in Chapter 4. Scaling issues in snow hydrology persist due to limitations in instrumentation and the inherent gap between sampled and true patterns and processes across scales. Chapter 2 assessed the difference in representation of snow processes and estimates of SWE and snow depth mean and variability of across scales. A relationship between snowpack metrics and forest cover was observed at the point scale but not the transect scale, which was attributed to the non-linear aggregation of complex snow processes across the transect and/or limitations in the study methodology. In general, the study found mean vegetative cover was not an effective metric for representing aggregate snow-vegetation processes and further research was suggested, which was addressed in Chapter 3. Point scale mean SWE and snow depth was found to be unrepresentative of the surrounding area, but bias was consistent within landscape units and time-periods suggesting that snowpack metrics within this environment could be bias corrected by scaling factors derived from a limited number of transect measurements. Consistency between upscaled estimates of snowpack properties suggested that a limited number of appropriately stratified point scale measurements may be a suitable replacement for transect scale mean values when it is not possible to collect transect data. Comparison of modelled products to field-based data highlighted the importance of understanding the scale and processes that ground truth measurements and model estimates represent. The modelled snow products were

reasonable estimates of SWE but bias correction during ablation is required in this environment.

In Chapter 3 relationships between forest-snowpack relationships were examined over two winters using field and remotely sensed estimates of tree canopy density, distance to tree boles and diameter at breast height. Orthophotography-derived 2D spectral metrics and photogrammetric point cloud 3D metrics correlated well with field estimates of canopy density derived from hemispheric photos while tree bole metrics were not successfully derived from LiDAR data. Significant differences in stand scale snowmelt rate and timing across forest types indicated that forests can be a significant driver of snow processes at this scale and suggests semi-distributed hydrologic models in this region should consider inclusion of forest cover in model discretization. Relationships between snowmelt rate, melt timing and canopy density metrics derived from both field and remotely sensed data were found at the point scale. Inter-annual differences in the snowmelt-forest structure relationship were attributed to contrasts in seasonal weather between years where canopy controlled solar radiation likely dominated melt in 2016 versus more spatially uniform turbulent flux-driven melt in 2017. Peak SWE and peak SWE timing were not correlated with canopy metrics. This is contrary to several previous studies that found stronger correlations between peak SWE and canopy structure and may be explained by a more consistent accumulation period and less mid-winter melt in those studies. Three-dimensional forest structure data derived from photogrammetric point cloud, and LiDAR data and simple orthophoto-derived spectral metrics were highly colinear. This was attributed to the characteristics of this study site and may not be applicable in other environments with different forest structure. The

findings in Chapter 3 indicates that the Ontario imagery program data sets can be used to describe forest-snowpack relationships and elucidate interannual variability in snow process in mixed wood, hardwood, and coniferous stands in the Great Lakes-St. Lawrence Forest region.

In Chapter 4, the Copernicus SWE product was found to provide a good estimate of mean basin SWE in the Petawawa River basin, which demonstrates promise for supporting water management decisions. Calibration of a hydrologic model to subbasin SWE substantially improved modelled basin scale SWE performance. However, assimilation of Copernicus data may provide little advantage over a well calibrated model. Assimilation of Copernicus SWE would likely improve modelled SWE skill when subbasin SWE values are not available for calibration, although this was not explicitly tested. All models evaluated in Chapter 4 had similar streamflow performance. This demonstrates that streamflow can be accurately estimated using a model with a poor representation of SWE, which may be sufficient for applications where estimating flow is the primary objective. However, applications where understanding the physical processes of snow accumulation, melt and streamflow generation are important require accurate representations of SWE. In this case, calibration to subbasin SWE and assimilation of Copernicus SWE can substantially improve modelled SWE.

This thesis has improved understanding of the influence of scale on snow processes and patterns, demonstrated that Ontario imagery can be used to describe forest-snowpack relationships in the Great Lakes-St. Lawrence Forest region and found that it may be unnecessary to assimilate SWE into a well-calibrated hydrologic model. Rapidly

improving technology that permits the deployment of inexpensive field-based measurement equipment and the quickly evolving field of remote sensing will further our ability to explore important scaling and forest-snowpack relationship research questions. The successful application of Ontario Imagery Program spectral and point cloud data demonstrated here should encourage future uses of these regularly acquired data to explore forest-snowpack relationships in other regions or investigate the impacts of forest change on snowpack metrics. Future research should evaluate the implications of climate variability on forest-snowpack relationships at more study sites and across a greater range of forest structure and climate conditions than were evaluated in this thesis. Exploration of flow process misrepresentation and model parameterization resulting in accurate flow simulation in models with poor SWE skill is recommended for future research. Testing the effects of calibration and data assimilation on subbasin scale model performance is also needed. Exploration of these suggested research areas will lead to better estimates of distributed SWE and streamflow at the subbasin and basin scale resulting in improved understanding of water balance components, ecosystem function, impacts of climate change and natural hazard risk in cold regions. (Sturm, 2015; Peters-Lidard *et al.*, 2017; Dong, 2018).

Chapter 6 Bibliography

Adams WP. 1976. Areal differentiation of snow cover in east central Ontario. *Water Resources Research* **12** (6): 1226–1234 DOI: 10.1029/WR012i006p01226

Anderson HW, Rice RM, West AJ. 1959. Snow in forest openings and forest stands. *Journal of Geophysical Research* **64** (8): 1093

Anderton SP, White SM, Alvera B. 2004. Evaluation of spatial variability in snow water equivalent for a high mountain catchment. *Hydrological Processes* **18** (3): 435–453 DOI: 10.1002/hyp.1319

Andreadis KM, Lettenmaier DP. 2006. Assimilating remotely sensed snow observations into a macroscale hydrology model. *Advances in Water Resources* **29** (6): 872–886 DOI: 10.1016/j.advwatres.2005.08.004

Arsenault R, Poulin A, Côté P, Brissette F. 2014. Comparison of Stochastic Optimization Algorithms in Hydrological Model Calibration. *Journal of Hydrologic Engineering* **19** (7) DOI: 10.1061/(asce)he.1943-5584.0000938

Asadzadeh M, Tolson B. 2012. Hybrid Pareto archived dynamically dimensioned search for multi-objective combinatorial optimization: Application to water distribution network design. *Journal of Hydroinformatics* **14** (1) DOI: 10.2166/hydro.2011.098

Asadzadeh M, Tolson B. 2013. Pareto archived dynamically dimensioned search with hypervolume-based selection for multi-objective optimization. *Engineering Optimization* **45** (12): 1489–1509 DOI: 10.1080/0305215X.2012.748046

Azar AE, Ghedira H, Romanov P, Mahani S, Tedesco M, Khanbilvardi R. 2008. Application of Satellite Microwave Images in Estimating Snow Water Equivalent. *JAWRA Journal of the American Water Resources Association* **44** (6): 1347–1362 DOI: 10.1111/j.1752-1688.2008.00227.x

Balsamo G, Albergel C, Beljaars A, Boussetta S, Brun E, Cloke H, Dee D, Dutra E, Munõz-Sabater J, Pappenberger F, et al. 2015. ERA-Interim/Land: A global land surface reanalysis data set. *Hydrology and Earth System Sciences* **19** (1): 389–407 DOI: 10.5194/hess-19-389-2015

Baltsavias EP. 1999. A comparison between photogrammetry and laser scanning. *ISPRS Journal of Photogrammetry and Remote Sensing* **54** (2–3): 83–94 DOI: 10.1016/S0924-2716(99)00014-3

Barnett TP, Adam JC, Lettenmaier DP. 2005. Potential impacts of a warming climate on water availability in snow-dominated regions. *Nature* **438** (7066): 303–309 DOI: 10.1038/nature04141

Beaton AD, Bradford A. 2013. Demonstration of a methodology for setting ecological flow and water level targets. *Canadian Water Resources Journal* **38** (4): 296–310 DOI: 10.1080/07011784.2013.830371

Beaton AD, Metcalfe RA, Buttle JM, Franklin SE. 2019. Investigating snowpack across scale in the northern Great Lakes–St. Lawrence forest region of Central Ontario, Canada. *Hydrological Processes* **33** (26): 3310–3329 DOI: 10.1002/hyp.13558

Bennett KE, Cherry JE, Balk B, Lindsey S. 2019. Using MODIS estimates of fractional snow cover area to improve streamflow forecasts in interior Alaska. *Hydrology and Earth System Sciences* **23** (5): 2439–2459 DOI: 10.5194/hess-23-2439-2019

Bergeron JM, Trudel M, Leconte R. 2016. Combined assimilation of streamflow and snow water equivalent for mid-term ensemble streamflow forecasts in snow-dominated regions. *Hydrology and Earth System Sciences* **20** (10): 4375–4389 DOI: 10.5194/hess-20-4375-2016

Beven K. 2012. *Rainfall-Runoff Modelling*. John Wiley & Sons, Ltd: Chichester, UK. DOI: 10.1002/9781119951001

Blöschl G. 1999. Scaling issues in snow hydrology. *Hydrological Processes* **13** (14–15): 2149–2175 DOI: 10.1002/(SICI)1099-1085(199910)13:14/15<2149::AID-HYP847>3.0.CO;2-8

Blöschl G. 2006. Hydrologic synthesis: Across processes, places, and scales. *Water Resources Research* **42** (3): 2–4 DOI: 10.1029/2005WR004319

Blöschl G, Sivapalan M. 1995. Scale issues in hydrological modelling: A review. *Hydrological Processes* **9** (3–4): 251–290 DOI: 10.1002/hyp.3360090305

Boon S. 2007. Snow accumulation and ablation in a beetle-killed pine stand in Northern Interior British Columbia. *Journal of Ecosystems and Management* (March) DOI: 10.22230/jem.2007v8n3a369

Bormann KJ, Westra S, Evans JP, McCabe MF. 2013. Spatial and temporal variability in seasonal snow density. *Journal of Hydrology* **484**: 63–73 DOI: 10.1016/j.jhydrol.2013.01.032

Brasnett B. 1999. A Global Analysis of Snow Depth for Numerical Weather Prediction. *Journal of Applied Meteorology* **38** (6): 726–740 DOI: 10.1175/1520-0450(1999)038<0726:AGAOSD>2.0.CO;2

Braun LN. 1991. Modelling of the snow-water equivalent in the mountain environment. In *Snow, Hydrology and Forests in High Alpine Areas. Proceedings of the Vienna Symposium*IAHS: Vienna; 3–17.

Breidenbach J, Næsset E, Lien V, Gobakken T, Solberg S. 2010. Prediction of species specific forest inventory attributes using a nonparametric semi-individual tree crown approach based on fused airborne laser scanning and multispectral data. *Remote Sensing of Environment* **114** (4): 911–924 DOI: 10.1016/j.rse.2009.12.004

Brown R, Brasnett B, Robinson D. 2003. Gridded North American monthly snow depth and snow water equivalent for GCM evaluation. *Atmosphere - Ocean* **41** (1): 1–14 DOI: 10.3137/ao.410101

Brown R, Tapsoba D, Derksen C. 2018. Evaluation of snow water equivalent datasets over the Saint-Maurice river basin region of southern Québec. *Hydrological Processes* **32** (17): 2748–2764 DOI: 10.1002/hyp.13221

Broxton PD, Harpold AA, Biederman JA, Troch PA, Molotch NP, Brooks PD. 2015. Quantifying the effects of vegetation structure on snow accumulation and ablation in mixed-conifer forests. *Ecohydrology* **8** (6): 1073–1094 DOI: 10.1002/eco.1565

Clark MP, Hendrikx J, Slater AG, Kavetski D, Anderson B, Cullen NJ, Kerr T, Örn Hreinsson E, Woods RA. 2011. Representing spatial variability of snow water equivalent in hydrologic and land-surface models: A review. *Water Resources Research* **47** (7) DOI: 10.1029/2011WR010745

Clark MP, Slater AG, Barrett AP, Hay LE, McCabe GJ, Rajagopalan B, Leavesley GH. 2006. Assimilation of snow covered area information into hydrologic and land-surface models. *Advances in Water Resources* **29** (8): 1209–1221 DOI: 10.1016/j.advwatres.2005.10.001

Cline D, Elder K, Bales R. 1998. Scale effects in a distributed snow water equivalence and snowmelt model for mountain basins. *Hydrological Processes* **12** (10–11): 1527–1536 DOI: 10.1002/(SICI)1099-1085(199808/09)12:10/11<1527::AID-HYP678>3.0.CO;2-E

Craig JR, Brown G, Chlumsky R, Jenkinson RW, Jost G, Lee K, Mai J, Serrer M, Sgro N, Shafii M, et al. 2020. Flexible watershed simulation with the Raven hydrological modelling framework. *Environmental Modelling and Software* **129** (December 2019): 104728 DOI: 10.1016/j.enversusoft.2020.104728

Cumming GH. 2009. Algonquin Park Forest Management Planning Manual. Algonquin Forest Authority, Pembroke, ON. Available at: http://www.algonquinpark.on.ca/pdf/forestry_fmp_phase1_2010-2020.pdf

Dash JP, Watt MS, Bhandari S, Watt P. 2016. Characterising forest structure using combinations of airborne laser scanning data, RapidEye satellite imagery and environmental variables. *Forestry* **89** (2): 159–169 DOI: 10.1093/forestry/cpv048

Davis RE, Hardy JP, Ni W, Woodcock C, McKenzie JC, Jordan R, Li X. 1997. Variation of snow cover ablation in the boreal forest: A sensitivity study on the effects of conifer canopy. *Journal of Geophysical Research: Atmospheres* **102** (D24): 29389–29395 DOI: 10.1029/97JD01335

Derksen C, Walker A, Goodison B. 2005a. Evaluation of passive microwave snow water equivalent retrievals across the boreal forest/tundra transition of western Canada. *Remote Sensing of Environment* **96** (3–4): 315–327 DOI: 10.1016/j.rse.2005.02.014

Derksen C, Walker AE, Goodison BE, Strapp JW. 2005b. Integrating in situ and multiscale passive microwave data for estimation of subgrid scale snow water equivalent distribution and variability. *IEEE Transactions on Geoscience and Remote Sensing* **43** (5): 960–972 DOI: 10.1109/TGRS.2004.839591

Dickinson WT, Whiteley HR. 1972. A sampling scheme for shallow snowpacks. *Hydrological Sciences Bulletin* **17** (3): 247–258 DOI: 10.1080/02626667209493832

Dietz AJ, Kuenzer C, Gessner U, Dech S. 2012. Remote sensing of snow – a review of available methods. *International Journal of Remote Sensing* **33** (13): 4094–4134 DOI: 10.1080/01431161.2011.640964

Dingman L. 2015. *Physical Hydrology*. Waveland Press: Long Grove, IL.

Dong C. 2018. Remote sensing, hydrological modeling and in situ observations in snow cover research: A review. *Journal of Hydrology* **561** DOI: 10.1016/j.jhydrol.2018.04.027

Dressler KA, Leavesley GH, Bales RC, Fassnacht SR. 2006. Evaluation of gridded snow water equivalent and satellite snow cover products for mountain basins in a hydrologic model. *Hydrological Processes* **20** (4): 673–688 DOI: 10.1002/hyp.6130

Duan QY, Gupta VK, Sorooshian S. 1993. Shuffled complex evolution approach for effective and efficient global minimization. *Journal of Optimization Theory and Applications* **76** (3) DOI: 10.1007/BF00939380

Duethmann D, Peters J, Blume T, Vorogushyn S, Güntner A. 2014. The value of satellite-derived snow cover images for calibrating a hydrological model in snow-dominated catchments in Central Asia. *Water Resources Research* **50** (3): 2002–2021 DOI: 10.1002/2013WR014382

Dunn OJ. 1964. American Society for Quality Multiple Comparisons Using Rank Sums Multiple Comparisons Using Rank Sums. *Source: Technometrics* **6** (3)

Dziubanski DJ, Franz KJ. 2016. Assimilation of AMSR-E snow water equivalent data in a spatially-lumped snow model. *Journal of Hydrology* **540**: 26–39 DOI: 10.1016/j.jhydrol.2016.05.046

Elder K, Dozier J, Michaelsen J. 1991. Snow accumulation and distribution in an Alpine Watershed. *Water Resources Research* **27** (7): 1541–1552 DOI: 10.1029/91WR00506

Ellis CR, Pomeroy JW, Link TE. 2013. Modeling increases in snowmelt yield and desynchronization resulting from forest gap-thinning treatments in a northern mountain headwater basin. *Water Resources Research* **49** (2): 936–949 DOI: 10.1002/wrcr.20089

Environment and Climate Change Canada. 2019. Canadian Climate Normals Available at: http://climate.weather.gc.ca/climate_normals/results_e.html?searchType=stnName&txtStationName=Traverse&searchMethod=contains&txtCentralLatMin=0&txtCentralLatSec=0&txtCentralLongMin=0&txtCentralLongSec=0&stnID=4197&dispBack=1 [Accessed 6 June 2019]

Erlandsson R, Stoessel M, Skånes H, Wennbom M, Angerbjörn A. 2019. An innovative

use of orthophotos – possibilities to assess plant productivity from colour infrared aerial orthophotos (N Horning and J Zhang, eds). *Remote Sensing in Ecology and Conservation* **5** (4): 291–301 DOI: 10.1002/rse2.108

Essery R, Bunting P, Rowlands A, Rutter N, Hardy J, Melloh R, Link T, Marks D, Pomeroy J. 2008. Radiative Transfer Modeling of a Coniferous Canopy Characterized by Airborne Remote Sensing. *Journal of Hydrometeorology* **9** (2): 228–241 DOI: 10.1175/2007JHM870.1

Essery R, Pomeroy J, Parviainen J, Storck P. 2003. Sublimation of Snow from Coniferous Forests in a Climate Model. *Journal of Climate* **16** (11): 1855–1864 DOI: 10.1175/1520-0442(2003)016<1855:SOSFCF>2.0.CO;2

European Commission Joint Research Centre. 2022. Copernicus Global Land Service Available at: https://land.copernicus.eu/global/products/swe [Accessed 6 July 2022]

Faria DA, Pomeroy JW, Essery RLH. 2000. Effect of covariance between ablation and snow water equivalent on depletion of snow-covered area in a forest. *Hydrological Processes* **14** (15): 2683–2695 DOI: 10.1002/1099-1085(20001030)14:15<2683::AID-HYP86>3.0.CO;2-N

Farnes PE, Peterson NR, Goodison BE, Richards RP. 1982. Metrication of manual snow sampling equipment. *50th Western Snow Conference*: 120–132

Feiccabrino J, Graff W, Lundberg A, Sandström N, Gustafsson D. 2015. Meteorological knowledge useful for the improvement of snow rain separation in surface based models. *Hydrology* **2** (4): 266–288 DOI: 10.3390/hydrology2040266

Finger D, Pellicciotti F, Konz M, Rimkus S, Burlando P. 2011. The value of glacier mass balance, satellite snow cover images, and hourly discharge for improving the performance of a physically based distributed hydrological model. *Water Resources Research* **47** (7): 1–14 DOI: 10.1029/2010WR009824

Finger D, Vis M, Huss M, Seibert J. 2015. The value of multiple data set calibration versus model complexity for improving the performance of hydrological models in mountain catchments. *Water Resources Research* **51** (4): 1939–1958 DOI: 10.1002/2014WR015712

Fletcher SJ, Liston GE, Hiemstra CA, Miller SD. 2012. Assimilating MODIS and AMSR-E Snow Observations in a Snow Evolution Model. *Journal of Hydrometeorology* **13** (5): 1475–1492 DOI: 10.1175/JHM-D-11-082.1

Fortin V, Jean M, Brown R, Payette S. 2015. Predicting Snow Depth in a Forest-Tundra Landscape using a Conceptual Model Allowing for Snow Redistribution and Constrained by Observations from a Digital Camera. *Atmosphere - Ocean* **53** (2): 200–211 DOI: 10.1080/07055900.2015.1022708

Franz KJ, Karsten LR. 2013. Calibration of a distributed snow model using MODIS snow covered area data. *Journal of Hydrology* **494**: 160–175 DOI:

10.1016/j.jhydrol.2013.04.026

Gao H, Ding Y, Zhao Q, Hrachowitz M, Savenije HHG. 2017. The importance of aspect for modelling the hydrological response in a glacier catchment in Central Asia. *Hydrological Processes* **31** (16): 2842–2859 DOI: 10.1002/hyp.11224

Gelaro R, McCarty W, Suárez MJ, Todling R, Molod A, Takacs L, Randles CA, Darmenov A, Bosilovich MG, Reichle R, et al. 2017. The Modern-Era Retrospective Analysis for Research and Applications, Version 2 (MERRA-2). *Journal of Climate* **30** (14): 5419–5454 DOI: 10.1175/JCLI-D-16-0758.1

Gelfan AN, Pomeroy JW, Kuchment LS. 2004. Modeling Forest Cover Influences on Snow Accumulation, Sublimation, and Melt. *Journal of Hydrometeorology* **5** (5): 785–803 DOI: 10.1175/1525-7541(2004)005<0785:MFCIOS>2.0.CO;2

Goodison BE, Glynn JE, Harvey KD, Slater JE. 1987. Snow Surveying in Canada: A Perspective. *Canadian Water Resources Journal* **12** (2): 27–42 DOI: 10.4296/cwrj1202027

Government of Canada. 2022. Canadian Climate Normals 1981-2010 Station Data Available at: https://climate.weather.gc.ca/climate_normals/results_1981_2010_e.html?searchType=stnProx&txtRadius=100&selCity=&selPark=&optProxType=custom&txtCentralLatDeg=45&txtCentralLatMin=32&txtCentralLatSec=51.554&txtCentralLongDeg=78&txtCentralLongMin=38&txtCentr [Accessed 4 February 2023]

Gray DM, Male DH. 1981. *Handbook of snow: principles, processes, management & use*. Pergamon Press.

Griessinger N, Seibert J, Magnusson J, Jonas T. 2016. Assessing the benefit of snow data assimilation for runoff modeling in Alpine catchments. *Hydrology and Earth System Sciences* **20** (9) DOI: 10.5194/hess-20-3895-2016

Grünewald T, Lehning M, Gru¨newald T, Lehning M. 2015. Are flat-field snow depth measurements representative? A comparison of selected index sites with areal snow depth measurements at the small catchment scale. *Hydrological processes* **29** (7): 1717–1728 DOI: 10.1002/hyp.10295

Gupta H V., Kling H, Yilmaz KK, Martinez GF. 2009. Decomposition of the mean squared error and NSE performance criteria: Implications for improving hydrological modelling. *Journal of Hydrology* **377** (1–2): 80–91 DOI: 10.1016/j.jhydrol.2009.08.003

Haala N, Hastedt H, Wolf K, Ressl C, Baltrusch S. 2010. Digital Photogrammetric Camera Evaluation – Generation of Digital Elevation Models. *Photogrammetrie - Fernerkundung - Geoinformation* **2010** (2): 99–115 DOI: 10.1127/1432-8364/2010/0043

Hammond JC, Saavedra FA, Kampf SK. 2018. How Does Snow Persistence Relate to

Annual Streamflow in Mountain Watersheds of the Western U.S. With Wet Maritime and Dry Continental Climates? *Water Resources Research* **54** (4): 2605–2623 DOI: 10.1002/2017WR021899

Han M, Shen H, Tolson BA, Craig JR, Mai J, Lin SGM, Basu NB, Awol FS. 2022. Basinmaker 3.0: A GIS Toolbox for Distributed Watershed Delineation of Complex Lake-River Routing Networks. *SSRN Electronic Journal* DOI: 10.2139/ssrn.4135646

Han M, Tolson BA, Metcalfe RA. 2021. Calibrating the Raven hydrological model to a dense network of continuously monitored natural lake levels on the Petawawa River Watershed. In *Canadian Water Resources Association National Conference*Saskatoon, Saskatchewan.

Hancock S, Baxter R, Evans J, Huntley B. 2013. Evaluating global snow water equivalent products for testing land surface models. *Remote Sensing of Environment* **128**: 107–117 DOI: 10.1016/j.rse.2012.10.004

Harder P, Pomeroy J. 2013. Estimating precipitation phase using a psychrometric energy balance method. *Hydrological Processes* **27** (13): 1901–1914 DOI: 10.1002/hyp.9799

He S, Guo S, Yang G, Chen K, Liu D, Zhou Y. 2020. Optimizing Operation Rules of Cascade Reservoirs for Adapting Climate Change. *Water Resources Management* **34** (1) DOI: 10.1007/s11269-019-02405-6

Hedrick A, Marshall H. 2014. Automated Snow Depth Measurements in Avalanche Terrain Using Time-Lapse Photography. (September) DOI: 10.13140/2.1.2049.6646

Hedstrom NR, Pomeroy JW. 1998. Measurements and modelling of snow interception in the boreal forest. *Hydrological Processes* **12** (10–11): 1611–1625 DOI: 10.1002/(SICI)1099-1085(199808/09)12:10/11<1611::AID-HYP684>3.0.CO;2-4

Heinzel J, Koch B. 2012. Investigating multiple data sources for tree species classification in temperate forest and use for single tree delineation. *International Journal of Applied Earth Observation and Geoinformation* **18**: 101–110 DOI: 10.1016/j.jag.2012.01.025

Huang C, Newman AJ, Clark MP, Wood AW, Zheng X. 2017a. Evaluation of snow data assimilation using the ensemble Kalman filter for seasonal streamflow prediction in the western United States. *Hydrology and earth system sciences* **21** (1): 635–650 DOI: 10.5194/hess-21-635-2017

Huang H, Chen Y, Clinton N, Wang J, Wang X, Liu C, Gong P, Yang J, Bai Y, Zheng Y, et al. 2017b. Mapping major land cover dynamics in Beijing using all Landsat images in Google Earth Engine. *Remote Sensing of Environment* **202**: 166–176 DOI: 10.1016/j.rse.2017.02.021

Huerta ML, Molotch NP, McPhee J. 2019. Snowfall interception in a deciduous

Nothofagus forest and implications for spatial snowpack distribution. *Hydrological Processes* **33** (13): 1818–1834 DOI: 10.1002/hyp.13439

Jenicek M, Seibert J, Zappa M, Staudinger M, Jonas T. 2016. Importance of maximum snow accumulation for summer low flows in humid catchments. *Hydrology and Earth System Sciences* **20** (2): 859–874 DOI: 10.5194/hess-20-859-2016

Jennings KS, Winchell TS, Livneh B, Molotch NP. 2018. Spatial variation of the rain–snow temperature threshold across the Northern Hemisphere. *Nature Communications* **9** (1): 1148 DOI: 10.1038/s41467-018-03629-7

Jiusto JE, Kaplan ML. 1972. Snowfall From Lake-Effect Storms. *Monthly Weather Review* **100** (1): 62–66 DOI: 10.1175/1520-0493(1972)100<0062:SFLS>2.3.CO;2

Jost G, Weiler M, Gluns DR, Alila Y. 2007. The influence of forest and topography on snow accumulation and melt at the watershed-scale. *Journal of Hydrology* **347** (1–2): 101–115 DOI: 10.1016/j.jhydrol.2007.09.006

Katoch S, Chauhan SS, Kumar V. 2021. A review on genetic algorithm: past, present, and future. *Multimedia Tools and Applications* **80** (5) DOI: 10.1007/s11042-020-10139-6

Kelly R. 2009. The AMSR-E Snow Depth Algorithm : Description and Initial Results. *Journal of The Remote Sensing Society of Japan* **29** (1): 307–317 DOI: 10.11440/rssj.29.307

Kennedy J, Eberhart R. 1995. Particle swarm optimization. In *Proceedings of ICNN'95 - International Conference on Neural Networks*1942–1948 vol.4. DOI: 10.1109/ICNN.1995.488968

Kim G, Rhim S, Lee S. 2007. Automated Visual Snow-Cover Measurement Using SRG and VMS. *IAENG International Journal of Computer Sciences* (August) Available at: http://citeseerx.ist.psu.edu/viewdoc/download?doi=10.1.1.148.7461&rep=rep1&type=pdf

Kinar NJ, Pomeroy JW. 2015. Measurement of the physical properties of the snowpack. *Reviews of Geophysics* **53** (2): 481–544 DOI: 10.1002/2015RG000481

King F, Erler AR, Frey SK, Fletcher CG. 2020. Application of machine learning techniques for regional bias correction of snow water equivalent estimates in Ontario, Canada. *Hydrology and Earth System Sciences* **24** (10): 4887–4902 DOI: 10.5194/hess-24-4887-2020

Kirkpatrick S, Gelatt CD, Vecchi MP. 1983. Optimization by simulated annealing. *Science* **220** (4598) DOI: 10.1126/science.220.4598.671

Kitagawa G. 1996. Monte Carlo Filter and Smoother for Non-Gaussian Nonlinear State Space Models. *Journal of Computational and Graphical Statistics* **5** (1): 1 DOI: 10.2307/1390750

Kuusisto E. 1986. The energy balance of a melting snow cover in different environments. *Modelling Snowmelt-Induced Processes* (155): 37–45

Land Information Ontario. 2020. COSINE Online Services Available at: https://www.gisapplication.lrc.gov.on.ca/cosineONT/Index.html?site=cosine&viewer=OntarioViewer&locale=en-US [Accessed 15 September 2020]

Land Information Ontario. 2022a. Ontario Imagery Program Available at: https://geohub.lio.gov.on.ca/pages/ontario-imagery-program [Accessed 28 December 2022]

Land Information Ontario. 2022b. Ontario Classified Point Cloud (Lidar-Derived) Available at: https://geohub.lio.gov.on.ca/maps/mnrf::ontario-classified-point-cloud-lidar-derived/explore?location=42.028146%2C-78.761366%2C3.00 [Accessed 28 December 2022]

Larue F, Royer A, De Sève D, Langlois A, Roy A, Brucker L. 2017. Validation of GlobSnow-2 snow water equivalent over Eastern Canada. *Remote Sensing of Environment* **194**: 264–277 DOI: 10.1016/j.rse.2017.03.027

Leach JM, Kornelsen KC, Coulibaly P. 2018. Assimilation of near-real time data products into models of an urban basin. *Journal of Hydrology* **563** (April): 51–64 DOI: 10.1016/j.jhydrol.2018.05.064

Van Leeuwen PJ. 2009. Particle filtering in geophysical systems. *Monthly Weather Review* **137** (12): 4089–4114 DOI: 10.1175/2009MWR2835.1

Leica Geosystems. 2011. Leica ADS80 Airborne Digital Sensor Digital Airborne Imaging Solution. Heerbrugg, Switzerland.

Leisenring M, Moradkhani H. 2011. Snow water equivalent prediction using Bayesian data assimilation methods. *Stochastic Environmental Research and Risk Assessment* **25** (2): 253–270 DOI: 10.1007/s00477-010-0445-5

Levene H. 1960. Robust tests for equality of variances. *Contributions to probability and statistics: Essays in …* **69** (346)

Liston GE, Pielke RA, Greene EM. 1999. Improving first-order snow-related deficiencies in a regional climate model. *Journal of Geophysical Research Atmospheres* **104** (D16) DOI: 10.1029/1999JD900055

Liu Y, Peters-Lidard CD, Kumar S, Foster JL, Shaw M, Tian Y, Fall GM. 2013. Assimilating satellite-based snow depth and snow cover products for improving snow predictions in Alaska. *Advances in Water Resources* **54**: 208–227 DOI: 10.1016/j.advwatres.2013.02.005

López-Moreno JI, Latron J. 2008. Influence of canopy density on snow distribution in a temperate mountain range. *Hydrological Processes* **22** (1): 117–126 DOI: 10.1002/hyp.6572

López-Moreno JI, Fassnacht SR, Beguería S, Latron JBP. 2011. Variability of snow depth at the plot scale: Implications for mean depth estimation and sampling strategies. *Cryosphere* **5** (3): 617–629 DOI: 10.5194/tc-5-617-2011

López-Moreno JI, Fassnacht SR, Heath JT, Musselman KN, Revuelto J, Latron J, Morán-Tejeda E, Jonas T. 2013. Small scale spatial variability of snow density and depth over complex alpine terrain: Implications for estimating snow water equivalent. *Advances in Water Resources* **55**: 40–52 DOI: 10.1016/j.advwatres.2012.08.010

Lovell JL, Jupp DLB, Culvenor DS, Coops NC. 2003. Using airborne and ground-based ranging lidar to measure canopy structure in Australian forests. *Canadian Journal of Remote Sensing* **29** (5): 607–622 DOI: 10.5589/m03-026

Lu X, Guo Q, Li W, Flanagan J. 2014. A bottom-up approach to segment individual deciduous trees using leaf-off lidar point cloud data. *ISPRS Journal of Photogrammetry and Remote Sensing* **94** (155): 1–12 DOI: 10.1016/j.isprsjprs.2014.03.014

Luce CH, Tarboton DG, Cooley KR. 1998. The infuence of the spatial distribution of snow on basin-averaged snowmelt. *Hydrological Processes* **12** (May 1997): 1671–1683 DOI: 10.1002/(SICI)1099-1085(199808/09)12:10/11<1671::AID-HYP688>3.0.CO;2-N

Lundberg A, Gustafsson D, Stumpp C, Kløve B, Feiccabrino J. 2016. Spatiotemporal Variations in Snow and Soil Frost—A Review of Measurement Techniques. *Hydrology* **3** (3): 28 DOI: 10.3390/hydrology3030028

Lundquist JD, Lott F. 2010. Using inexpensive temperature sensors to monitor the duration and heterogeneity of snow-covered areas. *Water Resources Research* **46** (4): 8–13 DOI: 10.1029/2008WR007035

Luojus K, Lemmetyinen J, Pulliainen J, Takala M, Moisander M, Cohen J, Ikonen J. 2017. Copernicus Global Land Operations “Cryosphere and Water” Algorithm Theoretical Basis Document. Helsinki. Available at: https://land.copernicus.eu/global/sites/cgls.vito.be/files/products/CGLOPS2_ATBD_SWE-NH-5km-V1_I1.01.pdf

Luojus K, Pulliainen J, Takala M, Derksen C, Rott H, Nagler T, Solberg R, Wiesmann A, Metsamaki S, Malnes E, et al. 2010. Investigating the feasibility of the globsnow snow water equivalent data for climate research purposes. *Geoscience and Remote Sensing Symposium (IGARSS), 2010 IEEE International* **19** (August 2010): 4851–4853 DOI: 10.1109/IGARSS.2010.5741987

Magnusson J, Gustafsson D, Hüsler F, Jonas T. 2014. Assimilation of point SWE data into a distributed snow cover model comparing two contrasting methods. *Water Resources Research* **50** (10): 7816–7835 DOI: 10.1002/2014WR015302

Magnusson J, Winstral A, Stordal AS, Essery R, Jonas T. 2017. Improving physically based snow simulations by assimilating snow depths using the particle filter. *Water*

Resources Research **53** (2): 1125–1143 DOI: 10.1002/2016WR019092

Mai JJ, Shen H, Tolson BA, Gaborit É, Arsenault R, Craig JR, Fortin V, Fry LM, Gauch M, Klotz D, et al. 2022. The Great Lakes Runoff Intercomparison Project Phase 4: the Great Lakes (GRIP-GL). *Hydrology and Earth System Sciences* **26** (13): 3537–3572 DOI: 10.5194/hess-26-3537-2022

Massmann C. 2019. Modelling Snowmelt in Ungauged Catchments. *Water* **11** (2): 301 DOI: 10.3390/w11020301

Mazzotti G, Currier WR, Deems JS, Pflug JM, Lundquist JD, Jonas T. 2019. Revisiting Snow Cover Variability and Canopy Structure Within Forest Stands: Insights From Airborne Lidar Data. *Water Resources Research* **55** (7): 6198–6216 DOI: 10.1029/2019WR024898

McCreight JL, Small EE. 2014. Modeling bulk density and snow water equivalent using daily snow depth observations. *Cryosphere* **8** (2): 521–536 DOI: 10.5194/tc-8-521-2014

Mekis E, Stewart RE, Theriault JM, Kochtubajda B, Bonsal BR, Liu Z. 2020. Near-0°C surface temperature and precipitation type patterns across Canada. *Hydrology and Earth System Sciences* **24** (4): 1741–1761 DOI: 10.5194/hess-24-1741-2020

Meromy L, Molotch NP, Link TE, Fassnacht SR, Rice R. 2013. Subgrid variability of snow water equivalent at operational snow stations in the western USA. *Hydrological Processes* **27** (17): 2383–2400 DOI: 10.1002/hyp.9355

Metcalfe RA, Buttle JM. 1995. Controls of Canopy structure on snowmelt rates in the boreal forest. In *Proceedings of the Eastern Snow Conference 52.*Toronto, ON; 249–257.

Metcalfe RA, Buttle JM. 1998. A statistical model of spatially distributed snowmelt rates in a boreal forest basin. *Hydrological Processes* **12** (10–11): 1701–1722 DOI: 10.1002/(SICI)1099-1085(199808/09)12:10/11<1701::AID-HYP690>3.0.CO;2-D

Micheletty P, Perrot D, Day G, Rittger K. 2021. Assimilation of Ground and Satellite Snow Observations in a Distributed Hydrologic Model for Water Supply Forecasting. *Journal of the American Water Resources Association* DOI: 10.1111/1752-1688.12975

Mizukami N, Perica S. 2008. Spatiotemporal Characteristics of Snowpack Density in the Mountainous Regions of the Western United States. *Journal of Hydrometeorology* **9** (6): 1416–1426 DOI: 10.1175/2008JHM981.1

Moeser D, Morsdorf F, Jonas T. 2015a. Novel forest structure metrics from airborne LiDAR data for improved snow interception estimation. *Agricultural and Forest Meteorology* **208**: 40–49 DOI: 10.1016/j.agrformet.2015.04.013

Moeser D, Roubinek J, Schleppi P, Morsdorf F, Jonas T. 2014. Canopy closure, LAI and radiation transfer from airborne LiDAR synthetic images. *Agricultural and Forest*

Meteorology **197**: 158–168 DOI: 10.1016/j.agrformet.2014.06.008

Moeser D, Stähli M, Jonas T. 2015b. Improved snow interception modeling using canopy parameters derived from airborne LiDAR data. *Water Resources Research* **51** (7): 5041–5059 DOI: 10.1002/2014WR016724

Molotch NP, Bales RC. 2005. Scaling snow observations from the point to the grid element: Implications for observation network design. *Water Resources Research* **41** (11): 1–16 DOI: 10.1029/2005WR004229

Molotch NP, Colee MT, Bales RC, Dozier J. 2005. Estimating the spatial distribution of snow water equivalent in an alpine basin using binary regression tree models: The impact of digital elevation data and independent variable selection. *Hydrological Processes* **19** (7): 1459–1479 DOI: 10.1002/hyp.5586

Moradkhani H. 2008. Hydrologic remote sensing and land surface data assimilation. *Sensors* **8** (5): 2986–3004 DOI: 10.3390/s8052986

Moradkhani H, Hsu K-L, Gupta H, Sorooshian S. 2005. Uncertainty assessment of hydrologic model states and parameters: Sequential data assimilation using the particle filter. *Water Resources Research* **41** (5): 1–17 DOI: 10.1029/2004WR003604

Morsdorf F, Kötz B, Meier E, Itten KI, Allgöwer B. 2006. Estimation of LAI and fractional cover from small footprint airborne laser scanning data based on gap fraction. *Remote Sensing of Environment* **104** (1): 50–61 DOI: 10.1016/j.rse.2006.04.019

Mudryk LR, Derksen C, Kushner PJ, Brown R. 2015. Characterization of Northern Hemisphere snow water equivalent datasets, 1981-2010. *Journal of Climate* **28** (20): 8037–8051 DOI: 10.1175/JCLI-D-15-0229.1

Murray CD, Buttle JM. 2003. Impacts of clearcut harvesting on snow accumulation and melt in a northern hardwood forest. *Journal of Hydrology* **271** (1–4): 197–212 DOI: 10.1016/S0022-1694(02)000352-9

Musselman KN, Lehner F, Ikeda K, Clark MP, Prein AF, Liu C, Barlage M, Rasmussen R. 2018. Projected increases and shifts in rain-on-snow flood risk over western North America. *Nature Climate Change* **8** (9) DOI: 10.1038/s41558-018-0236-4

Musselman KN, Molotch NP, Brooks PD. 2008. Effects of vegetation on snow accumulation and ablation in a mid-latitude sub-alpine forest. *Hydrological Processes* **22** (15): 2767–2776 DOI: 10.1002/hyp.7050

Musselman KN, Molotch NP, Margulis SA, Kirchner PB, Bales RC. 2012. Influence of canopy structure and direct beam solar irradiance on snowmelt rates in a mixed conifer forest. *Agricultural and Forest Meteorology* **161**: 46–56 DOI: 10.1016/j.agrformet.2012.03.011

Nemri S, Kinnard C. 2020. Comparing calibration strategies of a conceptual snow

hydrology model and their impact on model performance and parameter identifiability. *Journal of Hydrology* **582** (May 2019): 124474 DOI: 10.1016/j.jhydrol.2019.124474

Neumann NN, Derksen C, Smith C, Goodison B. 2006. Characterizing local scale snow cover using point measurements during the winter season. *Atmosphere-Ocean* **44** (3): 257–269 DOI: 10.3137/ao.440304

Nikon. 2010. Total Station DTM-322 Instruction Manual. Trimble, Westminster, CO.

Ontario Ministry of Natural Resources and Forestry. 2007. Forest Resources Inventory (FIM V2 2D) Packaged Product. Peterborough.

Ontario Ministry of Natural Resources and Forestry. 2014. Ontario Land Cover Compilation Data Specifications Version 2 . 0. Peterborough. Available at: https://www.sse.gov.on.ca/sites/MNR-PublicDocs/EN/CMID/Ontario Land Cover Compilation - Data Specification Version.pdf

Ontario Ministry of Natural Resources and Forestry. 2018. Provincial Digital Elevation Model User Guide. Peterborough. Available at: https://www.sse.gov.on.ca/sites/MNR-PublicDocs/EN/CMID/PDEM_UserGuide.pdf

Ontario Ministry of the Environment. 2016. Ontario's Great Lakes Strategy. Queen's Printer for Ontario, Toronto, ON.

Parajka J, Blöschl G. 2008. The value of MODIS snow cover data in validating and calibrating conceptual hydrologic models. *Journal of Hydrology* **358** (3–4): 240–258 DOI: 10.1016/j.jhydrol.2008.06.006

Parajka J, Haas P, Kirnbauer R, Jansa J, Blöschl G. 2012. Potential of time-lapse photography of snow for hydrological purposes at the small catchment scale. *Hydrological Processes* **26** (22): 3327–3337 DOI: 10.1002/hyp.8389

Parajka J, Merz R, Blöschl G. 2007. Uncertainty and multiple objective calibration in regional water balance modelling: case study in 320 Austrian catchments. *Hydrological Processes* **21** (4): 435–446 DOI: 10.1002/hyp.6253

Pearse GD, Dash JP, Persson HJ, Watt MS. 2018. Comparison of high-density LiDAR and satellite photogrammetry for forest inventory. *ISPRS Journal of Photogrammetry and Remote Sensing* **142** (March): 257–267 DOI: 10.1016/j.isprsjprs.2018.06.006

Penn CA, Wemple BC, Campbell JL. 2012. Forest influences on snow accumulation and snowmelt at the Hubbard Brook Experimental Forest, New Hampshire, USA. *Hydrological Processes* **26** (17): 2524–2534 DOI: 10.1002/hyp.9450

Peters-Lidard CD, Clark M, Samaniego L, Verhoest NEC, Van Emmerik T, Uijlenhoet R, Achieng K, Franz TE, Woods R. 2017. Scaling, similarity, and the fourth paradigm for hydrology. *Hydrology and Earth System Sciences* **21** (7): 3701–3713

DOI: 10.5194/hess-21-3701-2017

Pitt DG, Woods M, Penner M. 2014. A comparison of point clouds derived from stereo imagery and airborne laser scanning for the area-based estimation of forest inventory attributes in boreal Ontario. *Canadian Journal of Remote Sensing* **40** (3): 214–232 DOI: 10.1080/07038992.2014.958420

Pomeroy J, Essery R, Toth B. 2004. Implications of spatial distributions of snow mass and melt rate for snow-cover depletion: Observations in a subarctic mountain catchment. *Annals of Glaciology* **38**: 195–201 DOI: 10.3189/172756404781815275

Pomeroy J, Gray DM, Hedstrom NR, Janowicz JR. 2002. Prediction of seasonal snow accumulation in cold climate forests. *Hydrological Processes* **16** (18): 3543–3558 DOI: 10.1002/hyp.1228

Pomeroy J, Parviainen J, Hedstrom N, Gray DM. 1998. Coupled modelling of forest snow interception and sublimation. *Hydrological Processes* **12** (15): 2317–2337 DOI: 10.1002/(SICI)1099-1085(199812)12:15<2317::AID-HYP799>3.0.CO;2-X

Popescu SC, Wynne RH. 2004. Seeing the Trees in the Forest. *Photogrammetric Engineering & Remote Sensing* **70** (5): 589–604 DOI: 10.14358/PERS.70.5.589

Provincial Flood Forecasting and Warning Committee. 2014. Ontario Flood Forecasting and Warning Guidelines. Peterborough, ON.

Provincial Mapping Unit. 2020. Imagery User Guide. Queen's Printer for Ontario, Peterborough, ON.

Pulliainen J. 2006. Mapping of snow water equivalent and snow depth in boreal and sub-arctic zones by assimilating space-borne microwave radiometer data and ground-based observations. *Remote Sensing of Environment* **101** (2): 257–269 DOI: 10.1016/j.rse.2006.01.002

Pulliainen J, Hallikainen M. 2001. Retrieval of regional snow water equivalent from space-borne passive microwave observations. *Remote Sensing of Environment* **75** (1): 76–85 DOI: 10.1016/S0034-4257(00)00157-7

R Development Core Team R. 2011. *R: A Language and Environment for Statistical Computing*. DOI: 10.1007/978-3-540-74686-7

Raven : User's and Developer's Manual v3.6.

Riboust P, Thirel G, Moine N Le, Ribstein P. 2019. Revisiting a Simple Degree-Day Model for Integrating Satellite Data: Implementation of Swe-Sca Hystereses. *Journal of Hydrology and Hydromechanics* **67** (1): 70–81 DOI: 10.2478/johh-2018-0004

Rice R, Bales RC. 2010. Embedded-sensor network design for snow cover measurements around snow pillow and snow course sites in the Sierra Nevada of California. *Water Resources Research* **46** (3): 1–13 DOI: 10.1029/2008WR007318

Rich PM. 1990. Characterizing plant canopies with hemispherical photographs. *Remote Sensing Reviews* **5** (1): 13–29 DOI: 10.1080/02757259009532119

Rienecker MM, Suarez MJ, Gelaro R, Todling R, Bacmeister J, Liu E, Bosilovich MG, Schubert SD, Takacs L, Kim GK, et al. 2011. MERRA: NASA's modern-era retrospective analysis for research and applications. *Journal of Climate* **24** (14) DOI: 10.1175/JCLI-D-11-00015.1

Riggs G, Hall D. 2011. MODIS Snow Cover Algorithms and Products – Improvements for Collection 6. *68th Eastern Snow Conference*: 163–171

Rodell M, Houser PR, Jambor U, Gottschalck J, Mitchell K, Meng CJ, Arsenault K, Cosgrove B, Radakovich J, Bosilovich M, et al. 2004. The Global Land Data Assimilation System. *Bulletin of the American Meteorological Society* **85** (3) DOI: 10.1175/BAMS-85-3-381

Ross DB, Brasnett B. 2014. Canadian Meteorological Centre (CMC) Daily Snow Depth Analysis Data. *Canadian Meteorological Centre (CMC) Daily Snow Depth Analysis Data* DOI: http://dx.doi.org/10.5067/W9FOYWH0EQZ3

Rouse JW, Haas RH, Schell JA, Deeering D. 1973. Monitoring vegetation systems in the Great Plains with ERTS (Earth Resources Technology Satellite). In *Third Earth Resources Technology Satellite-1 Symposium*NASA SP-351; 309–317.

Rousse J-R, Auty D. 2020. Airborne LiDAR Data Manipulation and Visualization for Forestry Applications: R Package Version 2.2.4. Laval, QC. Available at: https://cran.r-project.org/package=lidR

Roy A, Royer A, Turcotte R. 2010. Improvement of springtime streamflow simulations in a boreal environment by incorporating snow-covered area derived from remote sensing data. *Journal of Hydrology* **390** (1–2): 35–44 DOI: 10.1016/j.jhydrol.2010.06.027

Scott RW, Huff FA. 1996. Impacts of the Great Lakes on Regional Climate Conditions. *Journal of Great Lakes Research* **22** (4): 845–863 DOI: 10.1016/S0380-1330(96)71006-7

Shapiro S, Wilk M. 1965. An analysis of variance test for normality (complete samples). *Biometrika* **52** (3–4): 591–611 DOI: 10.1093/biomet/52.3-4.591

Shawn Matott L-. 2017. OSTRICH – An Optimization Software Toolkit for Research Involving Computational Heuristics Documentation and User ' s Guide by L . Shawn Matott , Ph . D . State University of New York at Buffalo Center for Computational Research: 79 Available at: www.eng.buffalo.edu/~lsmatott/Ostrich/OstrichMain.html.

Sicart JE, Pomeroy J, Essery R, Hardy J. 2003. Snowmelt in a Canadian Spruce Forest : A Sensitivity Study to the Canopy Cover. In *60th Eastern Snow Conference*.

Singer SNN, Cheng CKK. 2002. An Assessment of the Groundwater Resources of

Northern Ontario. Toronto.

Smith AMS, Falkowski MJ, Hudak AT, Evans JS, Robinson AP, Steele CM. 2009. A cross-comparison of field, spectral, and lidar estimates of forest canopy cover. *Canadian Journal of Remote Sensing* **35** (5): 447–459 DOI: 10.5589/m09-038

Smyth EJ, Raleigh MS, Small EE. 2019. Particle Filter Data Assimilation of Monthly Snow Depth Observations Improves Estimation of Snow Density and SWE. *Water Resources Research* DOI: 10.1029/2018WR023400

Smyth EJ, Raleigh MS, Small EE. 2020. Improving SWE Estimation With Data Assimilation: The Influence of Snow Depth Observation Timing and Uncertainty. *Water Resources Research* **56** (5) DOI: 10.1029/2019WR026853

Snauffer AM, Hsieh WW, Cannon AJ. 2016. Comparison of gridded snow water equivalent products with in situ measurements in British Columbia, Canada. *Journal of Hydrology* **541**: 714–726 DOI: 10.1016/j.jhydrol.2016.07.027

Solberg S. 2010. Mapping gap fraction, LAI and defoliation using various ALS penetration variables. *International Journal of Remote Sensing* **31** (5): 1227–1244 DOI: 10.1080/01431160903380672

Solberg S, Brunner A, Hanssen KH, Lange H, Næsset E, Rautiainen M, Stenberg P. 2009. Mapping LAI in a Norway spruce forest using airborne laser scanning. *Remote Sensing of Environment* **113** (11): 2317–2327 DOI: 10.1016/j.rse.2009.06.010

St-Onge B, Audet F-AA, Bégin J. 2015. Characterizing the height structure and composition of a boreal forest using an individual tree crown approach applied to photogrammetric point clouds. *Forests* **6** (11): 3899–3922 DOI: 10.3390/f6113899

ter Steege H. 2018. HemiPhot.R Free R scripts to analyse hemispherical photographs for canopy openness, leaf area index and photosynthetic active radiation under forest canopies. Leiden, The Netherlands.

Steppuhn H, Dyck GE. 1974. Estimating true basin snowcover. *Interdisciplinary Symposium on Advances Concepts and Techniques in the Study of Snow and Ice Resources* (December): 314–328

Stigter EM, Wanders N, Saloranta TM, Shea JM, Bierkens MFP, Immerzeel WW. 2017. Assimilation of snow cover and snow depth into a snow model to estimate snow water equivalent and snowmelt runoff in a Himalayan catchment. *Cryosphere* **11** (4): 1647–1664 DOI: 10.5194/tc-11-1647-2017

Stone C, Webster M, Osborn J, Iqbal I. 2016. Alternatives to LiDAR-derived canopy height models for softwood plantations: a review and example using photogrammetry. *Australian Forestry* **79** (4): 271–282 DOI: 10.1080/00049158.2016.1241134

Sturm M. 2015. White water: Fifty years of snow research in WRR and the outlook for

the future. *Water Resources Research* **51** (7) DOI: 10.1002/2015WR017242

Sturm M, Wagner AM. 2010. Using repeated patterns in snow distribution modeling: An Arctic example. *Water Resources Research* **46** (12): 1–15 DOI: 10.1029/2010WR009434

Suriano ZJ, Leathers DJ. 2017. Synoptic climatology of lake-effect snowfall conditions in the eastern Great Lakes region. *International Journal of Climatology* **37** (12): 4377–4389 DOI: 10.1002/joc.5093

Takala M, Luojus K, Pulliainen J, Derksen C, Lemmetyinen J, Kärnä JP, Koskinen J, Bojkov B. 2011. Estimating northern hemisphere snow water equivalent for climate research through assimilation of space-borne radiometer data and ground-based measurements. *Remote Sensing of Environment* **115** (12): 3517–3529 DOI: 10.1016/j.rse.2011.08.014

Talbot J, Plamondon AP, Lévesque D, Aubé D, Prévos M, Chazalmartin F, Gnocchini M. 2006. Relating snow dynamics and balsam fir stand characteristics, Montmorency Forest, Quebec. *Hydrological Processes* **20** (5): 1187–1199 DOI: 10.1002/hyp.5938

Thirel, Salamon, Burek K. 2015. Assimilation of MODIS snow cover area data in a distributed hydrological model. *Hydrology and Earth System Sciences* **19** (4): 1887–1904 DOI: 10.5194/hessd-8-1329-2011

Thirel G, Salamon P, Burek P, Kalas M. 2013. Assimilation of MODIS snow cover area data in a distributed hydrological model using the particle filter. *Remote Sensing* **5** (11): 5825–5850 DOI: 10.3390/rs5115825

Tolson BA, Shoemaker CA. 2007. Dynamically dimensioned search algorithm for computationally efficient watershed model calibration. *Water Resources Research* **43** (1): 1–16 DOI: 10.1029/2005WR004723

Tukey JW. 1949. Comparing Individual Means in the Analysis of Variance. *Biometrics* DOI: 10.2307/3001913

Tuo Y, Marcolini G, Disse M, Chiogna G. 2018. A multi-objective approach to improve SWAT model calibration in alpine catchments. *Journal of Hydrology* **559**: 347–360 DOI: 10.1016/j.jhydrol.2018.02.055

Udnæs HC, Alfnes E, Andreassen LM. 2007. Improving runoff modelling using satellite-derived snow covered area? *Nordic Hydrology* **38** (1): 21–32 DOI: 10.2166/nh.2007.032

Ullah S, Dees M, Datta P, Adler P, Schardt M, Koch B. 2019. Potential of Modern Photogrammetry Versus Airborne Laser Scanning for Estimating Forest Variables in a Mountain Environment. *Remote Sensing* **11** (6): 661 DOI: 10.3390/rs11060661

Varhola A, Coops NC. 2013. Estimation of watershed-level distributed forest structure metrics relevant to hydrologic modeling using LiDAR and Landsat. *Journal of Hydrology* **487**: 70–86 DOI: 10.1016/j.jhydrol.2013.02.032

Varhola A, Coops N, Alila Y, Weiler M. 2014. Exploration of remotely sensed forest structure and ultrasonic range sensor metrics to improve empirical snow models. *Hydrological Processes* **28** (15): 4433–4448 DOI: 10.1002/hyp.9952

Varhola A, Coops NC, Bater CW, Teti P, Boon S, Weiler M. 2010a. The influence of ground- and lidar-derived forest structure metrics on snow accumulation and ablation in disturbed forests. *Canadian Journal of Forest Research* **40** (4): 812–821 DOI: 10.1139/X10-008

Varhola A, Coops N, Weiler M, Moore D. 2010b. Forest canopy effects on snow accumulation and ablation: An integrative review of empirical results. *Journal of Hydrology* **392** (3–4): 219–233 DOI: 10.1016/j.jhydrol.2010.08.009

Varhola A, Frazer GW, Teti P, Coops NC. 2012. Estimation of forest structure metrics relevant to hydrologic modeling using coordinate transformation of airborne laser scanning data. *Hydrology and Earth System Sciences Discussions* **9** (4): 5531–5573 DOI: 10.5194/hessd-9-5531-2012

Vuyovich C, Jacobs JM. 2011. Snowpack and runoff generation using AMSR-E passive microwave observations in the Upper Helmand Watershed, Afghanistan. *Remote Sensing of Environment* **115** (12): 3313–3321 DOI: 10.1016/j.rse.2011.07.014

Warren R, Bisset AR, Pond B, Voigt D. 1998. The Snow Network for Ontario Wildlife. *Ontario Ministry of Natural Resources. Queen's Printer for Ontario: Peterborough, ON.*

Watson FGR, Anderson TN, Newman WB, Alexander SE, Garrott RA. 2006. Optimal sampling schemes for estimating mean snow water equivalents in stratified heterogeneous landscapes. *Journal of Hydrology* **328** (3–4): 432–452 DOI: 10.1016/j.jhydrol.2005.12.032

White JC, Stepper C, Tompalski P, Coops NC, Wulder MA. 2015. Comparing ALS and Image-Based Point Cloud Metrics and Modelled Forest Inventory Attributes in a Complex Coastal Forest Environment. *Forests* **6** (12): 3704–3732 DOI: 10.3390/f6103704

Woods M, Lim K, Treitz P. 2008. Predicting forest stand variables from LiDAR data in the Great Lakes - St. Lawrence forest of Ontario. *Forestry Chronicle* **84** (6): 827–839 DOI: 10.5558/tfc84827-6

Yamazaki T, Kondo J. 1992. The snowmelt and heat balance in snow-covered forested areas. *Journal of Applied Meteorology* **31**: 1322–1327 DOI: 10.1175/1520-0450(1992)031<1322:TSAHBI>2.0.CO;2

Yang G, Guo S, Liu P, Li L, Liu Z. 2017. Multiobjective Cascade Reservoir Operation Rules and Uncertainty Analysis Based on PA-DDS Algorithm. *Journal of Water Resources Planning and Management* **143** (7) DOI: 10.1061/(asce)wr.1943-5452.0000773

Yatheendradas S, Peters Lidard CD, Koren V, Cosgrove BA, De Goncalves LGG, Smith M, Geiger J, Cui Z, Borak J, Kumar S V., et al. 2012. Distributed assimilation of satellite-based snow extent for improving simulated streamflow in mountainous, dense forests: An example over the DMIP2 western basins. *Water Resources Research* **48** (9): 1–18 DOI: 10.1029/2011WR011347

Yen H, Jeong J, Tseng W-H, Kim M-K, Records RM, Arabi M. 2015. Computational Procedure for Evaluating Sampling Techniques on Watershed Model Calibration. *Journal of Hydrologic Engineering* **20** (7) DOI: 10.1061/(asce)he.1943-5584.0001095

Zahmatkesh Z, Tapsoba D, Leach J, Coulibaly P. 2019. Evaluation and bias correction of SNODAS snow water equivalent (SWE) for streamflow simulation in eastern Canadian basins. *Hydrological Sciences Journal* **64** (13): 1541–1555 DOI: 10.1080/02626667.2019.1660780

Zhen Z, Quackenbush L, Zhang L. 2016. Trends in Automatic Individual Tree Crown Detection and Delineation—Evolution of LiDAR Data. *Remote Sensing* **8** (4): 333 DOI: 10.3390/rs8040333

Zheng Z, Ma Q, Qian K, Bales R. 2018. Canopy Effects on Snow Accumulation: Observations from Lidar, Canonical-View Photos, and Continuous Ground Measurements from Sensor Networks. *Remote Sensing* **10** (11): 1769 DOI: 10.3390/rs10111769